Analytical Evaluation of Restraint Mechanisms in Precast Concrete Double Tee Floor Systems Subjected to Fire Loading

Okasha, Nader; Pessiki, Stephen; Lee, Byoung-Jun
2006

ANALYTICAL EVALUATION OF RESTRAINT MECHANISMS IN PRECAST CONCRETE DOUBLE TEE FLOOR SYSTEMS SUBJECTED TO FIRE LOADING

by

Nader Okasha

Stephen Pessiki

Byoung-Jun Lee

ATLSS Report No. 06-24

December 2006

ATLSS is a National Center for Engineering Research on Advanced Technology for Large Structural Systems

117 ATLSS Drive
Bethlehem, PA 18015-4729

Phone: (610)758-3525
Fax: (610)758-5902

www.atlss.lehigh.edu
Email: inatl@lehigh.edu

ANALYTICAL EVALUATION OF RESTRAINT MECHANISMS IN PRECAST CONCRETE DOUBLE TEE FLOOR SYSTEMS SUBJECTED TO FIRE LOADING

by

Nader Okasha
Graduate Research Assistant
Department of Civil and Environmental Engineering

Stephen Pessiki
Professor and Chairperson
Department of Civil and Environmental Engineering

Byoung-Jun Lee
Research Scientist
ATLSS Center

ATLSS Report No. 06-24

December 2006

ATLSS is a National Center for Engineering Research on Advanced Technology for Large Structural Systems

117 ATLSS Drive
Bethlehem, PA 18015-4729

Phone: (610)758-3525
Fax: (610)758-5902

www.atlss.lehigh.edu
Email: inatl@lehigh.edu

TABLE OF CONTENTS

LIST OF TABLES

LIST OF FIGURES

ABSTRACT

The structural behavior of a precast prestressed concrete floor system subjected to fire is significantly influenced by the end restraint condition of its elements. Current design practice in the U.S. uses a dual classification for fire resistance of supporting members in floor and roof systems in buildings, depending upon whether these members are restrained or unrestrained at their ends. There are significant consequences in having a restrained versus unrestrained condition in terms the suitability of given section for a given span and loading condition.

Chapter 6 of Design for Fire Resistance of Precast Prestressed Concrete published by the precast/prestressed concrete institute suggests that restraint comes primarily from end supports. In actual precast structures, restraint may come from a variety of effects in addition to the conditions that exist at the end supports of a member. For example, restraint may be provided by connections between adjacent members not subjected to fire.

The objective of the research presented in this report is to analytically investigate the development of restraint mechanisms in precast prestressed concrete structures under fire loading. A prototype precast prestressed double tee beam typically used in practice for precast parking structures is considered in this research. The importance of various restraint mechanisms is investigated by evaluating their influence on the strength of the double tee beam section. The analytical approach consists of three sequential analysis steps: (1) nonlinear heat transfer analysis; (2) nonlinear structural analysis; and (3) nonlinear strength analysis. Each step uses the results from the previous analysis step.

Four different restraint cases, where restraint forces develop in the prototype double tee beam from different sources, are explored: (1) idealized single span restraints; (2) multiple span restraints; (3) flexible support elements restraints; and, (4) flange connectors restraints.

It is concluded from the results of this research that for the idealized single span cases, the strength is significantly less when only the flange is restrained, and even less when the beam is simply supported than when only the web is restrained and when the entire cross-section is restrained. The strength of the double tee beam when only the web is restrained is slightly higher, however, than when the entire cross-section is restrained. In addition, the strength of the double tee beam decreases as the number of spans increases in all restraint conditions (flange, web or entire cross section). Furthermore, the strength of the double tee beam restrained by spandrels or inverted tee girders is only slightly higher than the strength of the simply supported double tee beam. It is also concluded that the strength of the double tee beam restrained by any practical number of flange connectors is only slightly higher than the strength of the simply supported double tee beam.

CHAPTER 1

INTRODUCTION

1.1 INTRODUCTION

The structural behavior of a precast prestressed concrete system subjected to fire loads is significantly influenced by the end restraint condition of its elements. Current design practice in the U.S. uses a dual classification system for fire resistance of supporting members in floor and roof systems in buildings, depending upon whether these members are restrained or unrestrained at their ends. This dual classification system was first introduced in the ASTM E119 Standards in 1970 to recognize the practical difficulties of appropriately modeling the realistic boundary conditions (restraint conditions) in E119 tests (ASTM 1999).

Chapter 6 of Design for Fire Resistance of Precast Prestressed Concrete published by the precast/prestressed concrete institute suggests that restraint comes primarily from end supports. In actual precast structures, restraint may come from the conditions that exist at the end supports of a member and also from other sources such as connections to adjacent members not subjected to fire. There are significant consequences in having a restrained versus unrestrained condition in terms of the suitability of a given section for a given span and loading condition. This is particularly important in exterior bays where axial restraint may only be provided by the out-of-plane bending stiffness of a wall or weak-axis bending of a spandrel beam.

1.2 OBJECTIVE

The objective of the research presented in this report is to analytically investigate the development of restraint mechanisms in precast prestressed concrete structures under fire loading. The sources and magnitudes of restraint mechanisms in precast concrete structures are identified, and the impact of their restraint forces on the strength of members is evaluated.

The focus of this research is a prototype precast prestressed double tee beam typically used in practice for precast parking structures and also for occupied structures. The restraint mechanisms are investigated by evaluating their influence on the strength of the double tee beam section.

Four different restraint cases, where restraints forces develop in the prototype double tee beam from different sources, are explored: (1) idealized single span restraints; (2) multiple span restraints; (3) flexible support elements restraints; and, (4) flange connectors restraints. Each case is described in detail later in this report.

1.3 SUMMARY OF APROACH

The restraint mechanisms are studied for several cases of boundary conditions by evaluating the strength of the double tee beam at different fire durations. The strength of the double tee beam, restrained and unrestrained with idealized boundary conditions, which bound actual realistic boundary conditions, is first evaluated. The strength of the same double tee beam restrained by realistic boundary conditions is then evaluated and compared with the idealized bounding cases of boundary conditions.

The analytical approach used to evaluate the strength of the double tee beam for the different boundary condition cases consists of three sequential analysis steps: (1) nonlinear heat transfer analysis, (2) nonlinear structural analysis; and (3) nonlinear strength analysis. Each step uses the results from the previous analysis step as follows:

(1) Nonlinear heat transfer analyses are conducted to simulate the transfer of heat from the surfaces of the double tee beam through the cross-section and along the length of the individual members. The analytical models are developed and analyzed using the nonlinear finite element analysis program ABAQUS (2003). The ASTM E119 standard fire curve is used as the thermal input.

(2) Nonlinear structural analyses are conducted to simulate the structural behavior of the overall precast concrete system at elevated temperatures. The analytical models are developed and analyzed using the nonlinear finite element analysis program ABAQUS (2003), which has a sequential heat transfer-structural analysis option.

(3) Nonlinear strength analyses are conducted to determine the strength of the double tee beam at elevated temperatures and for the different restraint conditions considered. The analytical models are developed and analyzed using the DRAIN-2DX program by Prakash, Powell and Campbell (1993).

1.4 SCOPE OF REPORT

Chapters 2 and 3 present background information necessary to understand the work presented in this report. Chapter 2 reviews basic information about heat transfer and the analysis methods used in this research. Chapter 3 provides detailed information about the material properties used in the analyses conducted in this research.

Chapter 4 examines the influence of idealized boundary conditions on the strength of a single-span double tee beam under different fire durations. As will be shown, these analyses represent the bounding cases for the realistic boundary conditions.

Chapters 5, 6 and 7 examine the influence of realistic boundary conditions on the same double tee beam. Chapter 5 evaluates the impact of restraining the double tee beam with the axial restraint provided by the axial stiffness of additional floor members on the strength of that double tee beam under standard fire. Chapter 6 examines the restraint provided by an inverted tee girder and a pocket spandrel beam when these elements are used to support the double tee beam. Chapter 7 examines the restraint provided by flange connectors along the span of the double tee beam.

Chapter 8 summarizes the report and presents the conclusions of the study. Suggestions for future research are also presented in this chapter.

1.5 NOTATION

The following notation is used in this report:

a	=	Eurocode factor for deriving the stress strain relations of prestressing steel at elevated temperatures
A_p	=	area of the prestressing reinforcement, mm^2
b	=	Eurocode factor for deriving the stress strain relations of prestressing steel at elevated temperatures
c	=	Eurocode factor for deriving the stress strain relations of prestressing steel at elevated temperatures
C	=	specific heat of a material, $J/m^3°C$
e	=	eccentricity of the location of the restraint forces resultant to the centroid of the unheated cross-section of the double tee beam, m
E	=	modulus of elasticity, MPa
E_b	=	total amount of thermal radiation emitted by a black body
E(T)	=	modulus of elasticity of prestressing steel at temperature T, MPa
f_c	=	compressive strength of concrete at temperature T, MPa
$f_c^{'}$	=	cylinder strength of concrete at temperature T, MPa
$f_{co}^{'}$	=	cylinder strength of concrete at temperature 20 °C, MPa
f_{pe}	=	effective prestress of the prestressing reinforcement, MPa
f_{pu}	=	ultimate stress of the prestressing reinforcement, MPa
f_y	=	yield stress of prestressing steel, MPa
$f_y(T)$	=	yield stress of prestressing steel at temperature T, MPa
F_i	=	sum of restraint forces height i, kN
g	=	acceleration due to gravity (9.81 m/s^2)
h_a	=	overall heat exchange coefficients on the air side, W/m^2
h_f	=	overall heat exchange coefficients on the fire side, W/m^2
k	=	thermal conductivity of a material, W/mºC
M	=	moment, kN.m
Nc	=	number of connectors installed along the span of the beam
Ne	=	number of elements between every two connectors
P	=	Axial force, kN.
Pr	=	Prandtl number
Q	=	rate of the heat transfer
Q_w	=	latent heat of vapor, kJ/kg
R	=	resultant restraint force, kN

T	=	absolute air temperature, K or °C
T_a	=	overall heat exchange coefficients on the air side
T_f	=	temperature at the fire
T_{fi}	=	overall heat exchange coefficients on the fire side
T_{i1}	=	temperature at a point near the side of the object exposed to fire
T_{i2}	=	temperature at a point away from the side of the object exposed to fire
T_{surf}	=	temperature at the surface of the object exposed to fire
T_1	=	temperatures at the surface of the material on the fire side, °C
T_2	=	temperatures at the surface of the material on the air side, °C
w_c	=	moisture content by weight
$\overline{x}_i$	=	distance from the top of the flange of the double tee beam to the location of the restraint forces resultant, m
$\overline{X}$	=	distance from top of the flange of the double tee beam to the location of the restraint forces resultant, m
$\overline{y}$	=	distance from the top of the flange of the double tee beam to the centroid of the unheated cross-section of the double tee beam, m
α	=	thermal expansion coefficient
ΔT	=	temperature difference on both sides of an object, °C
ε	=	emissivity of the material
ε_c	=	strain of the concrete, mm/mm
ε_{max}	=	strain corresponding to maximum stress, mm/mm
ε_p	=	plastic strain, mm/mm
ε_{pr}	=	proportional limit strain (at the end of range I) of the prestressing steel
$\varepsilon_{pr}(T)$	=	proportional limit strain (at the end of range I) of the prestressing steel at temperature T
ε_r	=	resultant emissivity
ε_t	=	total strains, mm/mm
$\varepsilon(T)$	=	emissivity of prestressing steel at temperature T
ε_1	=	strain of the prestressing steel at the end of range II, mm/mm
ε_2	=	strain of the prestressing steel at the end of range III, mm/mm
ν	=	air viscosity, m^2/s
ρ	=	density of the material, N/m^3
ρ_c	=	density of concrete, N/m^3
σ	=	stress, MPa
σ_{pr}	=	proportional limit stress of the prestressing steel, MPa
$\sigma_{pr}(T)$	=	proportional limit stress of the prestressing steel at temperature T, MPa
σ_{SB}	=	Stefan-Boltzmann constant
$\sigma(T)$	=	stress of prestressing steel at temperature T, MPa

1.6 CONVERSION FACTORS

Values presented in this report are in SI units. The models are based on construction elements typically used in the U.S. and their dimensions and properties are given in British units. The conversion factors used in this report are listed below.

1 in	=	25.4 mm
1 kip	=	4.448 kN
1 ksi	=	6.895 MPa
1 lb/ft^3	=	16.02 kg/m^3
1 ft-lb	=	1.356 N-m

CHAPTER 2

BACKGROUND

2.1 INTRODUCTION

This chapter presents the background information that is relevant to this research. As explained in Chapter 1, the analytical approach used to study the structural performance of structural components consists of three sequential steps, where the results from each step are used to continue the analysis in the subsequent step. These steps are: (1) nonlinear heat transfer analysis, (2) nonlinear structural analysis; and (3) nonlinear strength analysis. A brief background explanation of each of these steps is presented in the following sections.

2.2 HEAT TRANSFER ANALYSES

Nonlinear finite element transient heat transfer analyses are conducted in order to determine the distribution and magnitude of temperature throughout a double tee at different fire durations. The analyses are nonlinear because material properties are temperature dependent. The analyses are transient because the temperatures vary with time in fire tests and an overall temperature history needs to be solved for the following structural analysis step.

The nonlinear heat transfer analyses of this project are conducted using ABAQUS program (ABAQUS 2005). ABAQUS conducts the analysis in an iterative fashion. The time incrementation is controlled automatically by ABAQUS, and is done with the backward Euler method. The size of the increment is selected based on the severity of the nonlinearity.

The element type that has been used throughout this study for the heat transfer analysis step is a solid (continuum) first order (eight nodes) hexahedra (brick) element and it is used with a full integration solution technique. This element is called DC3D8 in the ABAQUS elements library. Although second order elements provide higher accuracy in ABAQUS, first order elements are more efficient and less time costly if used in a fine mesh and used with full integration technique. In the full integration technique ABAQUS uses higher order integration to form the element stiffness, as opposed to the reduced integration technique where lower order integration is used for that purpose. In addition, to make the problem tractable, the element and mesh configuration has to be consistent with the element and mesh configuration used in the structural analysis finite element steps that follow, where first order elements are used with incompatible modes for reasons to be explained in Section 2.3. The reason for the element and mesh consistency between both the heat transfer analysis step and the structural analysis step elements is that the nodal temperature output of the heat transfer step is an input applied to the same nodes in the structural analysis step as thermal loads.

In typical studies of fire resistance, it is common to expose building elements to heating in accordance with a standard temperature-time relation. Standard time-temperature curves specify the furnace temperature as a function of time for a fire test. The most widely used standard fire tests are the ASTM E119 and the ISO 834 (Lie 1992), and they are both presented in Figure 2.1. For this project, the ASTM E119 time-temperature curve is adapted.

There are three basic mechanisms of heat transfer: (1) conduction; (2) convection; and, (3) radiation. These mechanisms are shown in Figure 2.2. As shown in the figure, the heat is transmitted from the fire to the surface of the object through radiation and convection. In other words, the thermal boundary conditions in fire problems consist of two parts: convection and radiation. Radiation however is the dominant mode in heat transfer analysis under fire conditions. To solve the heat transfer problem, the coefficients related to these boundary conditions need to be determined. Once the surface of the object is heated, the thermal energy transfers within the object by conduction. The following is a brief explanation of each of these mechanisms and their related coefficients used in this research. Additional information is provided in typical references such as Mills 1998.

2.2.1 Conduction

Conduction is the exchange of energy or heat on a molecular scale but without any movement of macroscopic portions of matter relative to one another. Equation 2.1 gives the basic equation for one dimensional steady state conductive heat transfer known as Fourier's law. The negative sign in the equation indicates that the heat flows from the higher temperature region to the lower temperature region.

$$Q = -k\left(\frac{dT}{dx}\right) \qquad (2.1)$$

where Q is the rate of the heat transfer, k is the thermal conductivity of the material, dx is the element thickness and dT is the temperature difference across the thickness dx. Equation 2.2 is the transient heat conduction equation for a 3D element dx*dy*dz with its edges parallel to the Cartesian coordinates x, y and z. Equation 2.2 is the basis of fire heat transfer problems.

$$r\ C\frac{\partial T}{\partial t} = k_x\frac{\partial^2 T}{\partial x^2} + k_y\frac{\partial^2 T}{\partial y^2} + k_z\frac{\partial^2 T}{\partial z^2} \qquad (2.2)$$

where C is the specific heat of the material and r is the density of the material. The thermal material properties (thermal conductivity and specific heat) of the materials used in this project are discussed in Chapter 3.

2.2.2 Convection

In convection, heat is transferred at the interface between a fluid and a solid surface. The exchange of heat is due to fluid motion. This motion may be the result of an external force, causing the fluid to flow over the solid surface. This is called forced convection. It may also be the result of buoyancy-induced flow when there is a temperature gradient in the flow, causing a density gradient. This is called natural convection. In either case, the flow is either turbulent or laminar. Turbulent flow takes place when eddy motion of small fluid elements occurs, producing fluctuations in the flow velocities of individual fluid elements, both in the direction of the surface and perpendicular to it. Laminar flow takes place when the fluid moves in a continuous path without mixing with the adjacent paths. Convective heat transfer in fire is mainly by natural convection. At the fire/solid interface, convective heat transfer is usually turbulent. On the air side, which is the side of the solid not exposed to fire, however, laminar flow is usually the case. Convective heat transfer can be described by Equation 2.3a on the fire side of the material, and by Equation 2.3b on the air side.

$$Q = h_f (T_{fi} - T_1) \tag{2.3a}$$

$$Q = h_a (T_2 - T_a) \tag{2.3b}$$

where Q is the rate of heat transfer (heat flux across the thickness), h_f, h_a are the overall heat exchange coefficients on the fire side and air side respectively, and T_1,T_2 are the temperatures at the surface of the material on the fire and air side respectively.

According to Wang (2002), the convective heat transfer coefficient on the fire side can be found from Equation 2.4.

$$h_f = B\left[\left(\frac{g \times P_r}{T \times n^2}\right)\right]^{1/3} k(\Delta T)^{1/3} \tag{2.4}$$

where DT is the temperature difference, B has a value of (0.14) for horizontal surfaces, which is the dominant case in this research, g is the acceleration of gravity (9.81 m/s^2) and P_r, T, n and k are air properties and they are shown in Table 2.1. P_r is the Prandtl number, T is the absolute air temperature, n is the air viscosity and k is the air conductivity.

Figure 2.3 shows the relation between h_f and DT. As shown in the figure, the convection heat transfer coefficient varies depending on the temperature difference. It increases up to 7.32 W/m^2 at a temperature difference of 200 °C and then reduces slowly to 6.27 W/m^2 at a temperature difference of 1200 °C. Therefore, a constant approximate value of 6.5 W/m^2 is used for the convection heat transfer coefficient in this report.

Convective heat transfer can be also described by Equation 2.5 on the air side of the material. Eurocode 1 Part 1.2 recommends the use of a constant value of heat transfer coefficient on the air side of 10 W/m^2. This value is used for this report.

$$h_a = B\left[\left(\frac{g \times P_r}{T \times n^2}\right)\right]^{1/3} k(\Delta T)^{1/4} \qquad (2.5)$$

2.2.3 Radiation

Radiation is the exchange of energy by electromagnetic waves that can be absorbed, transmitted or reflected at a surface. When a radiant thermal energy passes through a medium, an object that is on the path can absorb, reflect and/or transmit fractions of that energy. The relation between the absorptivity a, reflectivity, r and transmittivity t of a material can be described by Equation 2.6.

$$t + r + a = 1 \qquad (2.6)$$

An extreme case is that an object will absorb all incident thermal radiation, i.e. a = 1. The object in this case is called a blackbody. The most important property of the blackbody is that it is a perfect emitter. The total amount of thermal radiation, E_b, emitted by a black body is given by Equation 2.7.

$$E_b = s_{SB} T^4 \qquad (2.7)$$

where s_{SB} is the Stefan-Boltzmann constant and T is the absolute air temperature, K or °C. In most realistic cases, and in fire engineering studies, an additional term is introduced to Equation 2.7, which becomes:

$$E = e s_{SB} T^4 \qquad (2.8)$$

where e is the emissivity and it is defined as the ratio of the total energy emitted by a surface to that of that of a blackbody surface at the same temperature.

A fire surrounding a construction element can be considered as a case of two bodies with one inside the other and are a small distance apart compared with their dimensions so that their areas are effectively equal. The total radiant energy exchange between these two bodies having surfaces 1 and 2, with a surface area A, can be given by Equation 2.9.

$$Q = \frac{e_1 e_2}{1 - r_1 r_2} s \left(T_1^4 - T_2^4\right) A \qquad (2.9)$$

Assuming the transitivity to be negligible, then from Equation 2.6, $r = 1 - a$ (and by Kirchoff's law $r = 1 - e$) and after some mathematical manipulation, Equation 2.9 becomes:

$$Q = \frac{e_1 e_2}{e_1 + e_2 - e_1 e_2} s \left(T_1^4 - T_2^4\right) A = e_r s \left(T_1^4 - T_2^4\right) A \qquad (2.10)$$

where e_r is the resultant emissivity. The Eurocode 1 Part 1.2 gives the emissivity of fire and general construction element as 0.8 and 0.7 respectively. Therefore, the resultant emissivity used in this report is 0.6.

2.3 RESTRAINT FORCES ANALYSES

Nonlinear structural analyses are conducted sequentially after the heat transfer analyses to determine the restraint forces developed in the models and resulting from various different restraint conditions prescribed at different fire durations. The structural analyses are also conducted using the ABAQUS program.

ABAQUS provides an option of running the structural analysis either coupled or uncoupled with the heat transfer analysis. In this project, sequential uncoupled analyses are performed. This option assumes that the structural analysis results have no bearing on the heat transfer analysis (e.g. the thermal properties are not dependent upon dependant upon stress)

ABAQUS uses Newton's method to solve the nonlinear equilibrium equations. Therefore, the solution is reached through a series of time increments, in which ABAQUS iterates to obtain equilibrium. Automatic time incrementation is used, where ABAQUS selects the size of the increments based on the severity of the nonlinearity. The analysis includes large-displacement effect, material nonlinearity and geometric nonlinearity.

The element type that has been used throughout this study for the structural analysis step is a solid (continuum) first order (eight nodes) hexahedra (brick) element enhanced with incompatible modes and used with a full integration technique. This element is called C3D8I in the ABAQUS element library. Although second order elements provide higher accuracy than first order elements, first order incompatible mode elements can produce results in bending problems that are comparable to quadratic elements but at significantly lower computational cost. In addition, using the element in a fine mesh and using the full integration technique enhances the accuracy of the results even further. With the full integration technique, ABAQUS uses higher order integration to form the element stiffness, as opposed to the reduced integration technique where lower order integration is used for that purpose. Incompatible modes are used to improve the bending behavior of the element, if any. In addition to the standard displacement degrees of freedom, incompatible deformation modes are added internally to the elements. The primary effect of these modes is to eliminate the parasitic shear stresses that cause the response of the regular first-order displacement elements to be too stiff in bending. In addition, these modes eliminate the artificial stiffening due to Poisson's effect in bending.

2.4 STRENGTH ANALYSES

In this step, the results from the previous steps are used to determine the section strength at the different fire durations and for the restraint forces developed under the different boundary conditions considered by using nonlinear fiber analysis with the DRAIN-2DX program by Prakash, Powell and Campbell (1993). A different fiber model is built at each fire duration. The loads are applied to the model in the following sequence: (1) the prestressing forces resulting from the prestressing steel, (2) the restraint forces resulting from the previous structural analysis step; and (3) curvature is applied until failure of the section is reached. The outcome of these analyses is the strength of the double tee beam subjected to different restraint conditions at different fire durations. This provides the insight needed to understand the effect of fire on precast concrete members subject to different restraint conditions.

The fiber analysis model is composed of one short fiber element. For pure bending strength analysis, the element is fixed at one end and free at the other end. The fiber model contains one or more segments. The behavior of the segments are monitored at their centers, which are called the slices. The slices, and hence the segments, are made up of a number of fibers. The fibers are formed by descretizing the segments into a number of partial areas. The fineness of the descretization provides greater accuracy in the analysis results. The fibers are defined by their areas, material properties and distance to a selected datum. The datum is usually chosen to be the centroid of the cross section. Each fiber is assigned a different stress-strain relationship with either concrete or steel material properties. In this report, the fibers are built by discretizing the thermal distribution contours resulting from the finite element heat transfer analyses. The fibers are assigned the properties corresponding to the temperatures closest to their temperatures.

Once the model is built, the analysis is performed to find the strength of the section. The analysis process conducts a series of iterations to find a strain distribution across the section that results into an equilibrium of forces on the section. In each iteration, the depth of the neutral axis is varied and the stress-strain diagram of each fiber is used to find the stress in each fiber, from which the forces are computed. The process is repeated until equilibrium is achieved. The flexural moment capacity of the section is then determined by summing the moments of the individual fibers with respect to the reference datum.

Table 2.1: Property values of air at atmospheric pressure (Wang 2002).

Air temperature		Viscosity	Conductivity	Prandtl Number
T (K)	T (°C)	n ($\times 10^6$ m^2/s)	k (W/m°C)	P_r
200	-73	7.49	0.01809	0.739
250	-23	9.49	0.02227	0.722
300	27	15.68	0.02624	0.708
350	77	20.76	0.03003	0.697
400	127	25.90	0.03365	0.689
450	177	28.86	0.03707	0.683
500	227	37.90	0.04038	0.680
550	277	44.34	0.04360	0.680
600	327	51.34	0.04659	0.680
650	377	58.51	0.04953	0.682
700	427	66.25	0.05230	0.684
750	477	73.91	0.05509	0.686
800	527	82.29	0.05779	0.689
850	577	90.75	0.06028	0.692
900	627	99.30	0.06279	0.696
950	677	108.20	0.06525	0.699
1000	727	117.80	0.06752	0.702
1100	827	138.60	0.07320	0.704
1200	927	159.10	0.07820	0.707
1300	1027	182.10	0.08370	0.705
1400	1127	205.50	0.08910	0.705
1500	1227	229.10	0.09460	0.705

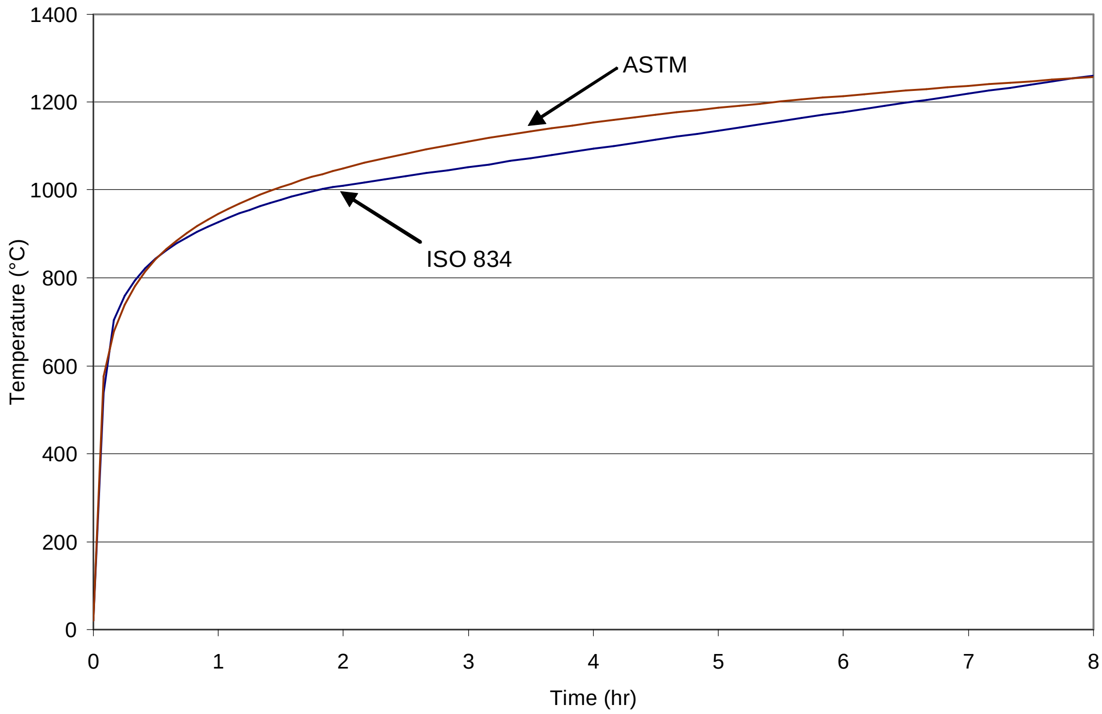

Figure 2.1: Standard fire time-temperature curves.

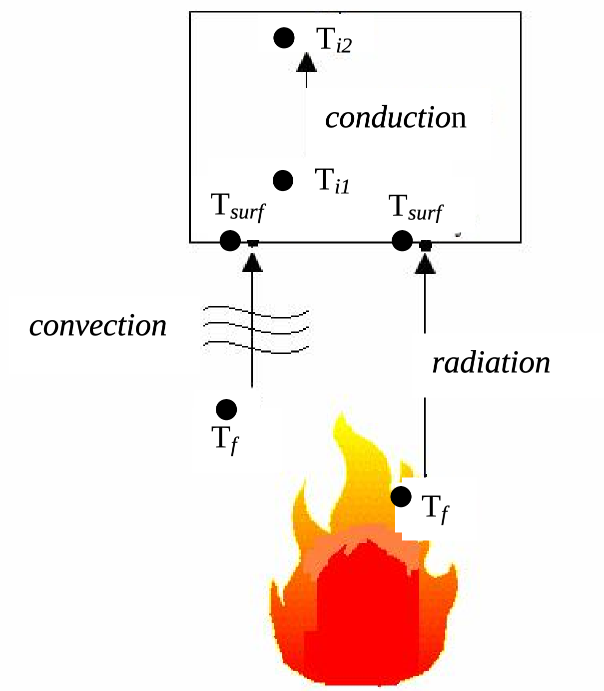

Figure 2.2: A schematic drawing of the three heat transfer mechanisms.

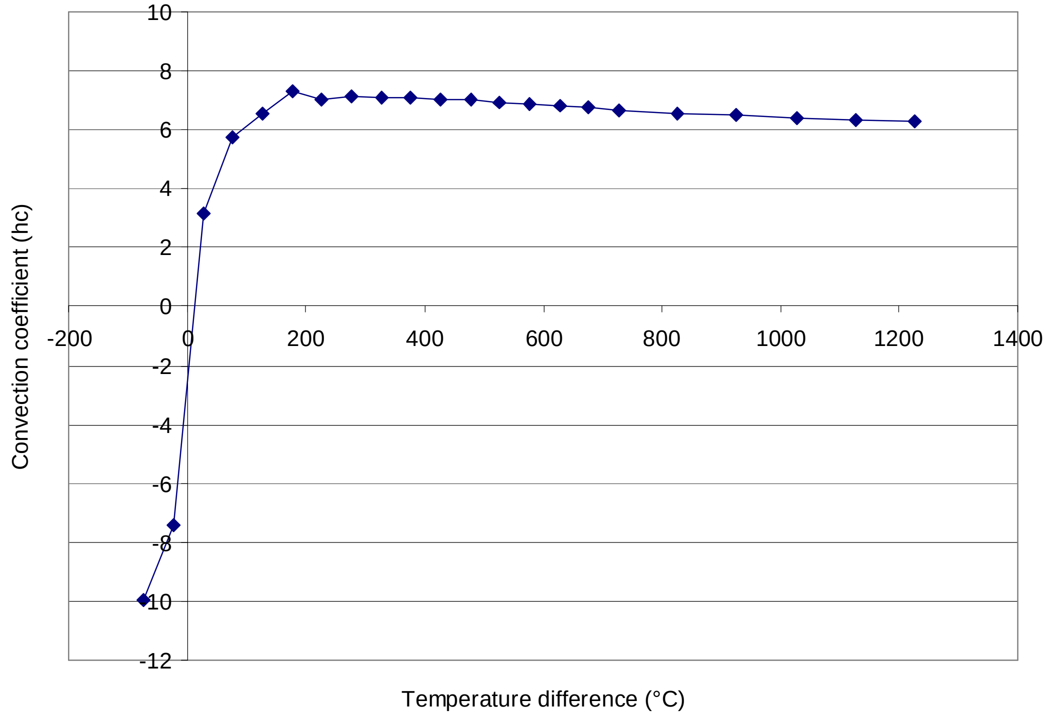

Figure 2.3: Convection heat transfer coefficient on the fire side of concrete.

CHAPTER 3

MATERIAL PROPERTIES

3.1 INTRODUCTION

Nonlinear material properties are used throughout this report. All building material properties experience various degrees of degradation when exposed to fire. In order to effectively carry out the analysis of this project, the relation between the different properties of the materials used for the models, and the increase in temperature, must be correctly modeled.

For a precast concrete structure, the two main materials to be modeled are the concrete and the prestressing steel. Gross section analysis is assumed in both the thermal and structural analysis steps in part to avoid the numerical issues that are encountered by modeling cracking in the concrete. The prestressing steel reinforcement is neglected in the heat transfer model because it does not contribute to a significant degree in the resulting thermal distribution over the cross-section of the model. The prestressing steel is also excluded from the structural analysis model because it does not contribute greatly to the stiffness of the gross section. It is included, however, in the strength analysis step.

The same mechanical properties assigned to the concrete are used for both tension and compression in the structural analysis models. This was done to avoid the numerical difficulties involved in modeling the cracking damage of the concrete in the finite element analysis. Had the cracking in concrete been accounted for, the restraint forces developing would have been less as a result of limiting the force input in the system. Thus, the restraint forces in the theses analyses are expected to be conservative. However, as will be shown in the subsequent chapters, the restraint forces are found not to be too conservative. Furthermore, the steel reinforcement in the actual structure would carry the tension forces after the concrete has cracked. Hence, the tension properties in the finite element model will act in lieu of the excluded reinforcement.

Section 3.2 presents the properties used for the concrete. Both the thermal and mechanical properties are presented in this section. Section 3.3 presents the properties used for the prestressing steel. Only the mechanical properties are presented since the prestressing steel is included only in the strength analysis.

3.2 CONCRETE

3.2.1 Thermal Material Properties

The thermal properties of concrete vary with the type and amount of aggregates in the concrete. Normal weight concrete with siliceous aggregates is the type of concrete used in this project. The thermal material properties that affect the heat transfer analysis are the thermal conductivity and the specific heat.

Thermal Conductivity: Thermal conductivity is the property of a material that indicates its ability to conduct heat. The thermal conductivity of concrete tends to decrease with the rise in temperature for normal weight concrete. This is illustrated in Figure 3.1. The value and the change in thermal conductivity of concrete depend on the degree of crystallinity of the aggregates. The thermal conductivity of concrete is governed by Equation 3.1 (Lie 1992).

$$k = -0.000625T + 1.5 \qquad \text{for} \quad 0\ ^{\circ}\text{C} \leq T \leq 800\ ^{\circ}\text{C} \qquad (3.1\text{a})$$

$$k = 1.0 \qquad \text{for} \quad T > 800^{\circ}\text{C} \qquad (3.1\text{b})$$

where k is the thermal conductivity (W/m°C) and T is the temperature (°C).

Specific Heat: Specific heat of a material is the amount of energy required to raise the temperature of one gram of that material by one degree Celsius. Equation 3.2 governs the relation between the volumetric specific heat (product of specific heat and density) and temperature for siliceous aggregates, and Figure 3.2 displays this relation. As shown in the figure, the specific heat of siliceous aggregate concrete increases slowly with the increase in temperature except at temperature 110 °C where the specific heat reaches a peak. This peak is not accounted for in Equation 3.2, but will be explained next.

$$r_c C = (0.005T + 1.7) \times 10^6 \qquad \text{for } 0 \leq T \leq 200\ ^{\circ}\text{C} \qquad (3.\ 2\text{a})$$
$$r_c C = 2.7 \times 10^6 \qquad \text{for } 200 < T \leq 400\ ^{\circ}\text{C} \qquad (3.\ 2\text{b})$$
$$r_c C = (0.013T - 2.5) \times 10^6 \qquad \text{for } 400 < T \leq 500\ ^{\circ}\text{C} \qquad (3.\ 2\text{c})$$
$$r_c C = (-0.013T + 10.5) \times 10^6 \qquad \text{for } 500 < T \leq 600\ ^{\circ}\text{C} \qquad (3.\ 2\text{d})$$
$$r_c C = 2.7 \times 10^6 \qquad \text{for } T > 600\ ^{\circ}\text{C} \qquad (3.\ 2\text{e})$$

where r_c is the density of concrete (24000 N/m^3), T is temperature (°C) and C is the specific heat (J/m^3°C).

The heat transfer process is affected by the migration of water within the concrete. To accurately model that effect, a laborious combined temperature and mass transfer analysis should be carried out. Instead, and as done here, an approximate method is to add the energy consumed by water evaporation at 110 °C to the specific heat. Accordingly, the maximum increase in the specific heat of the hygroscopic concrete over that of the dry material may be obtained by Equation 3.3.

$$\Delta C = (2w_c \times Q_w) / \Delta T \qquad (3.3)$$

where w_c is the moisture content by weight, and Q_w is the latent heat of vapor. In this report, w_c =2%, Q_w=2260 kJ/kg and DT is the range during which water evaporation occurs, approximately 50 °C (Wang 2002).

3.2.2 Structural Material Properties

The concrete used for the double tee beams and spandrel beams is normal weight concrete with siliceous aggregates and compressive strength of 34.8 MPa (5 ksi). The compressive strength of concrete in the inverted tee girders is 69.5 MPa (10 ksi). This section describes the calculations conducted to determine the mechanical material properties at elevated temperatures of the 34.8 MPa concrete.

Constitutive Relations: Equation 3.4 provides a family of stress-strain relations for a 34.8 MPa compressive strength siliceous aggregate concrete (Lie 1992).

$$e_{\max} = 0.0025 + (6.0T + 0.04T^2) \times 10^{-6} \qquad (3.4a)$$

$$f_c^{'} = f_{co}^{'} \qquad \text{for } T<450\ °C \qquad (3.4b)$$

$$f_c^{'} = f_{co}^{'}[2.011 - 2.353\frac{T-20}{1000}] \qquad \text{for } T\geq 450\ °C \qquad (3.4c)$$

$$f_c = f_c^{'}[1 - \left(\frac{e_{\max} - e_c}{e_{\max}}\right)^2] \qquad e_c \leq e_{\max} \qquad (3.4d)$$

$$f_c = f_c^{'}[1 - \left(\frac{e_c - e_{\max}}{3e_{\max}}\right)^2] \qquad e_c > e_{\max} \qquad (3.4e)$$

where, f_c is the compressive strength of concrete at temperature T, $f_c^{'}$ is the cylinder strength of concrete at temperature T, $f_{co}^{'}$ is the cylinder strength of concrete at temperature 20 °C, e_c is the strain of the concrete, and $e_{\max}$ is the strain corresponding to maximum stress.

These relations are presented in curves shown in Figure 3.3. Each one of these curves present a constitutive model for concrete at a given temperature value. In addition, information about the modulus of elasticity and compressive strength of the concrete as a function of temperature can be extracted from these relations. The elastic modulus of concrete experiences rapid losses as the temperature is increased regardless of the type of aggregates used. This is shown for the 34.8 MPa concrete in Figure 3.4. On the other hand, the compressive strength of concrete at elevated temperatures depends on the type of aggregate, cement to aggregate ratios and the degree of loading among other factors. According to the ACI-318 (2005) the linear limit of concrete is reached at 45% of the compressive strength, so the elastic modulus has the value of the slope of the stress-strain curve up to that value of stress. Equation 3.4 provides the compressive stress and strain of the concrete for any given temperature, and it shows that the compressive strength remains unaffected by the increase in temperature until a temperature of 450°C is reached, where it starts to decay. This is shown in Figure 3.5.

In order to input the stress-strain relationships in ABAQUS to perform the structural analysis, these relationships have to be edited to comply with the ABAQUS approach of treating this type of information. ABAQUS separates the elastic strains from the plastic strains, which add up to the total strains that are used in the curves above. This is shown in Figure 3.6. ABAQUS reads the stresses with their corresponding plastic strains. Therefore, the elastic strain components had to be excluded from the total strains as shown in Equation 3.5.

$$e_p = e_t - s\ / E \tag{3.5}$$

where, e_p is the plastic strains, e_t is the total strains, s is the stress and E is the modulus of elasticity. The modified stress-strain curves are shown in Figure 3.7.

The family of concrete stress-strain curves shown in Figure 3.3 is used for the strength analysis with the following modification. The DRAIN-2DX program, which is the software used for the strength analysis, has a limit to the number of linear segments used to approximate the actual stress-strain curve. This limit is only five linear segments. Therefore, the curves are descretized to five linear segments as demonstrated in Figure 3.8.

Thermal expansion: The thermal expansion coefficient of concrete, a, varies linearly with temperature as shown in Equation 3.6.

$$a = (0.008T + 6)\times 10^{-6} \tag{3.6}$$

3.3 PRESTRESSING STEEL

Since the prestressing steel is only considered in the strength analysis part, only the mechanical properties are considered in this report. The prestressing steel considered has an ultimate stress of f_{pu}= 1860 MPa (270 ksi) and effective stress of f_{pe}= 1221 MPa (177 ksi). Another family of stress-strain curves is derived here for the prestressing steel at various elevated temperatures. These curves are derived according to the Eurocode 2 part 1.2, which provides a set of equations and parameters valid for various types of steels. These equations are listed in Figure 3.9 and the parameters given for prestressing steel strands are shown in Table 3.1. The Eurocode approach divides the strain-strain curves generated into four ranges with a corresponding set of equations. Range I is the range where the curve behaves linear elastically. Range II is the range where the curve behaves in a non-linear manner. Range III is the range where the curve experiences plastic behavior. Range IV is defined for numerical purposes.

The resulting family of stress strain curves is shown in Figure 3.10 and their descretized curves, with the DRAIN-2DX limited five linear segments, in Figure 3.11. The curves have ranges of strains from 0 to 0.02 mm/mm because DRAIN-2DX is programmed so that strains in the model higher than the last strain value provided will have corresponding stresses equal to the last stress value provided. The curves in Figure 3.11

are derived at the temperatures of the given parameters and at other intermediate temperatures chosen for their proximity to the temperatures of some of the prestressing strands at the various fire durations considered. These temperatures are found in the heat transfer analysis part of Chapter 4. To obtain suitable parameters for these intermediate temperatures, a linear interpolation between the nearest parameters is performed. All the parameters are illustrated in Figure 3.12, with the interpolated points shown in symbols larger than the originals.

Since DRAIN-2DX program doesn't account for prestresses in steel, a rational approach was adapted and successfully used by Thompson (2004) to include the prestressing forces in the model. This approach is also adapted in this report. This is done by both modifying the stress-strain diagram of the prestressing steel to model the initial stresses in the strands and applying an equivalent prestressing force to the model at the end nodes equal to the forces provided by the prestressing strands on the concrete beam. This process is illustrated in Figure 3.13.

In an actual double tee in service, the strands are stressed to the point of effective stress, f_{pe} on the stress-strain curve. The remaining part of the curve is the amount of stress that the strands can accumulate if the beam were overloaded to failure. Therefore, a new set of axes ($Stress_2$, $Strain_2$) is used in the fiber model with the intersection point being the origin of the shifted curve. The shifted origin accounts for the initial stresses that are not present in the fiber model. Starting from a stress value of f_{pe}, rather than zero, the strands can accumulate stresses equal to the difference between the ultimate stress, f_{pu} and the effective stress, f_{pe}.

In the double tee beam, the compressive force is a compressive force acting at the centroid of the prestressing steel. This is modeled in the fiber model by applying a force equal to $f_{pe} \cdot A_p$ where A_p is the area of the prestressing steel.

This process needs to be applied to the stress-strain curves corresponding to the prestressing steel at elevated temperatures. However, no information on the effect of the elevated temperatures on the effective stresses to which the origin of the stress-strain diagrams would be shifted to was found in the literature. To overcome this difficulty, the following approach is adapted. Figure 3.14 illustrates two arbitrary stress-strain diagrams of prestressing steel at two different temperatures. One of them has an ultimate stress value, f_{pu1} higher than the effective stress of the prestressing steel at room temperature, f_{pe} and the other has a lower ultimate stress value, f_{pu2} than f_{pe}. The origin of the first curve is shifted to f_{pe} and a prestressing force of $f_{pe} \cdot A_p$ is applied to the end nodes. The second curve is completely disregarded; since the strands are deemed to have already yielded due to the fire load, and a prestressing force of $f_{u2} \cdot A_p$ is applied to the beam. In other words, the strands that experience temperatures causing their ultimate stresses to drop below the effective stress at room temperature are not considered in the analysis but the force they apply to the concrete are.

This approach might not present the true characteristics of the steel accurately enough to result in the real load deflection path the analysis would take, but it does lead to an accurate estimate of the ultimate capacity of the model, which is particularly what this study is interested in. This is verified by results from strain-compatibility calculations for a few samples conducted according to the ACI-216 (1989). The results of shifting the family of prestressing steel stress-strain curves are illustrated in Figure 3.15. Once again, only the curves that are applicable to the shifting process are shown in Figure 3.15b and the other higher temperature curves are disregarded.

Since the loads can only be applied to one node at each end in DRAIN-2DX, the prestressing forces are all shifted to the location of that node, producing a moment from each strand. The forces and moments of all strands are collected and applied to the end node, which is chosen to be at the level of the centroid of the original section at room temperature. Table 3.2 demonstrates the values of the temperature, temperature of the assigned stress-strain curve, unshifted stress in the strand, prestressing force and moment at each strand level, where level 1 is the closest to the web bottom, and the total to be applied at the node for each fire duration considered. The initial stress is either, as explained previously, the effective stress at room temperature (f_{pe}=1221 MPa) or the ultimate stress of the prestressing steel at the given temperatures.

Table 3.1: Eurocode parameters for stress-strain relations for prestressing steel.

Temp (°C)	E(T)/E(20)	Fpr(T)/Fy(20)	Fy(T)/Fy(20)
20	1	1	1
100	0.98	0.68	0.99
200	0.95	0.51	0.87
300	0.88	0.32	0.72
400	0.81	0.13	0.46
500	0.54	0.07	0.22
600	0.41	0.05	0.1
700	0.1	0.03	0.08
800	0.07	0.02	0.05
900	0.03	0.01	0.03
1000	0	0	0

Table 3.2: Summary of the prestressing forces and moment calculations.

Fire duration = 0.5 hr					
Level	T (°C)	Curve T (°C)	Stress (MPa)	P (kN)	M (kN.mm)
1	181	180	1221	482	292532
2	101	100	1221	482	271103
3	87	85	1221	482	249674
4	84	85	1221	241	114122
5	81	85	1221	4821	163957
Σ				2169	1091388
Fire duration = 1.0 hr					
Level	T (°C)	Curve T (°C)	Stress (MPa)	P (kN)	M (kN.mm)
1	407	400	856	338	204988
2	263	260	1221	482	271103
3	218	200	1221	482	249674
4	203	200	1221	241	114122
5	188	180	1221	482	163957
Σ				2025	1003844
Fire duration = 1.5 hr					
Level	T (°C)	Curve T (°C)	Stress (MPa)	P (kN)	M (kN.mm)
1	542	540	320	109	65953
2	405	400	856	338	189972
3	355	340	1146	414	214509
4	334	340	1146	207	98049
5	304	300	1221	482	163957
Σ				1625	771955
Fire duration = 2.0 hr					
Level	T (°C)	Curve T (°C)	Stress (MPa)	P (kN)	M (kN.mm)
1	646	650	167	66	40106
2	507	500	409	162	90855
3	453	440	677	232	120187
4	430	440	677	116	54936
5	398	400	856	338	114891
Σ				966	447573

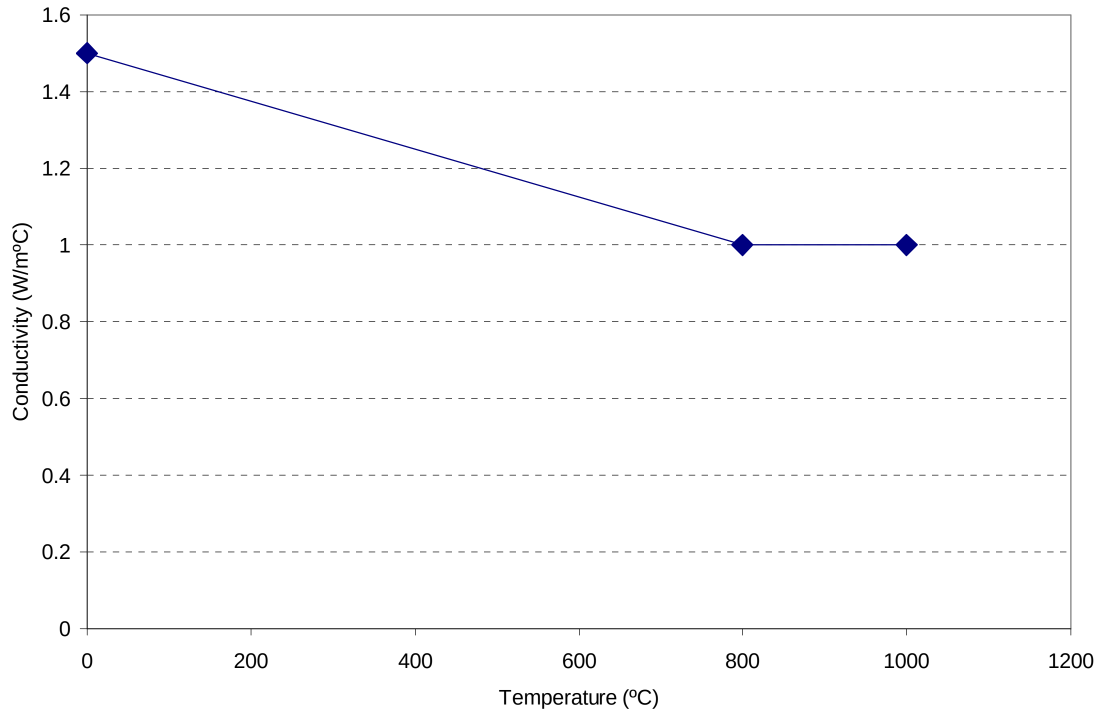

Figure 3.1: The variation of concrete thermal conductivity with temperature (based on Lie 1992).

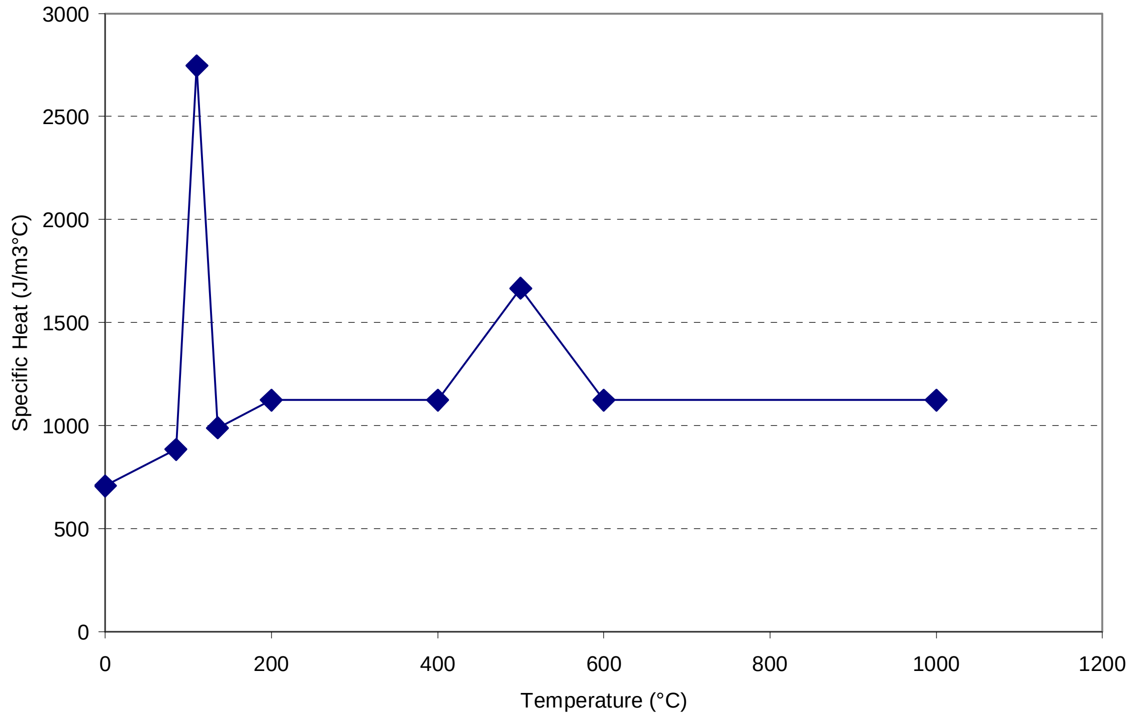

Figure 3.2: The variation of concrete specific heat with temperature (based on Lie 1992).

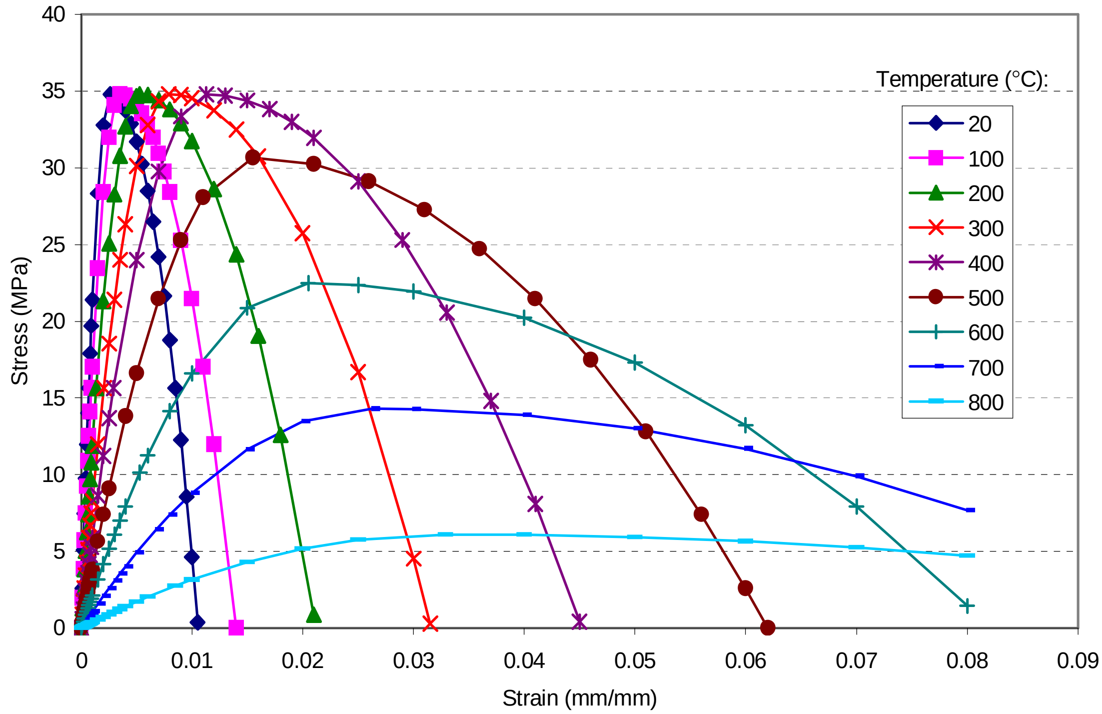

Figure 3.3: Temperature dependent stress-strain curves for concrete (based on Lie 1992).

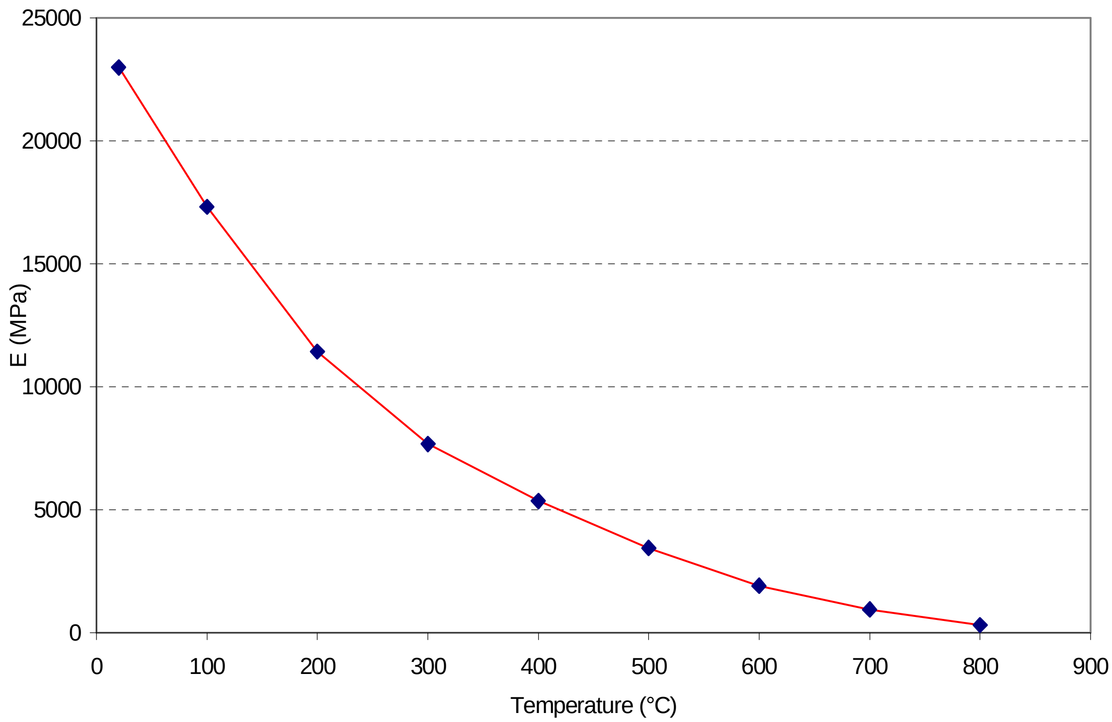

Figure 3.4: Variation of the modulus of elasticity of concrete, E, with temperature for a 34.8 MPa compressive strength concrete.

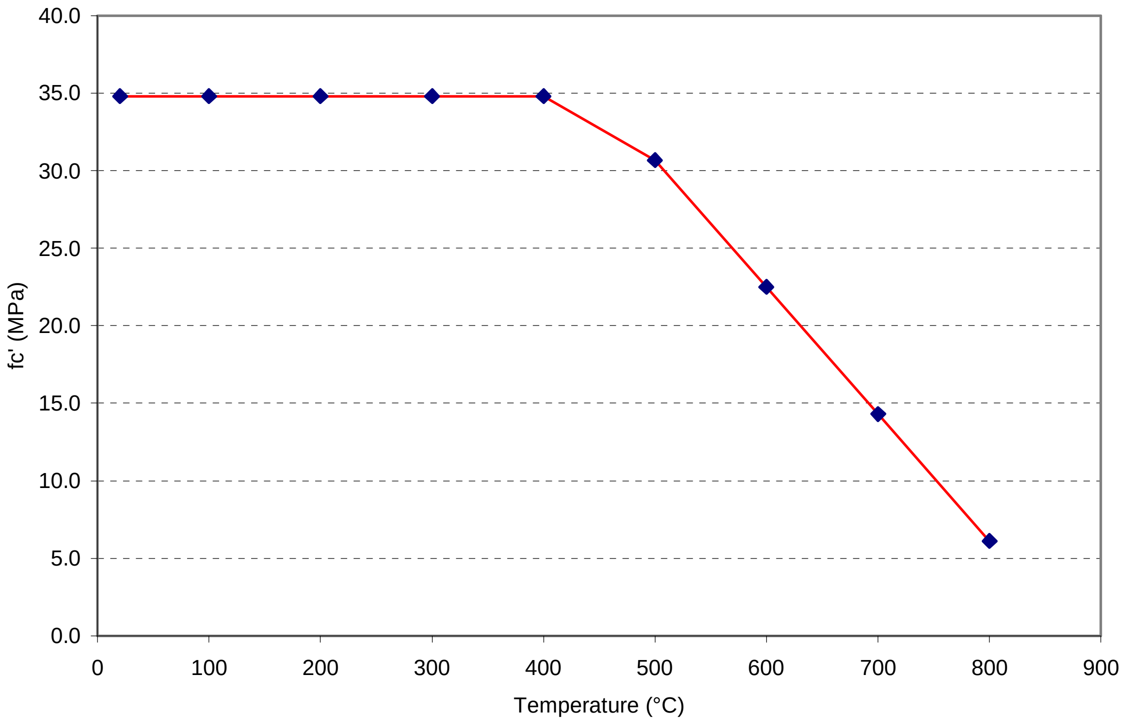

Figure 3.5: Variation of the compressive strength of concrete, f_c', with temperature for a 34.8 MPa compressive strength concrete.

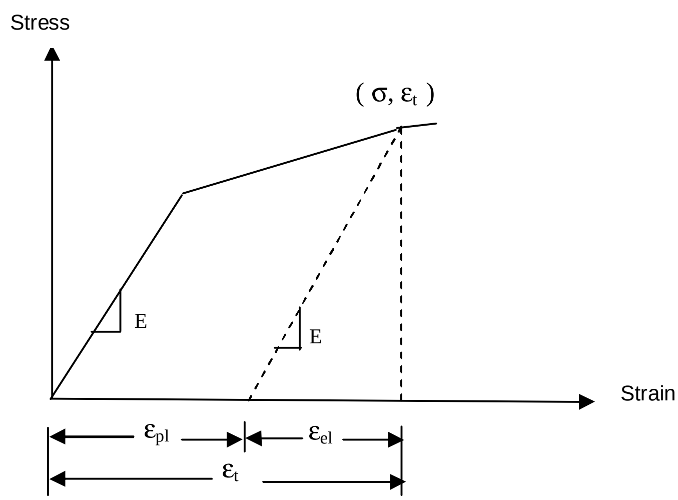

Figure 3.6: A schematic of an arbitrary point of stress-strain with its plastic strain ε_p, elastic strain ε_{el}, and total strain ε_t.

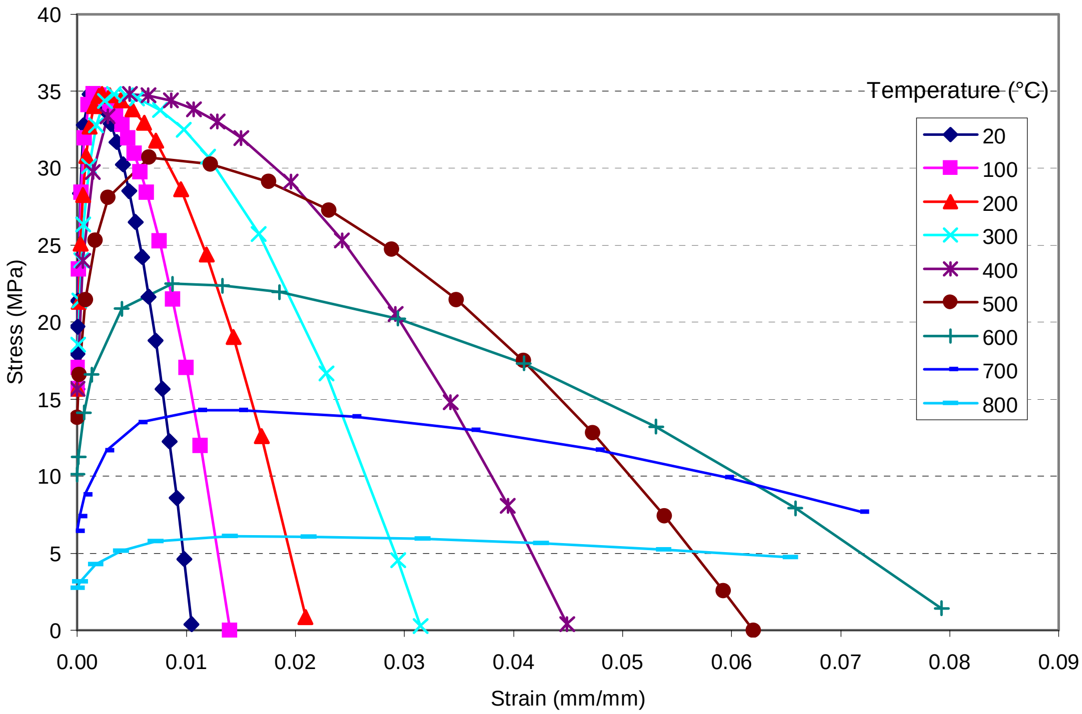

Figure 3.7: Modified stress-strain curves for concrete for ABAQUS.

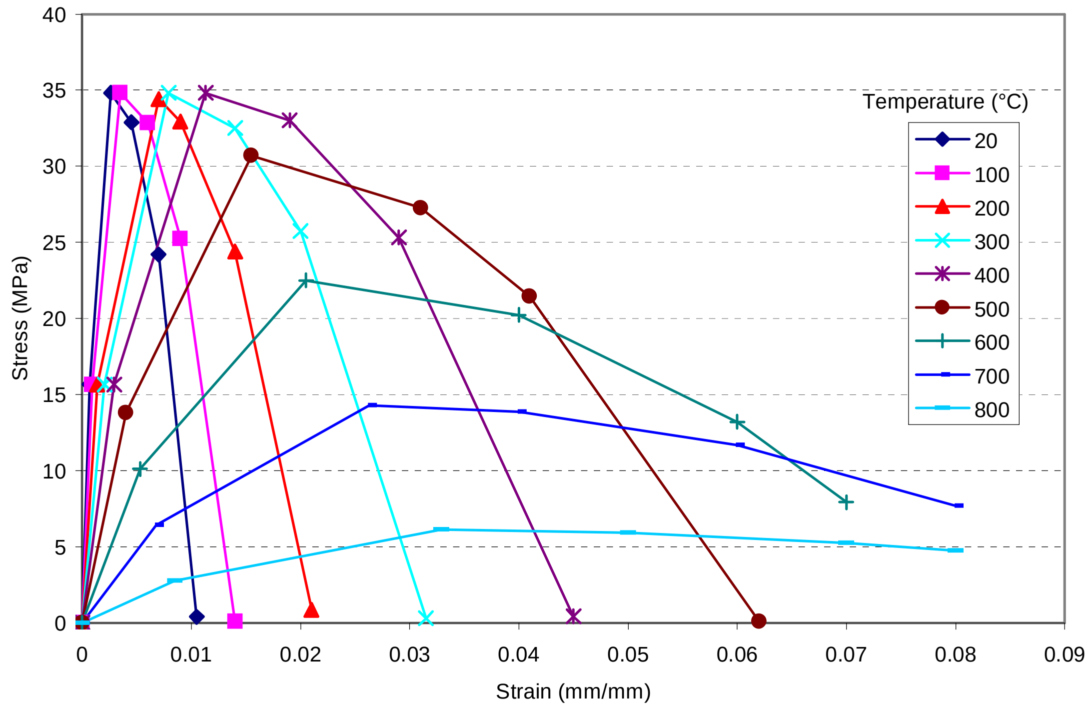

Figure 3.8: Stress-strain curves for concrete for DRAIN-2DX.

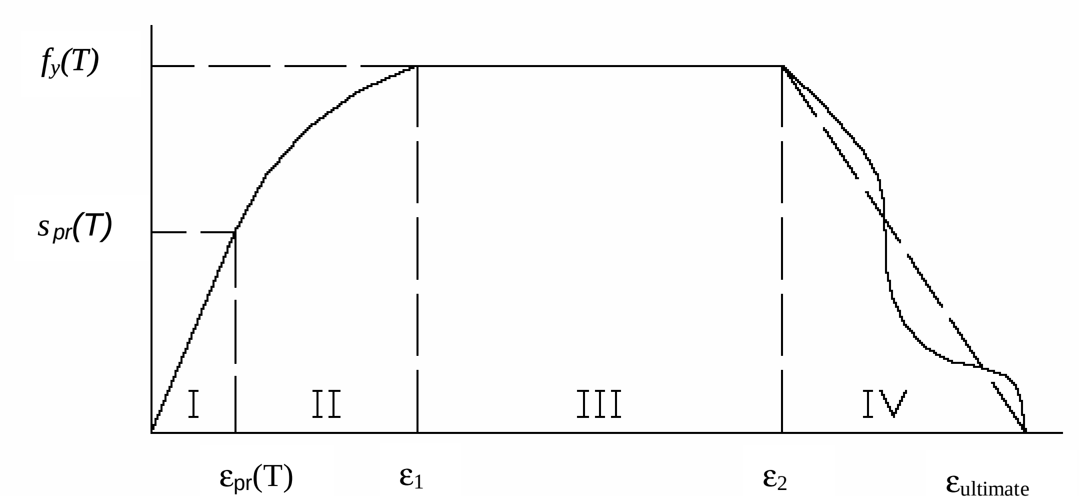

Range I Elastic	$s(T) = E(T)\times e(T)$
Range II Non-Linear	$s(T) = b/2\times\sqrt{a^2-(e_1-e(T))^2} + s_{pr}(T) - c$ $E(T) = (b\times(e_1-e(T)))/(a\times\sqrt{a^2-(e_1-e(T))^2})$ *with* $e_1 = 0.02$ $a^2 = (E(T)\times(e_1-e_{pr}(T))^2 + c\times(e_1-e_{pr}(T))/E(T)$ $b^2 = E(T)\times(e_1-e_{pr}(T))\times c + c^2$ $c = (f_y(T)-s_{pr}(T))^2/(2\times(s_{pr}(T)-f_y(T))+E(T)\times(e_1-e_{pr}(T)))$
Range III Plastic	$s(T) = f_y(T)$ $E(T) = 0$
Range IV	For numerical purposes a descending branch should be adapted. Linear and nonlinear models are permitted.

Figure 3.9: Equations for stress-strain relations for prestressing steel (Eurocode 1996).

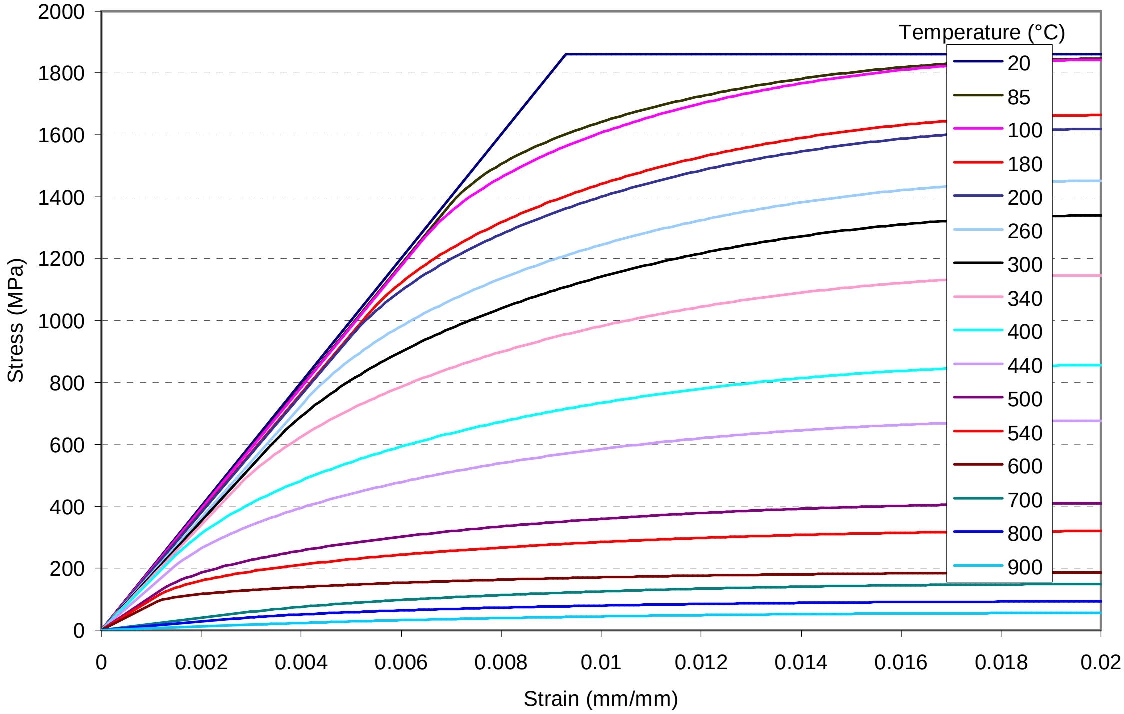

Figure 3.10: Stress-strain curves for prestressing steel computed using Eurocode equations (Figure 3.9).

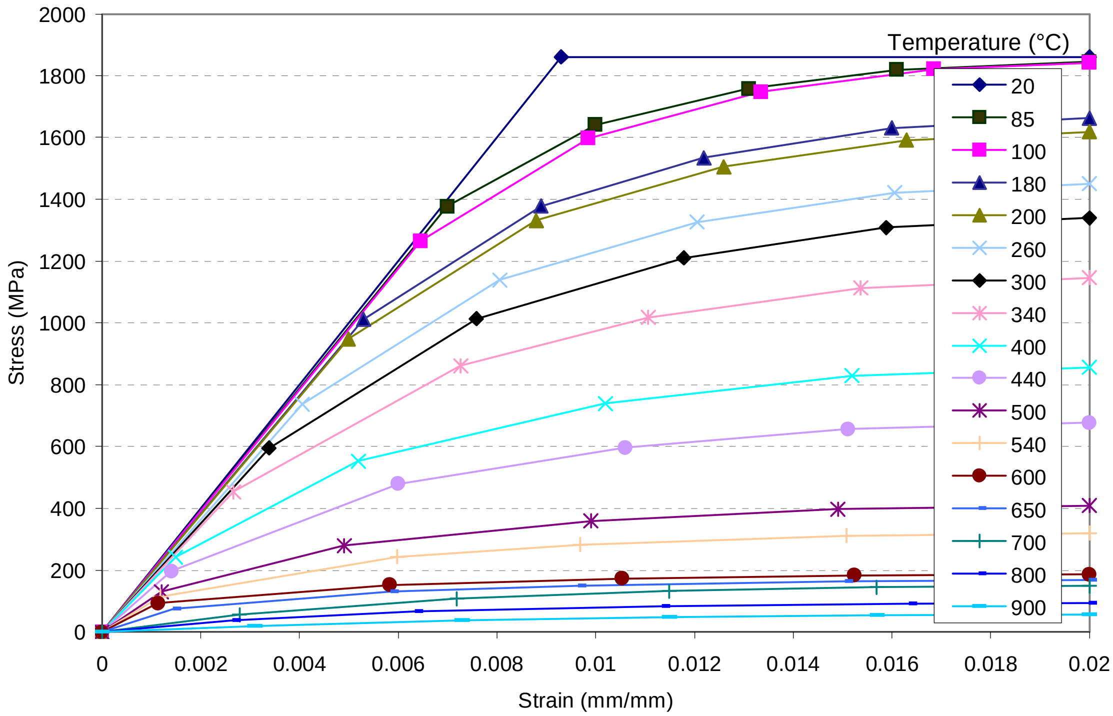

Figure 3.11: Stress-strain curves for prestressing steel for DRAIN-2DX.

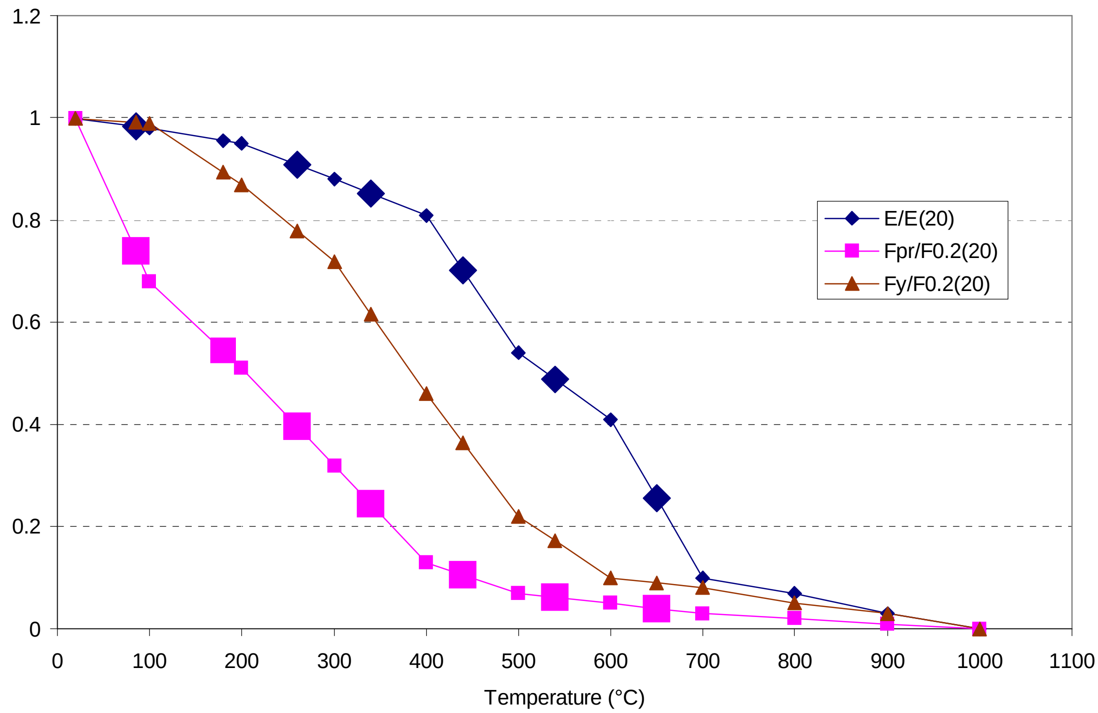

Figure 3.12: Values for the parameters of the stress-strain relationship for prestressing steel.

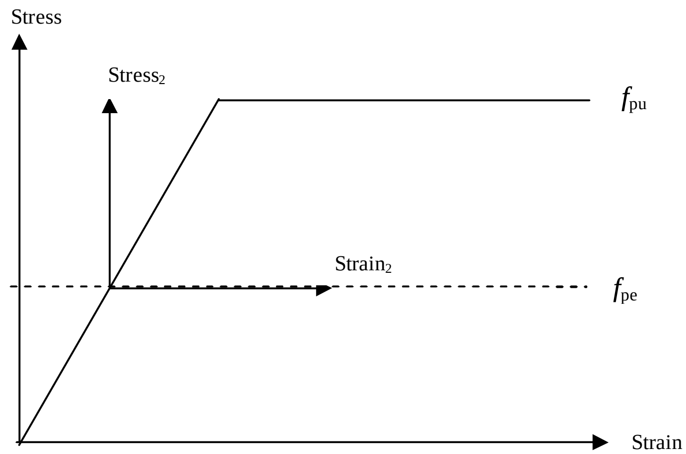

Figure 3.13: Modeling approach for prestressing steel stress-strain curves at room temperature.

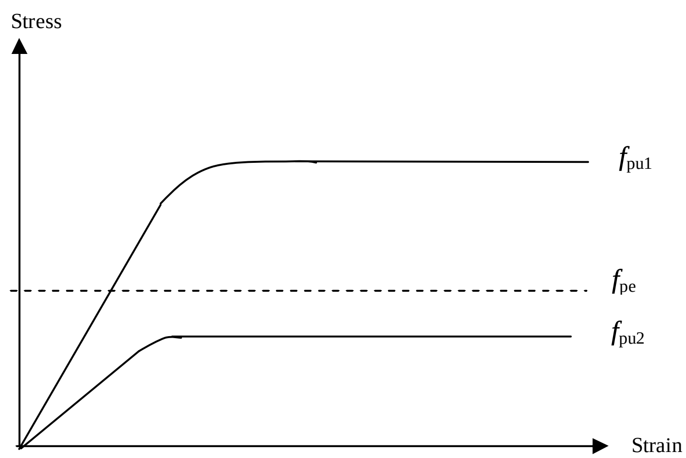

Figure 3.14: Modeling approach for prestressing steel stress-strain curves at elevated temperatures.

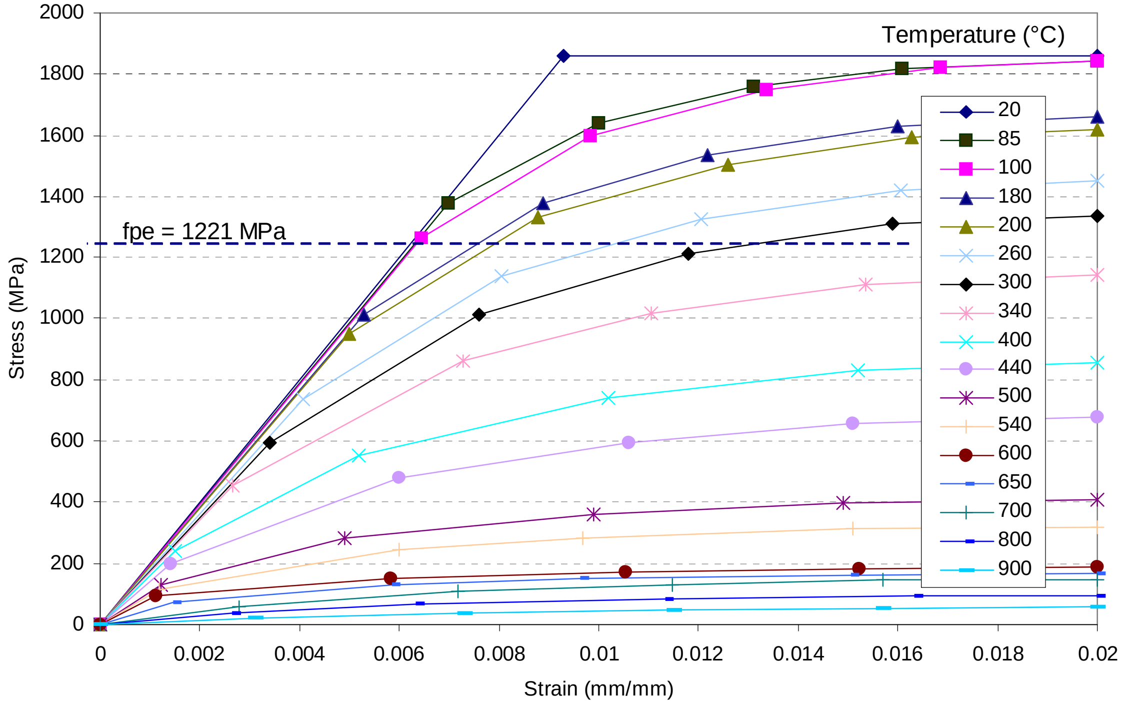

(a)

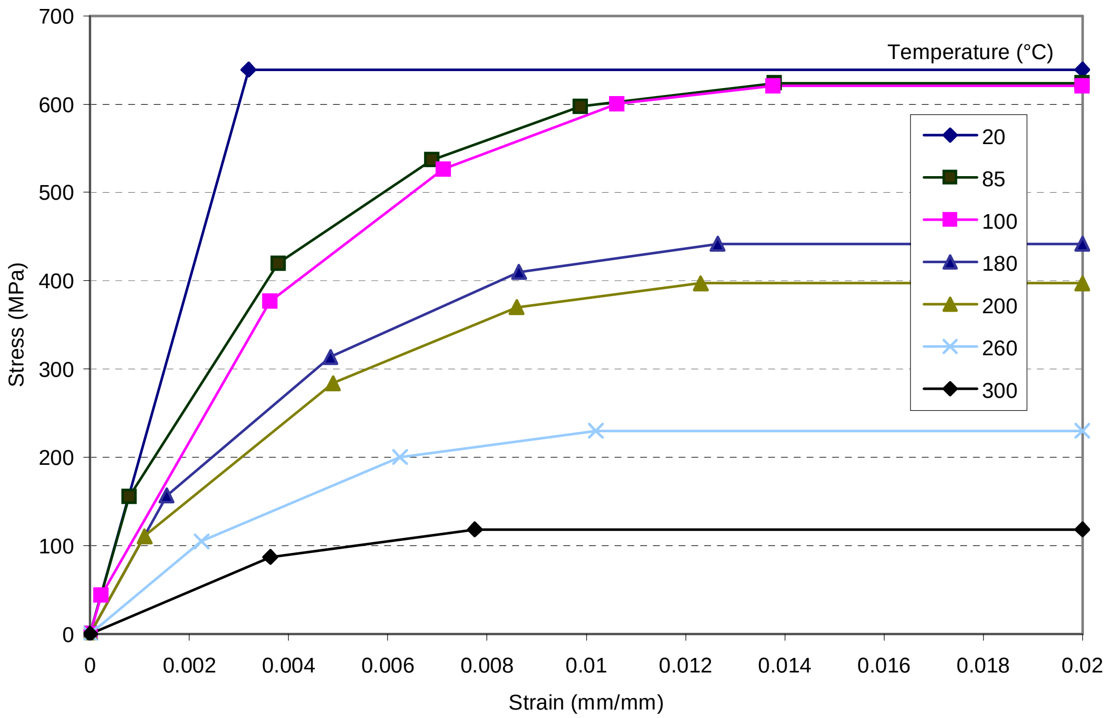

(b)

Figure 3.15: Prestressing steel stress-strain curves: (a) before being shifted; and (b) after being shifted.

CHAPTER 4

IDEALIZED BOUNDARY CONDITIONS

4.1 INTRODUCTION

This chapter presents analyses results of idealized boundary conditions chosen to be the bounding cases for the other realistic boundary conditions, some of which are presented in the following chapters. In these analyses, a single span double tee beam is analyzed having four different prescribed boundary conditions and the strength of the double tee beam at four different fire durations (0.5 hr, 1.0 hr, 1.5 hr, and 2.0 hr) is examined. These analyses are conducted through nonlinear finite element analysis followed by nonlinear fiber analysis. The finite element analysis includes nonlinear heat transfer analysis followed by nonlinear structural analysis.

A simply supported beam is considered as an unrestrained boundary condition case, and three other restrained boundary condition cases present the four idealized boundary conditions studied in this chapter. These idealized boundary condition cases are shown in Figure 4.1. The restrained cases are: full-restraint case, where the entire section of the double tee beam at the supports is restrained, flange-restraint case, where only the flange part of the section of the double tee beam at the supports is restrained and web-restraint, where only the web part of the section of the double tee beam at the supports is restrained. These boundary conditions are described more fully in section 4.3.
These boundary conditions are bounding cases in the sense that the restrained parts of the models are attached to an infinitely stiff element, called the ground in ABAQUS terminology, providing infinite compression restraint to these parts and the unrestrained parts have infinite freedom to translate. In real structures, double tee beams are attached to other members or systems of members possessing finite stiffness, and providing finite restraints.

Section 4.2 presents results of the nonlinear finite element heat transfer analysis. The finite element model of the double tee beam is assigned non-linear thermal material properties and its underside is exposed to a standard fire, modeled by the ASTM-E119 time-temperature cure. The rest of the double tee beam surface is exposed to air at room temperature (20 °C). This heat transfer analysis provides thermal histories for each node of the model.

Section 4.3 presents results of the nonlinear finite element structural analysis. The finite element model of the double tee beam is assigned nonlinear mechanical properties and the thermal histories found in the previous step are used as a thermal load input for this analysis step. This structural analysis provides the resulting restraint forces for the different boundary conditions cases sought.

In Section 4.4, the strength is determined by performing nonlinear fiber analysis of the double tee beam section. The double tee beam section is divided to fibers to accommodate the variation of temperature over the section that is found from the previous finite element heat transfer analysis. Each fiber is assigned stress-strain properties corresponding to the temperature that dominates the area of that fiber. The restraint forces found from the previous finite element structural analyses are applied to the related fiber model. The resulting strength of the section of the double tee beam is then presented and discussed. Section 4.5 summarizes the results presented in this chapter.

4.2 HEAT TRANSFER ANALYSES

Nonlinear finite element heat transfer analyses are conducted on the double tee beam model in order to find the thermal histories at the element nodes at the four different fire durations by using the ABAQUS program. These thermal histories are applied in the finite element structural analyses conducted next in order to find the restraint forces developed in the double tee beam at the four fire durations.

4.2.1 Description of The Model

As noted earlier, a prototype precast prestressed double tee beam typically used in practice in precast parking structures is studied in this research. A cross-section of the prototype double tee beam is shown in Figure 4.2. The prototype is a 15DT34 beam and strand pattern 188-S (18 strands with 0.5 in. diameter) beam provided by the PCI Handbook 6th Edition. The beam has a span of 61 ft, flange depth of 4 in., flange width of 15 ft, web depth of 30 in., web upper width of 9 in. and lower width of 6.5 in. The prestressing strands are placed as shown in Figure 4.2 and they have an ultimate stress of 1860 MPa (270 ksi), and effective prestress of 1221 MPa (177 ksi).

4.2.2 Mesh Convergence Studies

The mesh configuration for the double tee beams is selected based on heat transfer convergence studies and providing an appropriate number of nodes on the sides of the model to accommodate the various cases of mechanical boundary conditions prescribed in the structural analysis steps. Four different meshes, shown in Figure 4.3, are studied at two different fire durations (1.0 hr and 2.0 hr), and their nodal temperatures results are compared with results provided by the PCI Handbook.

The four meshes differ in the number of elements in the web cross-section, and share the same mesh in the flange cross-section and along the span of beam. This convergence study focuses only on the mesh configuration of the web due to the fact that the flange mesh configuration is dictated by the number and location of connectors anticipated to be used in the different cases of structural analysis. Three elements are made over the depth of the flange to make installing the flange connectors at two thirds of the height of the flange possible. Using more than 3 elements over the depth of the flange would make the analysis running time unaffordable. The number of elements along the flange width is chosen to satisfy a reasonable aspect ratio for the element. By using 132 elements along the span of the beam, several different flange connecter patterns can be installed meanwhile keeping common nodes to study and compare the behavior at these location for the different cases. Four different flange connectors cases are considered, where the number of flange connectors are varied along the span: (a) 3 flange connectors; (a) 5 flange connectors; (a) 9 flange connectors; and (a) 17 flange connectors. Figure 4.4 shows the top view of the 3 flange connectors case. The flange connectors in the other three cases are distributed evenly along the span between the flange connectors shown in Figure 4.4.

Figures 4.5 and 4.6 present thermal distribution contours over the cross-section for the two fire durations 1.0 hr and 2.0 hr respectively and for the four different meshes. The PCI handbook contains curves that provide the temperature distribution of stemmed precast concrete members during fire tests at different fire durations. Figures 9.3.7.6 and 9.3.7.7 of the PCI Handbook are shown here in Figure 4.7 and they are used to generate two curves for this model that are compared with the curves generated from results of the other four meshes analyzed. Figure 4.8 compares the results found from the finite element heat transfer analyses and from the PCI Handbook charts. The finite element heat transfer analysis results are extracted at the nodes of the meshes; however the corresponding PCI handbook results are found from the curves pertaining to the given heights. The results provided in the figure show the variation of temperature along the centerline of the stemmed web of the double tee beam from the bottom of the web to the last height presented in the PCI Handbook charts, which is 10 in.

The results shown in Figure 4.8 show that mesh T4 is the most accurate mesh to be used for this project. Being the finest mesh, mesh T4 is also chosen to enhance the efficiency of using first order type elements. In addition, mesh T4 provides closer nodes to the locations of the prestressing steel, which makes the linear interpolation process to find the temperatures at the steel strand locations, where no element nodes exist, more accurate. Therefore, mesh T4 is used throughout this project as the mesh configuration for both the heat transfer and structural analysis steps.

4.2.3 Thermal Histories

Using the model chosen from the convergence tests results, a nonlinear heat transfer analysis is conducted for the model to generate the nodal thermal histories at four different fire durations (0.5 hr, 1.0 hr, 1.5 hr, and 2.0 hr). The nonlinear thermal material properties and the element type (DC3D8) presented in Chapter 3 are used in this analysis step. Figure 4.9 shows the resulting temperature contours over the double tee beam section at the end of each fire duration. These contours are used later to build the fiber analysis model and the thermal histories are also used in the finite element structural analysis as thermal load.

Temperatures of the prestressing steel are extracted from the results of these analyses by linear interpolation between the temperatures of the adjacent nodes. The prestressing steel strands are placed at five levels, and the strands of each level have the same temperature in both webs and at both sides of the centerline of the web since they are at the same distance from the centerline. As shown in Figure 4.2, Level 1 is the closest to the bottom web. Temperatures at these five levels for the four different fire durations are presented in Table 4.1. These temperatures are used later in the strength analysis to assign the appropriate mechanical properties for each strand.

4.3 RESTRAINT FORCES ANALYSES

Nonlinear finite element structural analyses are conducted on the double tee beam models in order to find the restraint forces resulting from various different restraint conditions prescribed at the four different fire durations by using the ABAQUS program. These forces are applied in the strength analyses conducted next to compute the strengths of the double tee beam section at the four fire durations.

4.3.1 Description of the Models

The heat transfer finite element models described in Section 4.2 are modified to perform the structural analyses. It is necessary to use the same mesh used in the heat transfer analyses for the reason that the thermal histories recorded in the heat transfer analysis for each node in the mesh are used in this analysis step as a thermal load input to the same nodes. In other words, the same node configuration used in the heat transfer analysis step has to be kept for use in this analysis step. The nonlinear mechanical material properties and the element type (C3D8I) presented in Chapter 3 are used in this analysis step.

By giving the nonlinear mechanical material properties to all the elements in the model, the analysis in ABAQUS failed to converge to a solution in the flange-restraint case due to numerical difficulties that arose from experiencing excessive strains and severe element distortions at few locations. These locations are at the discontinuities of the boundary conditions, especially at the top of the web for the flange-restraint case. To overcome this problem, several elements in these regions are assigned linear elastic temperature degrading properties in all restraint cases. Thus, only the elastic modulus (temperature dependant), which is presented in Figure 3.4, is assigned to these elements. These elements are shown in Figure 4.10. Had these elements been assigned the nonlinear properties and the analyses managed to converge, the restraint forces would have been expected to decrease due to limiting the force input into the elements due to yielding of the material. Therefore, the results of these analyses are expected to be conservative. The conservativeness of the results are found, as will be shown in Section 4.3.3, to be acceptable since the restraint forces developed in the flange-restraint case are small compared to the simply supported case anyways.

4.3.2 Boundary Conditions

Attention in this report is focused on the impact of the axial thermal deformations of the structural elements on the strength of these elements. Therefore, mechanical boundary conditions are prescribed to provide restraint in the longitudinal direction only and freedom of expansion is granted in the other directions by providing minimum constraints to prevent instabilities and rigid body motions in the model and matrix singularity problems in the analysis.

The double tee beam model is restrained in the vertical direction at four nodes, one at each vertical reaction point, to prevent free body motion of the model. These nodes are chosen on the bottom of the webs near the supports. In order to capture the behavior of practical double tee beams sitting on other structural elements, such as a flange of an inverted tee girder, a kinematic coupling constraint is used between these nodes, known as the reference points (RP1, RP2, RP3, R4), and the faces of the eight surrounding elements as shown in Figure 4.11. In addition, this is done to avoid the concentration of loads at one single node. Large point loads can cause numerical difficulties in finite element analysis. The rest of the model is able to expand freely in the vertical direction. Vertical reactions develop in neither the single span cases nor the multiple span cases. They develop in small values, however, in the double case adjoined by flange connectors case and the flexible supports case. These reactions are found to bee small compared to the opposing reactions developed be the self weight and dead loads acting on the double tee beam.

Four cases of mechanical boundary conditions are considered to restrain the double tee beam in the longitudinal direction. These four cases are: simply supported, full-restraint, where all the nodes on the section of the double tee beam at the support are restrained, flange-restraint, where only the nodes on the flange part of the section of the double tee beam at the support are restrained and web-restraint, where only the nodes on the web part of the section of the double tee beam at the support are restrained.

In the first case (simply supported), only the two reference points (RP3, RP4) are restrained. In the other three cases the restraints prescribed are one-way restraints. In other words, the nodes restrained are allowed to move away from the support and not towards the support, resulting only in compression forces at the support. This is done to provide freedom of rotation at the support and to capture the behavior of double tee beams in real structures were the restraint results from the double tee beam pushing against the adjacent structural components due to thermal expansion. This compression-only property is provided to the support using nonlinear springs having infinite stiffness in the compression direction and negligible stiffness in the tension direction. This is shown in Figure 4.12. These springs are connected between all the nodes located in the region restrained and the ground (an infinitely rigid object). The forces developed in these springs are the restraint forces sought.

4.3.3 Restraint Forces

Among the four cases considered, the first case (simply supported) develops no restraint forces. For the other three cases, the restraint forces are extracted as follows: The forces in the springs are summed at each horizontal row of nodes in the mesh, forming a group of resultants, F_i’s, one at each level of nodes across the depth of the double tee beam and along the vertical centerline of the cross section. Moments of these resultants with respect to the top of the cross-section are summed and divided by the total, R, of these sums to find the location of the total resultant of the restraint forces as shown in Equation 4.1.

$$
\begin{aligned}
R &= \sum F_i \\
\overline{X} &= \frac{\sum\left(F_i \cdot \overline{x}_i\right)}{R} \\
e &= \overline{y} - \overline{X} \\
M &= R \cdot e
\end{aligned}
\qquad (4.1)
$$

The total force is then referenced to the centroid of the uncracked gross non-heated section generating a moment equal to (R·e), where the eccentricity, e, is the distance between the location of R and the centroid as shown in Figure 4.13.

Since the model is symmetric, the forces in the springs developing on each longitudinal side of the double tee beams are the same. Therefore the forces in the springs on one longitudinal side are found and doubled, resulting in the axial restraint forces and moments that are tabulated in Table 4.2 and they are used next in the strength analysis step to compute the strength of the double tee beam for each case.

It is clear from Table 4.2 that the direction of the restraint moment is consistent with the restraint condition. The flange-restraint case experiences positive restraint moments throughout the fire duration and the web-restraint case experiences negative restraint moments. The full-restraint case, however, experiences negative restraint moment during the early stages of the fire and then the moment reverses. In other words, the beam starts behaving as being restrained from the web and then continues to behave as being restrained from the flange. This is attributed to the effect of the material softening due to the high temperatures towards the bottom of the beam causing the location of the resultant to move vertically upwards.

4.4 STRENGTH ANALYSES

In this section, the results from the previous steps are used to find the section strength of the double tee beam at the four different fire durations and for the different boundary conditions considered by using nonlinear fiber analyses with the DRAIN-2DX program by Prakash, Powell and Campbell (1993). Unlike the previous finite element analyses, the prestressing steel is considered in these analyses. The outcome of these analyses is the strength of the double tee beam subjected to different restraint conditions at different fire durations. This provides the insight needed to understand the effect of different restraint conditions on precast concrete members subject to fire. The restraint cases considered here are the idealized bounding cases for the other realistic cases that are to be studied in the next chapters.

4.4.1 Description of the Models

The fiber analysis model used in this model is composed of one short fiber element (20mm length). This element is fixed at one end and free at the other end. The fiber model used contains one segment only. The behavior of this element (segment) is monitored at the center of the element, which is called the slice. The slice, and hence the element, is made up of a number of fibers.

The fibers are defined by their areas, material properties and distance to a selected datum. The datum is chosen to be the centroid of the original unheated cross section. This is because DRAIN-2DX applies the axial loads prescribed on the level of that datum, and the centroid of the original section is where the restraint forces are arbitrarily chosen to apply. Each fiber is assigned a different stress-strain relationship with either concrete or steel material properties. The material properties for both the concrete and the reinforcing steel were explained in details in Chapter 3. The concrete fibers are built by discretizing the thermal distribution contours resulting from the previous finite element heat transfer analyses presented in Figure 4.8. These contours are specially assigned a uniform scale from 50 °C to 850 °C with 100 °C intervals, so each grayscale shade presents a range of temperature with an average to be a multiple of 100. Thus, each grayscale shade is assigned one of the stress-strain curves that are related to the temperatures in the multiples of 100 °C. Therefore the fibers are disctretized so that each fiber is assigned the grayscale shade that dominates its area, and hence assigned the corresponding stress-strain relation. For example, the contour grayscale shade presenting the range between 750 °C and 850 °C has the average of 800 °C and the fibers that are dominated by this contour grayscale shade are assigned the stress-strain relation of concrete at temperature of 800 °C. The highest temperature considered is 800 °C and any fibers with higher than that are still assigned the 800 °C relations. Any fibers with lower than 50 °C are assigned room temperature properties (20°C).

The number of fibers in the models ranges from 200 to 250 fibers. The fineness of the descretization provides greater accuracy in the analysis results. Figures 4.14 to 4.17 show one half of the double tee beam sections with their discretized fibers at the end of each fire duration. Although, due to the symmetry of the cross section, the two stems of the double tee beam have the same fiber configuration shown in the figures, only one half is shown to provide closer details.

The steel fibers are assigned the properties corresponding to the temperatures closest to their temperatures that are found by interpolating between the nodal temperatures in the heat transfer analysis step. Once the model is built for each fire duration, it is run for each boundary condition case considered. A model is also run to find the strength of the double tee beam at room temperature. The loads are applied to the model in the following sequence: prestressing forces (Table 3.2), restraint forces (Table 4.2), and finally curvature is applied until failure is achieved. For the simply supported case, however, there are no restraint forces in the previously mentioned loading sequence.

4.4.2 Strength Analyses Results

Figure 4.18 presents a bar chart containing the summary of all the results achieved in the fiber analyses. In light of the results presented in Figures 4.18, the strength of the double tee beam varies significantly with the type of boundary conditions prescribed and subjected to a given duration of standard fire. It is evident from the figure that the strength is significantly less in the flange-restraint case, and even less in the simply supported case than the web-restraint case and the full-restraint case. Figure 4.19 provides normalized values of the analyses results in terms of the self-weight midspan moment of the simply supported double tee beam (i.e. M = 778 kN.m). Values in the chart higher than unity present the case where the double tee beam is expected to withstand its own self weight at the particular fire duration. Consequently, the simply supported double tee beam is expected to fail under its self weight if exposed to two hours of fire. Figure 4.20 provides a series of curves presenting the results of the fiber analysis that are previously explained in Figure 4.18. This figure shows that the strength of the double tee beam in the web-restraint case is slightly higher than in the full-restraint case. This is attributed to the fact that the flange contributes to the restraint in the full-restraint case, which tends to decrease the strength, and doesn't in the web-restraint case.

4.5 SUMMARY

This chapter presents analyses results of idealized boundary conditions chosen to be the bounding cases for the other realistic boundary conditions, some of which are presented in the following chapters. A simply supported beam is considered as an unrestrained boundary condition case, and three other restrained boundary condition cases present the four idealized boundary conditions studied in this chapter. The restrained cases are: full-restraint case, where the entire section of the double tee beam at the supports is restrained, flange-restraint case, where only the flange part of the section of the double tee beam at the supports is restrained and web-restraint, where only the web part of the section of the double tee beam at the supports is restrained. In all cases, restraint is provided by compression only reactions to resist axial thermal expansion.

The direction of the restraint moment is found to be consistent with the restraint condition in all restraint cases. The flange restraint case experiences positive restraint moments throughout the fire duration and the web restraint case experiences negative restraint moments. The full restraint case, however, experiences negative restraint moment during the early stages of the fire and then the moment reverses. This is attributed to the effect of the material softening due to the high temperatures towards the bottom of the beam causing the location of the resultant to move vertically upwards.

The strength of the double tee beam varies significantly with the type of boundary conditions prescribed and subjected to a given duration of standard fire. The strength is significantly less in the flange-restraint case, and even less in the simply supported case than the web-restraint case and the full-restraint case. It is found that the simply supported double tee beam is expected to fail under its self weight if exposed to two hours of fire.

Table 4.1: Temperature at the levels of the prestressing steel strand levels.

Level	Temperature at fire durations (°C)			
	0.5 hr	1.0 hr	1.5 hr	2.0 hr
1	181	408	542	646
2	101	263	406	507
3	88	218	355	453
4	85	203	334	430
5	81	188	304	398

Table 4.2: Restraint forces results for the ideal boundary conditions.

	0.5 hr	1.0 hr	1.5 hrs	2.0 hrs
Full-Restraint	8597 KN 294 KN.m	10363 KN 6 KN.m	170 KN.m 10786 KN	282 KN.m 10532 KN
Flange-Restraint	712 KN.m 6116 KN	963 KN.m 7815 KN	1040 KN.m 8369 KN	1042 KN.m 8365 KN
Web-Restraint	7479 KN 486 KN.m	8897 KN 265 KN.m	9267 KN 100 KN.m	9073 KN 21 KN.m

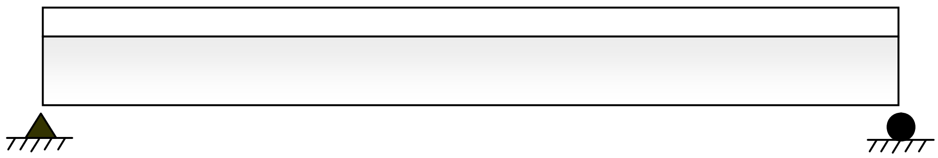

(a)

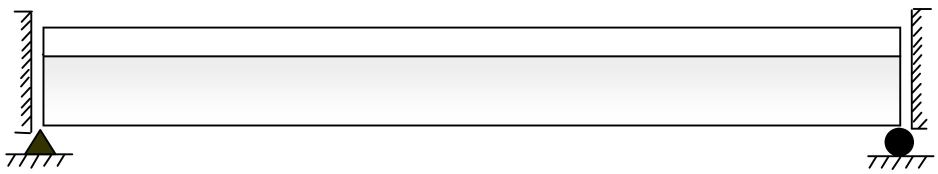

(b)

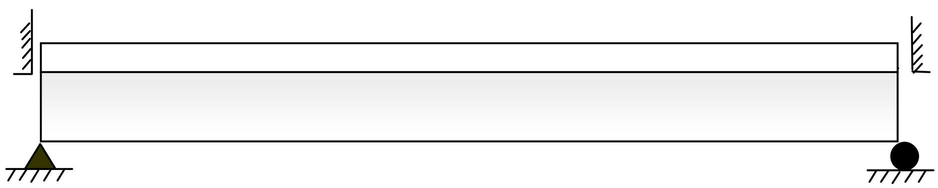

(c)

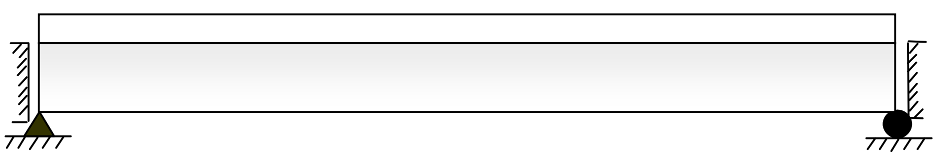

(d)

Figure 4.1: Boundary condition cases: (a) simply supported; (b) full-restraint; (c) flange-restraint; and (d) web-restraint.

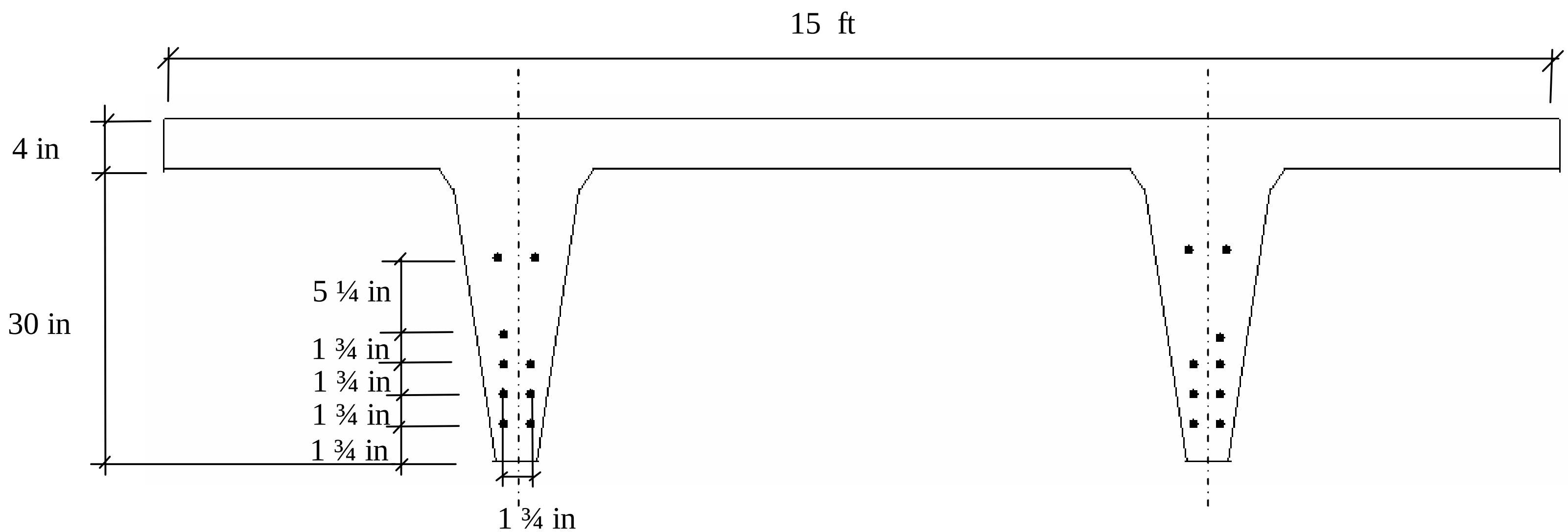

Figure 4.2: Prototype double tee beam used for this research (not to scale).

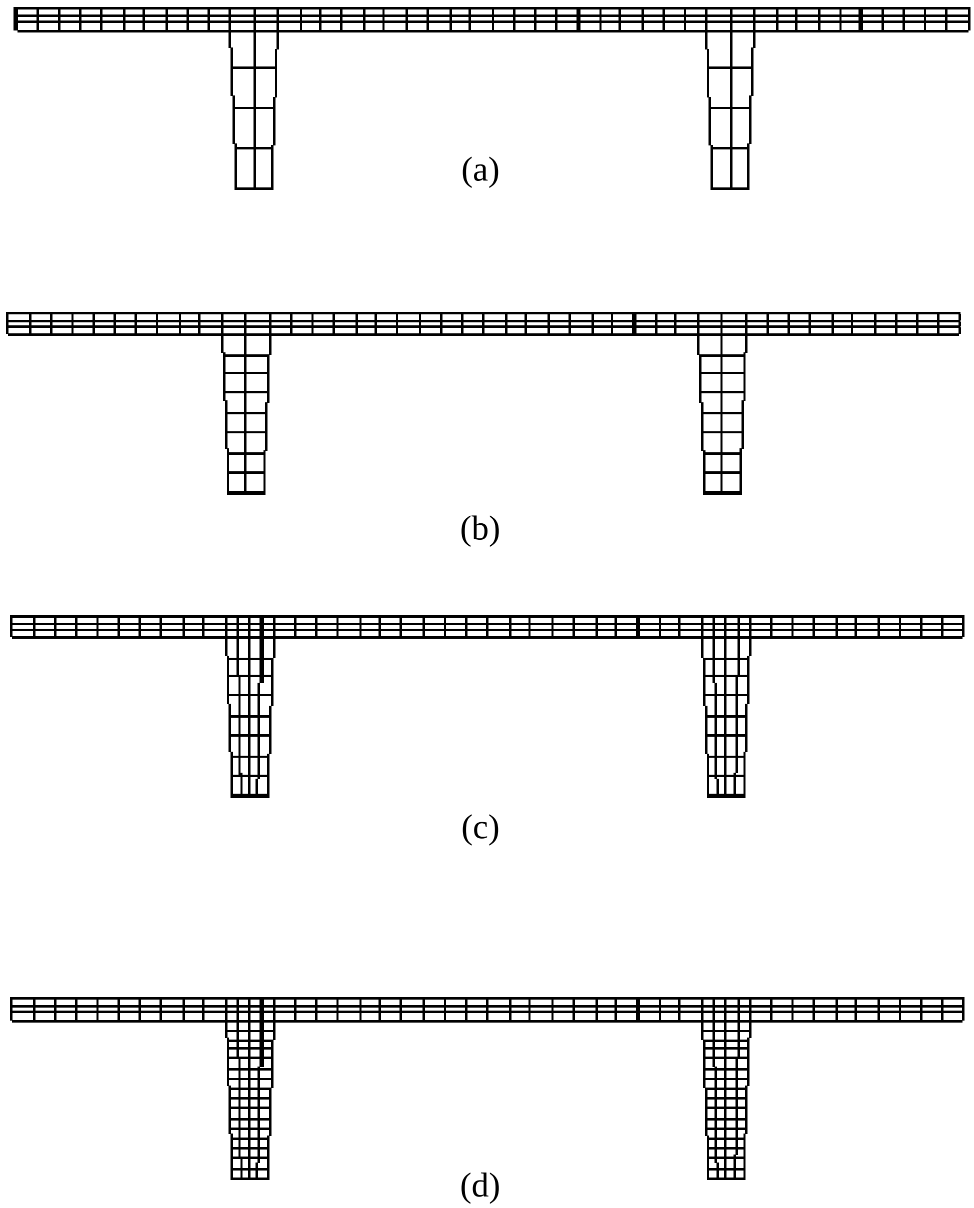

Figure 4.3: Mesh configurations used in the convergence study: (a) mesh 1; (b) mesh 2; (c) mesh 3; and (d) mesh 4.

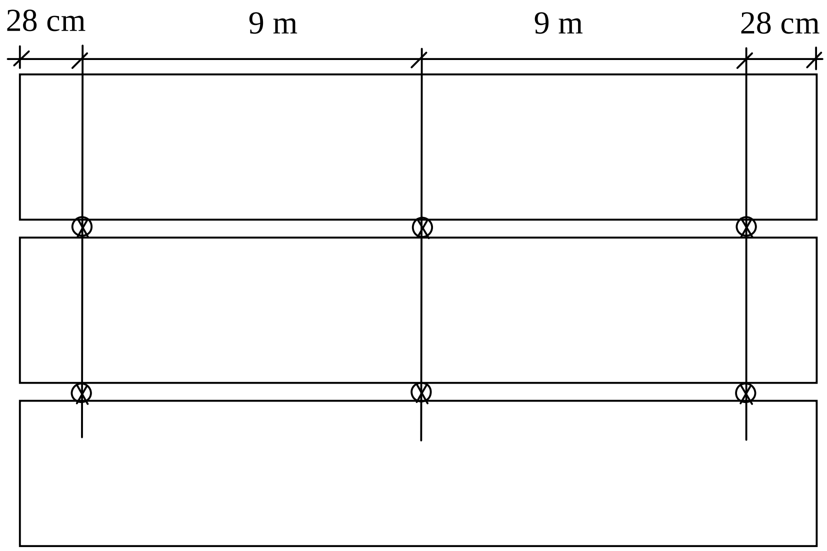

Figure 4.4: Top view of the 3 flange connectors case.

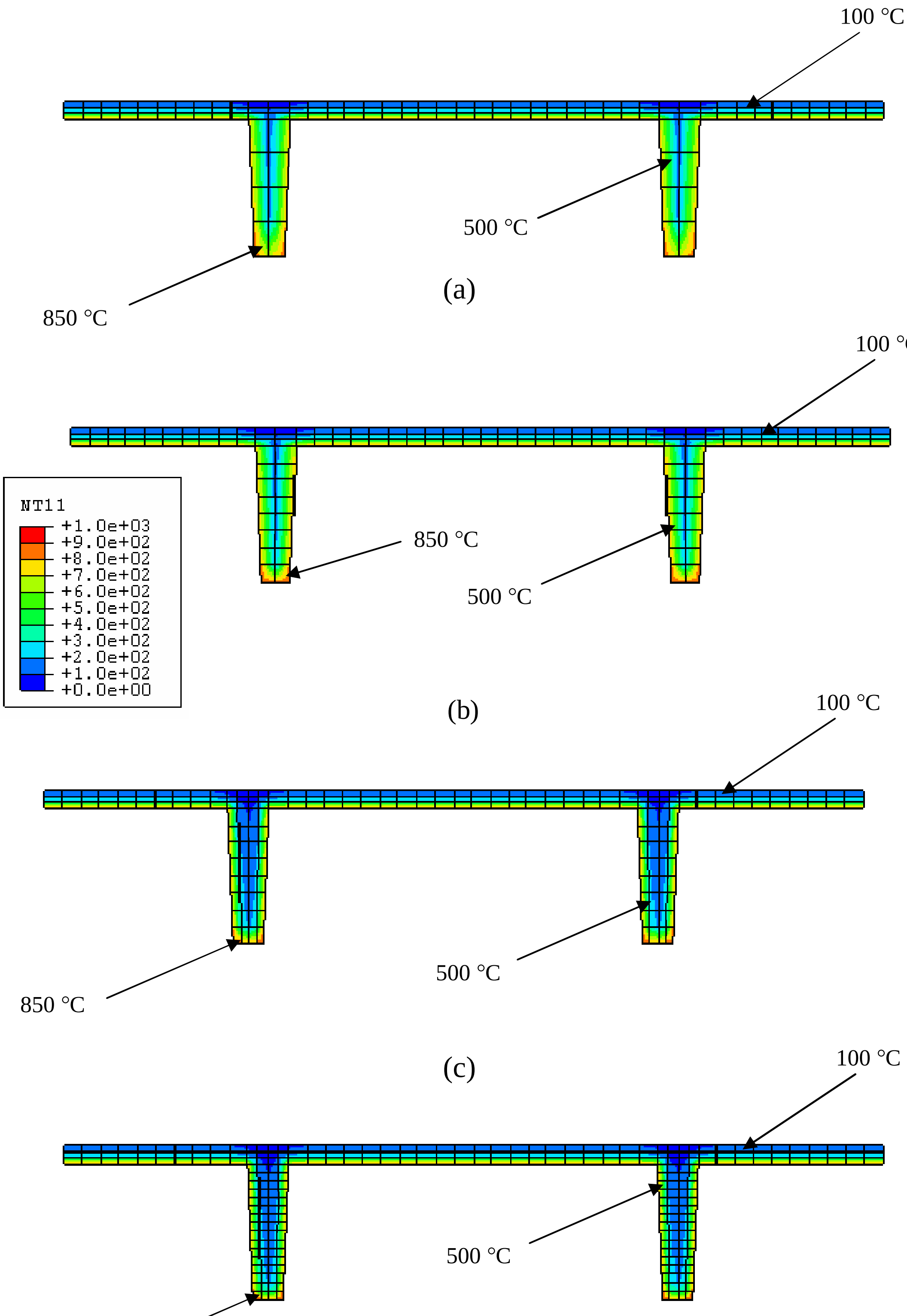

Figure 4.5: Temperature distribution contours at 1.0 hr fire duration for: (a) mesh T1; (b) mesh T2; (c) mesh T3; and (d) mesh T4.

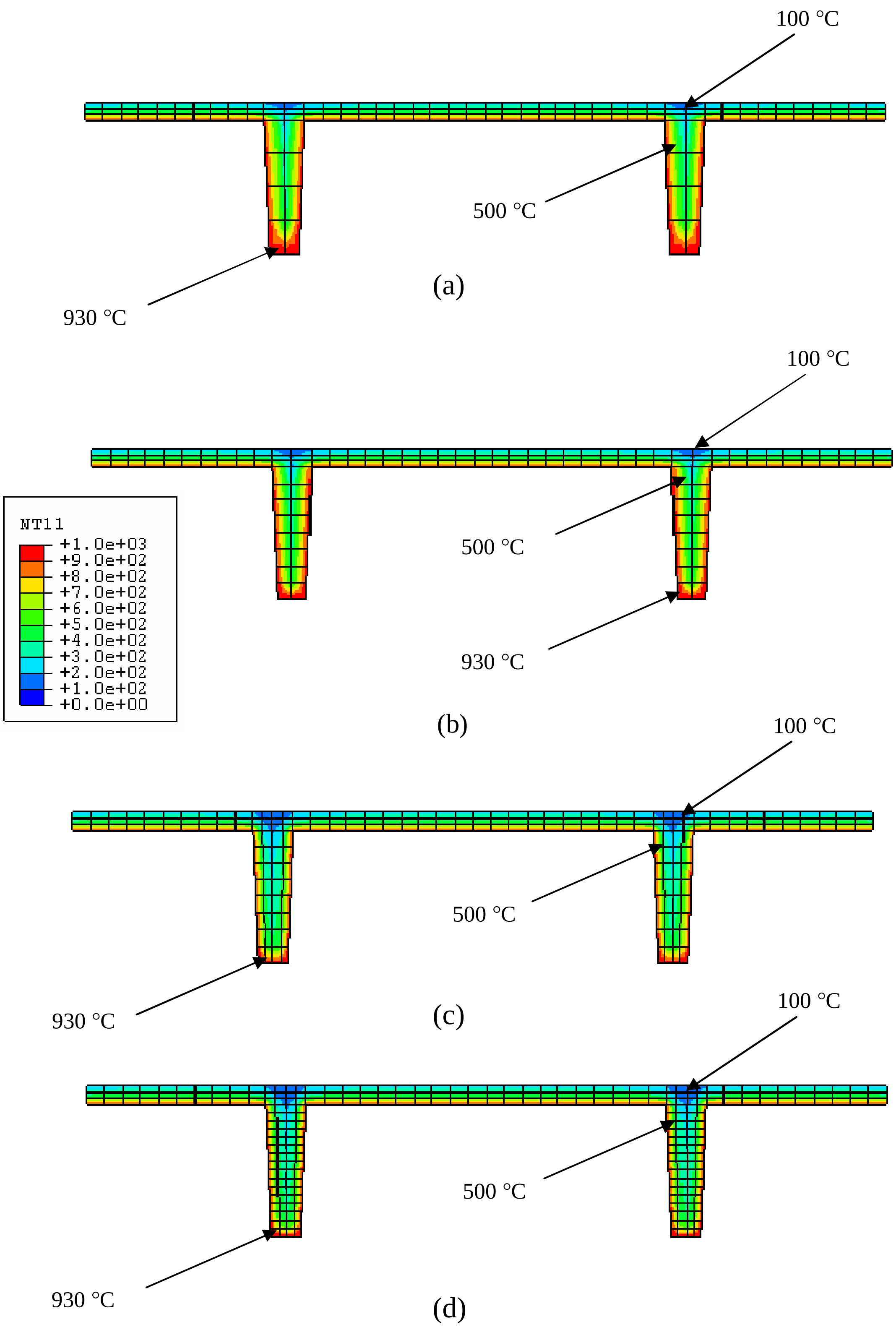

Figure 4.6: Temperature distribution contours at 2.0 hr fire duration for: (a) mesh T1; (b) mesh T2; (c) mesh T3; and (d) mesh T4.

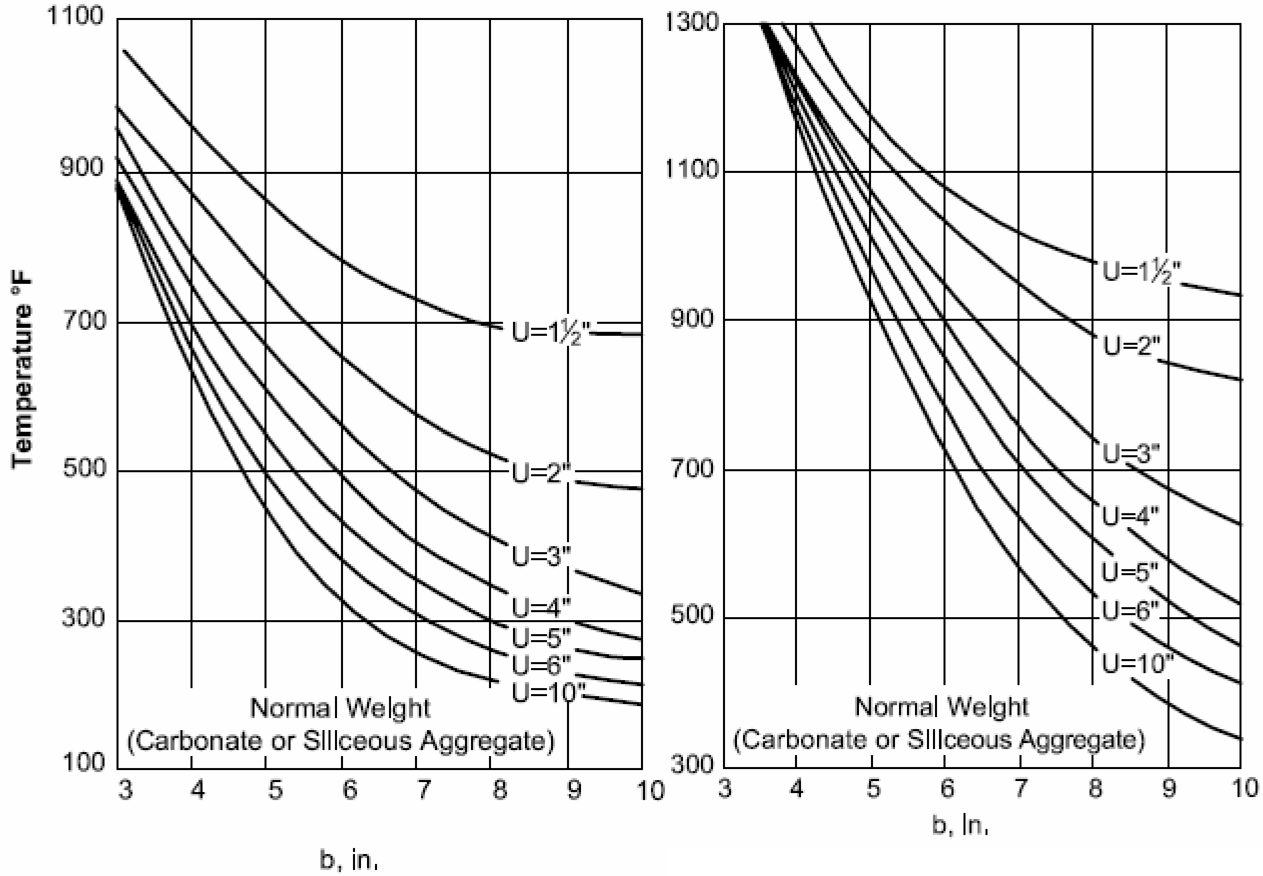

(a) (b)

Figure 4.7: PCI Handbook Figures: (a) 9.3.7.6; and (b) 9.3.7.7 showing thermal distribution of stemmed precast elements at 1.0 hr and 2.0 hr respectively.

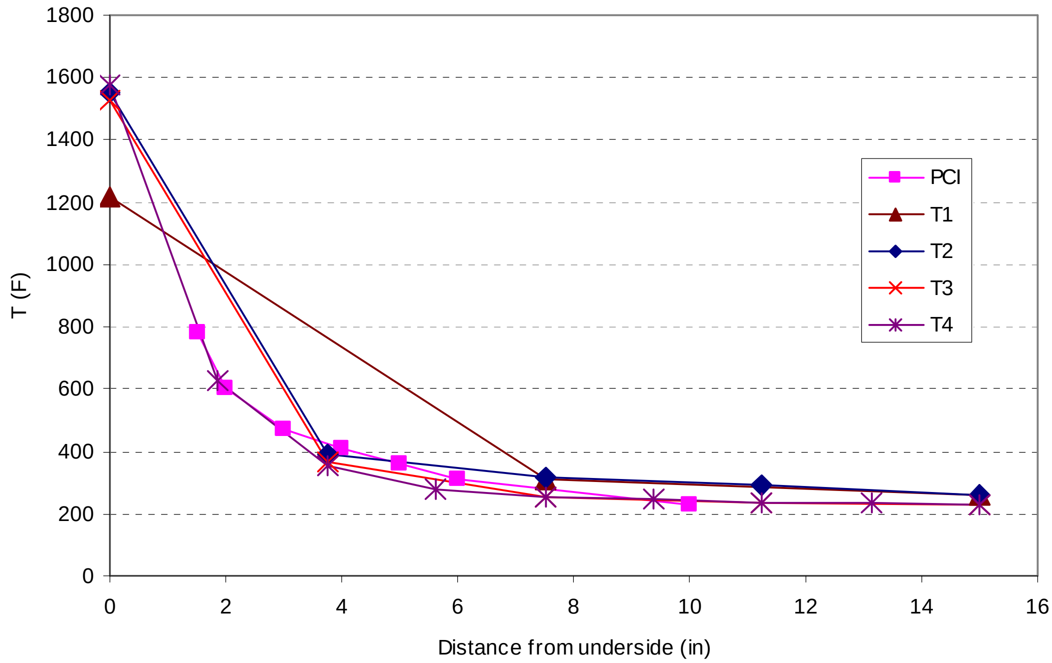

(a)

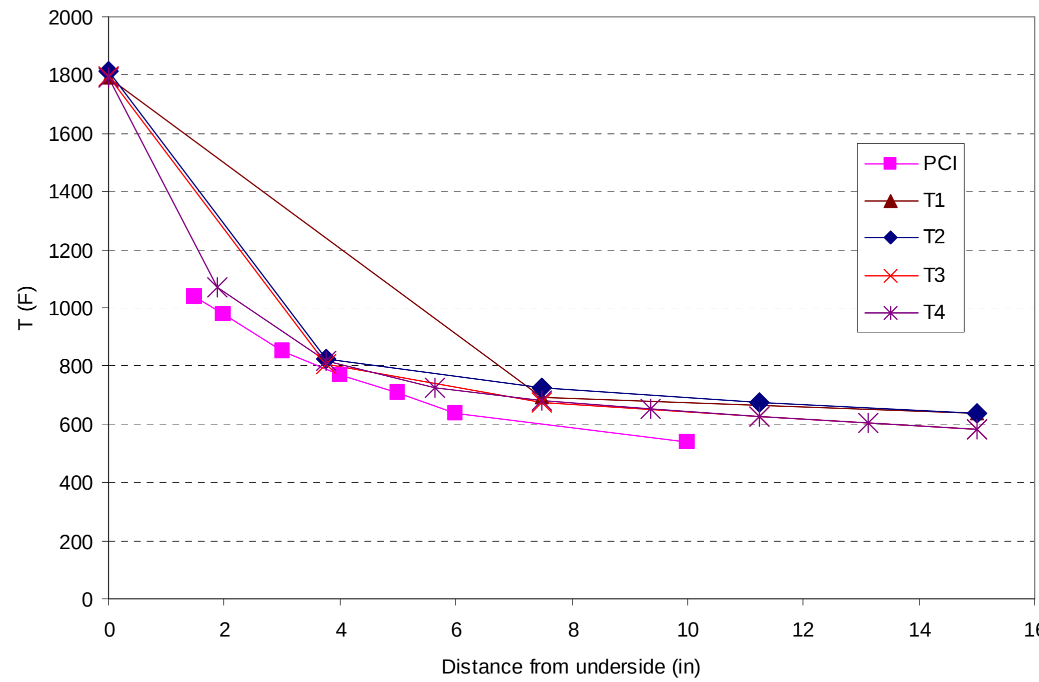

(b)

Figure 4.8: Results of the convergence studies at: (a) 1.0 hr; and (b) 2.0 hr.

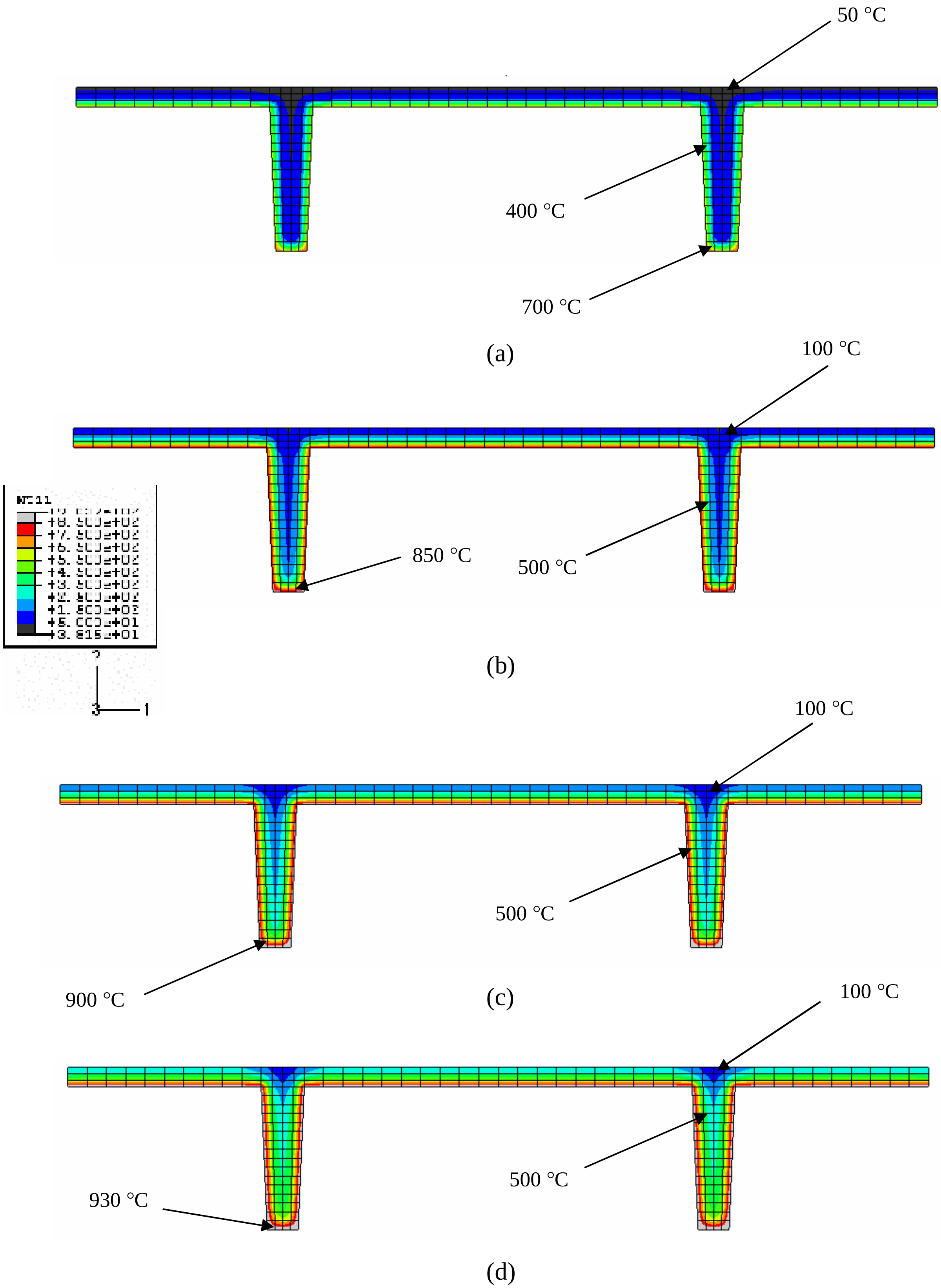

Figure 4.9: Temperature distribution contours over the cross-section of the double tee beam for fire duration of: (a) 0.5 hr; (b) 1.0 hr; (c) 1.5 hr; and (d) 2.0 hr.

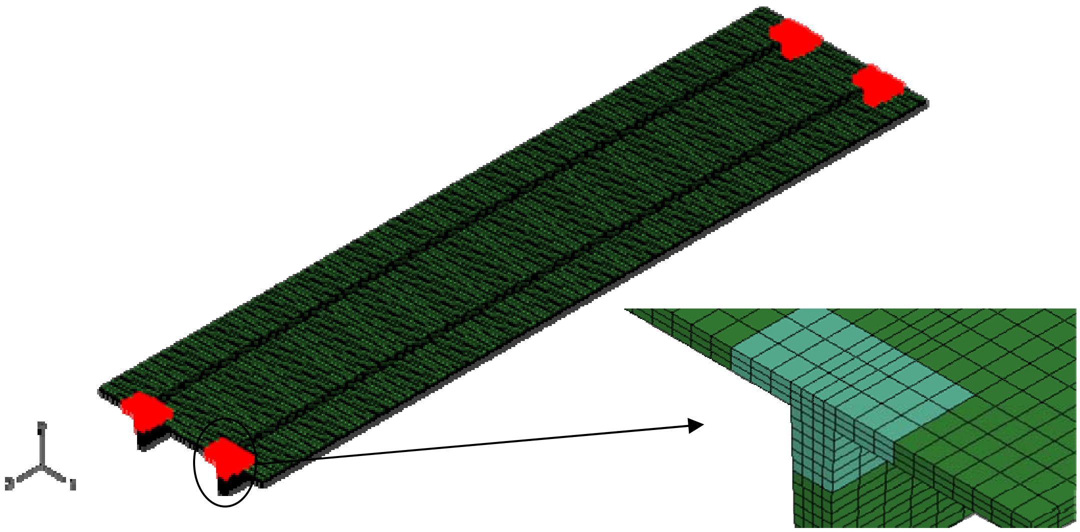

Figure 4.10: The elements assigned linear elastic properties in the restraint force analyses.

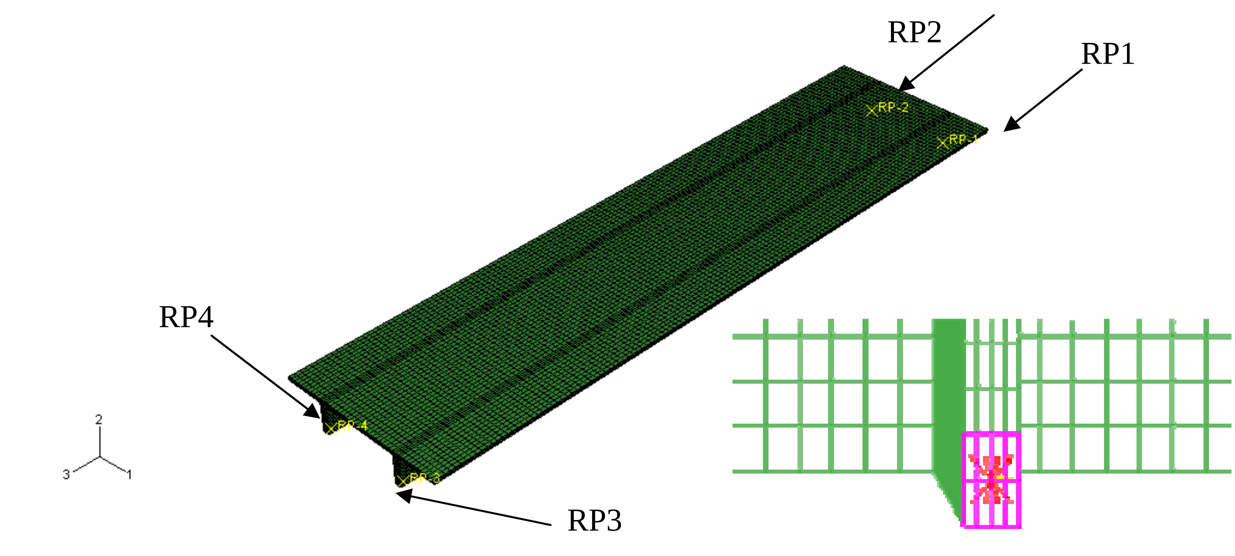

(a) (b)

Figure 4.11: Boundary conditions in structural analyses: (a) isometric view showing the locations of the four reference points (RP1, RP2, RP3, RP4); and (b) bottom view of a web showing the kinematic coupling constraint area.

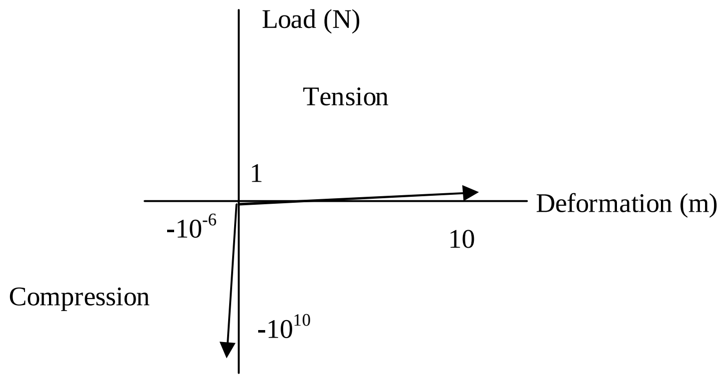

Figure 4.12: Stiffness of the compression only nonlinear springs used for axial restraint at the supports.

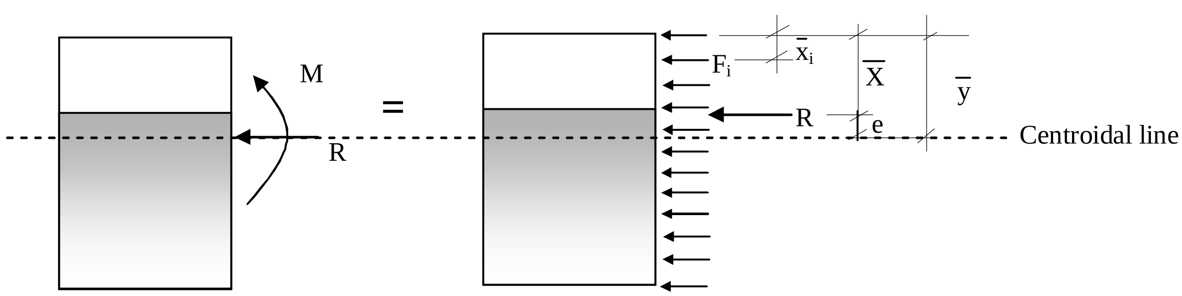

Figure 4.13: Restraint forces and their equivalent resultant.

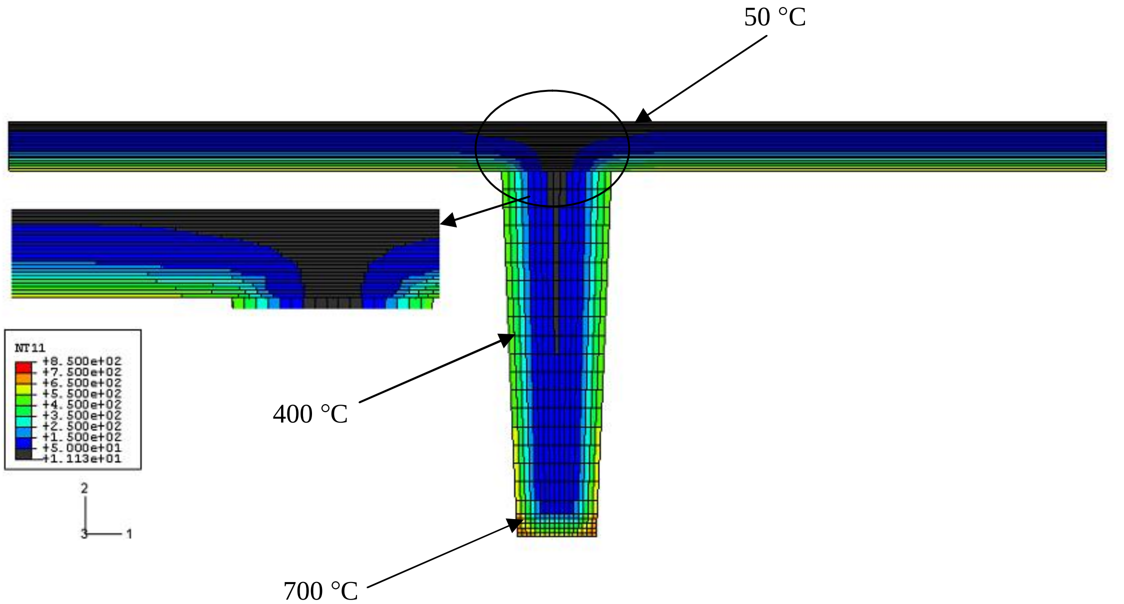

Figure 4.14: Cross-section of one half of the double tee beam with the DRAIN-2DX fibers at fire duration of 0.5 hr.

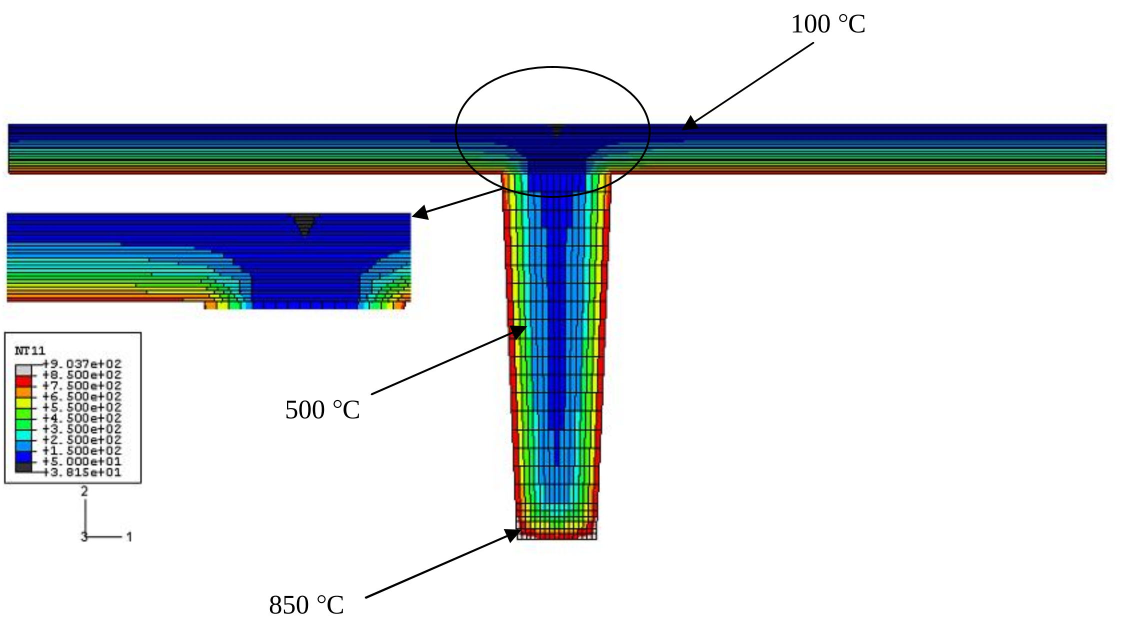

Figure 4.15: Cross-section of one half of the double tee beam with the DRAIN-2DX fibers at fire duration of 1.0 hr.

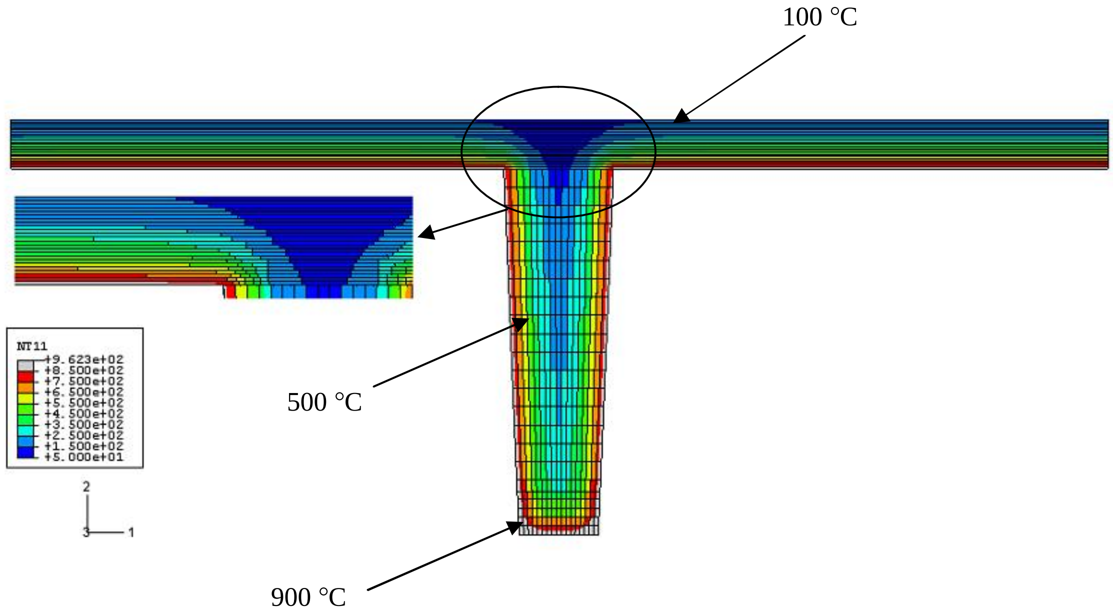

Figure 4.16: Cross-section of one half of the double tee beam with the DRAIN-2DX fibers at fire duration of 1.5 hr.

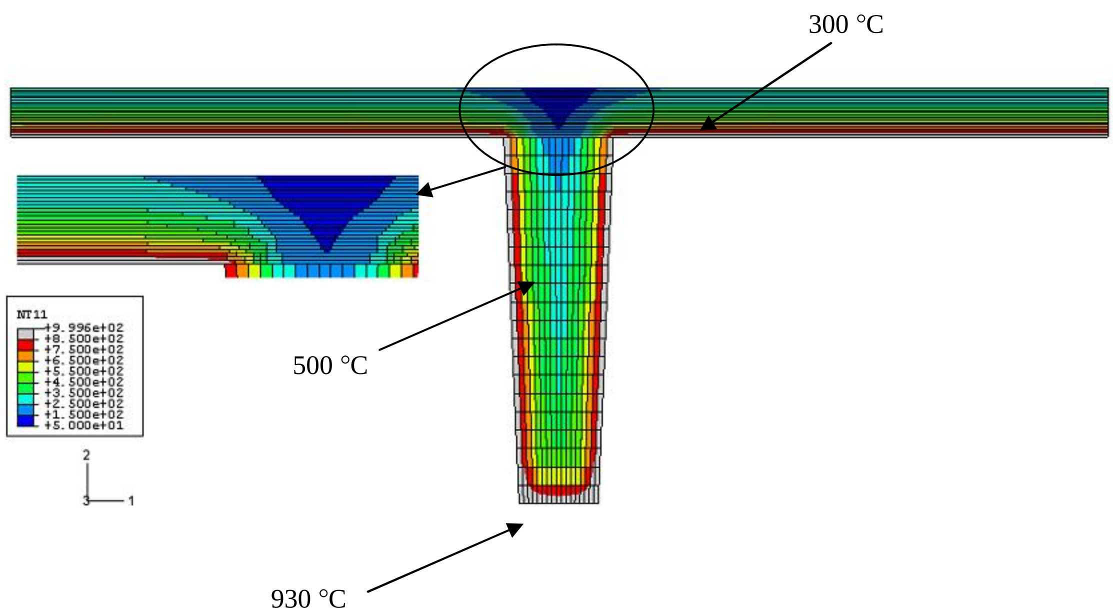

Figure 4.17: Cross-section of one half of the double tee beam with the DRAIN-2DX fibers at fire duration of 2.0 hr.

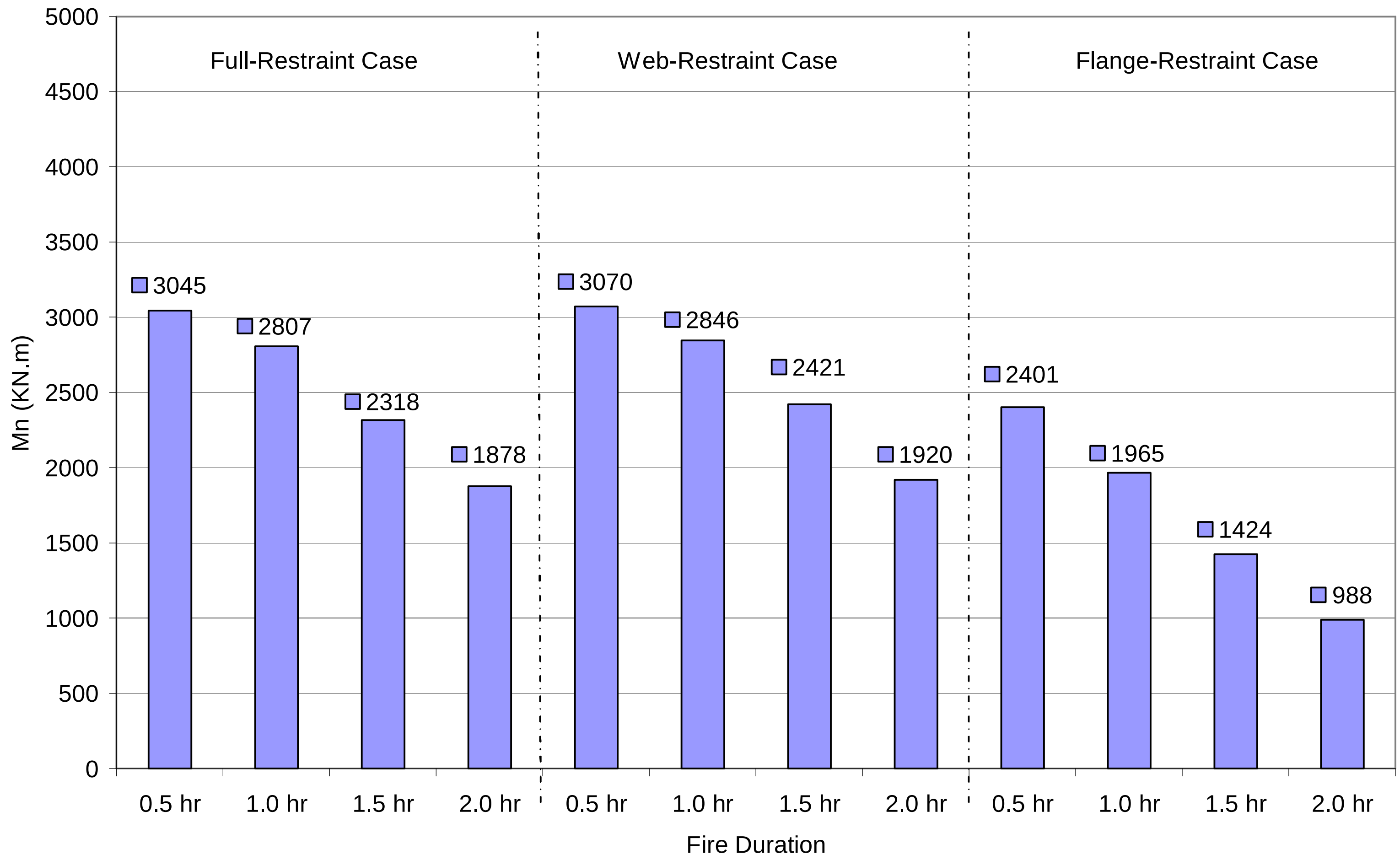

Figure 4.18: Bar chart summary of the strength analyses for the idealized boundary condition cases.

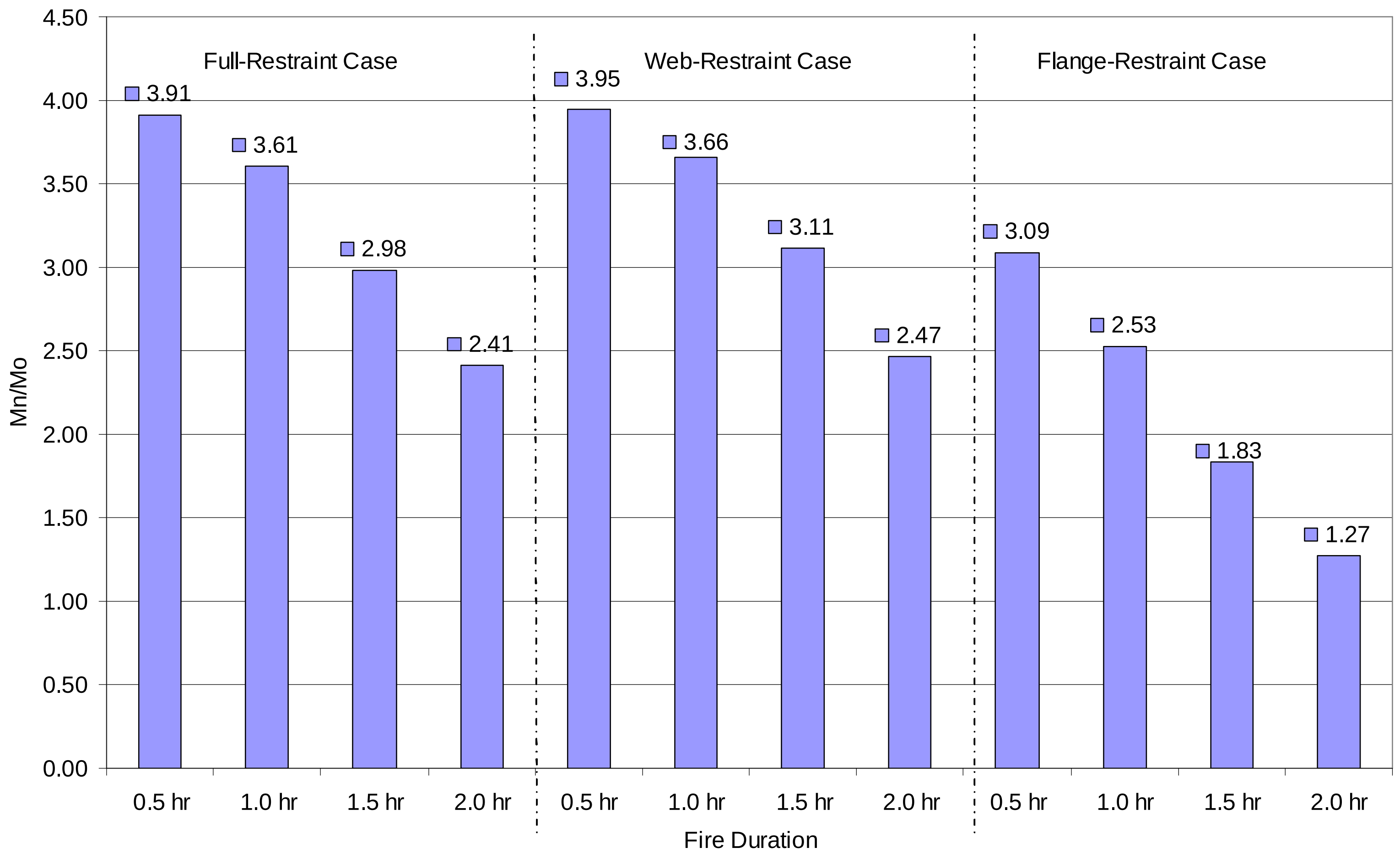

Figure 4.19: Normalized summary of the strength analyses for the idealized boundary condition cases.

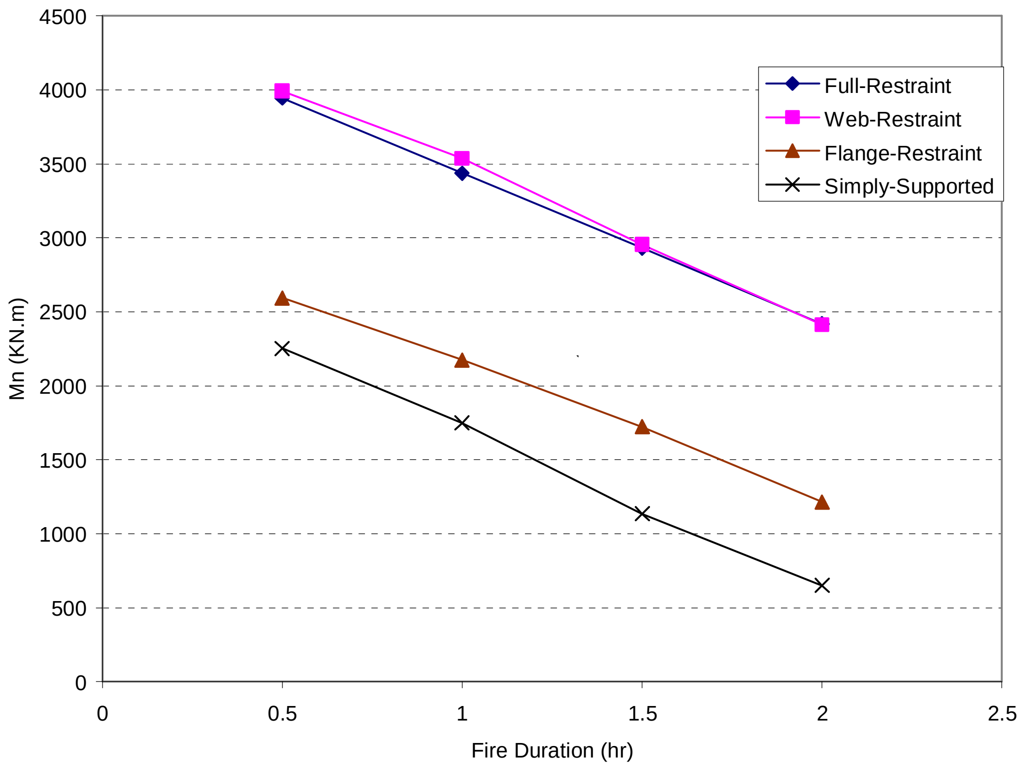

Figure 4.20: Summary of the strength analyses for the idealized boundary condition cases.

CHAPTER 5

MULTIPLE SPAN RESTRAINTS

5.1 INTRODUCTION

This chapter presents results from the analyses of the prestressed double tee beam restrained longitudinally by other double tee beams at each end with different types of connections and subjected to fire at four different durations (0.5 hr, 1.0 hr, 1.5 hr, and 2.0 hr). These analyses are conducted to capture the behavior of one of the cases of real restraints in precast concrete structures. It's the case where double tee beams are arranged in series with other double tee beams and the restraint forces develop from the interaction of these double tee beams together. The restraint forces generated in the double tee, hence, depend on the stiffness of the other double tee beams connected to it and the type of connection provided. Two systems of double tee beams are considered, and they are shown in Figure 5.1. The two systems are referred to as the 3 double tee system and the 5 double tee system. In both cases, only the intermediate double tee beam is subjected to standard fire, modeled by the ASTM-E119 time-temperature curve, from below and the other double tee beams remain at room temperature, 20 °C.

Three different restraint cases are considered in these analyses. The three different restraint cases are the same ones used in Chapter 4 for the idealized restraint cases, and they are shown in Figure 5.2. These cases are: full-restraint, web-restraint, and flange-restraint. In all these restraint cases, the restraint is provided by compression only springs, as described in Section 4.3, at the end of each double tee beam except at the node connecting each two adjacent frame elements in the 5 double tee beam system, where full connectivity is provided. These different cases are modeled and their impact on the strength of the double tee beam is studied.

Section 5.2 presents results from the structural analysis including the restraint forces developing in the double tee beam. The structural analyses models are described and the results are presented. Section 5.3 presents the strength analysis results in which the strength of the double tee beam is determined. Section 5.4 presents a summary of this chapter.

5.2 RESTRAINT FORCES ANALYSES

5.2.1 Description of the Models

In both of the two systems considered, the middle double tee beam has the same geometry, mesh, element type, and material properties that were discussed and used in Chapter 3. In addition, only the middle double tee beam is exposed to the standard fire from below. The other double tee beams remain at room temperature and their properties remain at the room temperature properties. Thus, the same thermal histories generated in Chapter 4 can be used in theses analyses. Therefore, only the nonlinear finite element structural analyses are conducted using ABAQUS program and the thermal histories are used as a thermal load input. These analyses result in the restraint forces that are then used in subsequent fire analysis to find the strength of the double tee beam for each case.

To reduce analysis time, the room temperature double tee beams modeled by 3D frame elements attached to a transition mesh at the support ends. In the 3 double tee beam system, each room temperature double tee beam is made of one frame element attached to a transition mesh at each end, as shown in Figure 5.3. In the 5 double tee beam system, however, there are two frame elements directly connected to each other on each side of the middle heated double tee beam and attached to a transition mesh at each support end, as shown in Figure 5.4.

The frame elements are assigned linear elastic properties and the transition meshes are assigned both elastic properties at the elements near the supports, as done in Chapter 4 and inelastic properties elsewhere. The frame elements are assigned the elastic time varying modulus of concrete, the gross moment of inertia of the uncracked section of the double tee beam and the gross area of that section. Since the middle heated double tee beam is connected to the transition meshes through node-to-node nonlinear springs, these meshes have to provide the same pattern of nodes so that each node in the double tee beam has a corresponding node on the transition mesh at the same level to connect with. Therefore, as shown in Figure 5.5 the transition mesh has the same mesh configuration and element type as the mesh of the middle double tee beam. All elements in the transition mesh are assigned the room temperature nonlinear properties shown in Figure 5.6 except a few elements at the ends that are shown in Figure 5.7 that are assigned linear elastic room temperature properties for reasons explained in Section 4.3.

The frame elements are connected to the transition meshes by imposing a kinematic coupling constraint between the end node of the frame element, which is the reference node, and the nodes located on the surface of the transition mesh elements. This is shown in Figure 5.8. This imposes that the surface between the constrained nodes on the transition meshes remains plane, which is consistent with the beam theory assumptions.

5.2.2 Boundary Conditions

The mechanical boundary conditions that were prescribed to the double tee beam model in Chapter 4 are prescribed similarly to the intermediate double tee beam. In the 3 double tee beam system, the transition mesh elements are restrained from a node, called the reference point. This node constrains the surfaces of the adjacent elements at each far end of the double tee beam on the bottom of the web, as done in Section 4.3. This is shown in Figure 5.9. These reference points are all restrained in the vertical direction; to prevent free body motion. The reference points on the left side of the system only are restrained in the transverse direction; only to prevent free body motion. The same thing is done to the side beams of the 5 double tee beam system, besides that the node connecting the two frame elements on each side is restrained in both the vertical and transverse directions. The same connection case is used across the span of the entire system in each case except at the node connecting each two adjacent frame elements in the 5 double tee beam system, where full connectivity is provided. For instance, in the flange-only restraint case, the middle double tee beam is connected to the adjacent transition meshes at each end through the flange-only connection, and the transition meshes at the far ends are connected to the ground through the flange-only connection as well.

5.2.3 Restraint Forces

The models are run for each of the connection cases and for each of the fire durations. Since the systems are symmetric, the spring forces developing on each side of the double tee beam are the same. The forces in the springs between the transition mesh and the double tee beam on one side are found using the technique explained in Section 4.3. These forces are the restraint forces sought and they are shown in Table 5.1 for the 3 double tee beam system and Table 5.2 for the 5 double tee beam system. The stresses developed in the frame element are checked to ensure that the use of linear elastic properties for those elements is appropriate. These stresses are found to be less than 45% of f_c', which is the limit of the linear elastic behavior of concrete according to the ACI-318 (2005). Therefore, assigning linear elastic properties to the frame elements is indeed applicable.

Tables 5.1 and 5.2 summarize the restraint forces that develop in the 3 double tee and 5 double tee beam systems, respectively, for the four different fire durations considered. It is clear from Tables 5.1 and 5.2 that the direction of the restraint moment is consistent with the restraint condition. The flange restraint case experiences positive restraint moments throughout the fire duration and the web restraint case experiences negative restraint moments. The full restraint case, however, experiences negative restraint moment during the early stages of the fire and then the moment reverses in the 3 double tee beams system but doesn't reverse in the 5 double tee beams system. The reverse in moment direction in the 3 double tee beams system takes place at the 2.0 hr fire duration, but the reverse takes place at the 1.5 hr fire duration in the single span idealized boundary condition.

The magnitudes of the restraint forces in the 5 double tee beam system are less than the corresponding values of the restraint forces in the 3 double tee beam system. The restraint forces in both cases are less than the corresponding restraint forces in the idealized single span cases. This shows that the restraint forces in a structural member tend to decrease as the flexibility of the system they exist in increase. The lower flexibility in the 5 double tee beam system compared to the 3 double tee system is attributed to the larger lower axial stiffness in the former due to its larger length.

5.3 STRENGTH ANALYSES

The resulting restraint forces from the previous step are used to analyze the moment capacity of the section of the intermediate double tee beam, at the four different fire durations and for the different restraint cases considered, by using nonlinear fiber analysis with DRAIN-2DX program. The prestressing steel is included in these analyses. The outcome of these analyses is the strength of the double tee beam subjected to different restraint conditions at different fire durations. This is to provide the insight needed to understand the effects of different restraint conditions on the precast concrete double tee beam subject to fire. The restraint cases considered here are the three different connection types within the 3 double tee beam system and the 5 double tee beam system.

The same fiber models that have been explained and used in Chapter 4 are used here after replacing the previous restraint forces with the ones presented in Tables 5.1 and 5.2. Figure 5.10 is a bar chart displaying the summary of all the results achieved in the strength analyses. It is evident from this chart that for both the 3 and 5 double team beam systems and at any given fire duration the strength of the double tee beam is slightly less when prescribed the full-restraint boundary conditions than the web-restraint boundary conditions. This is because the full-restraint case has its flange contributing to the restraint and thus diminishing the strength of the double tee. The strength is significantly less in the flange-only restraint case, and even less in the simply supported case. Figure 5.11 provides normalized values of the strength analyses results in terms of the self-weight midspan moment of one simply supported double tee beam (i.e. M = 778 kN.m). Values in the chart higher than unity present the case where the double tee beam is expected to withstand its own self weight at the particular fire duration. Therefore, from the results shown in the chart, the double tee beam is expected to withstand its self weight in all restraint cases and at all fire durations.

Figure 5.12 presents curves for the summary of the results achieved in the strength analyses of this chapter. These curves show again that in both 3 and 5 double tee beam systems the strength of the beam in the web-restrained case is slightly higher than that of the full-restraint case, and it's considerably higher in both cases than in the flange-restraint case

Figure 5.13 compares between the results of the double tee beam systems of this chapter and the results of the idealized restraints applied to the single span beam in Chapter 4. The curves in the figure show that the strength of the double tee beam decreases as the number of spans increases in all restraint conditions. This effect, however, is lower in the flange-restraint case than in the other restraint cases.

5.4 SUMMARY

This chapter presents results from the analyses of the prestressed double tee beam supported longitudinally by other double tee beams from each end with different types of connections and subjected to fire at four different durations (0.5 hr, 1.0 hr, 1.5 hr, and 2.0 hr). These analyses are conducted to capture the behavior of one of the cases of real restraints in precast concrete structures. It's the case where double tee beams are connected to other double tee beams and the restraint forces develop from the interaction of these double tee beams together. Two systems of double tee beams are considered. The two systems are referred to as the 3 double tee system and the 5 double tee system. In both cases, only the intermediate double tee beam is subjected to standard fire, modeled by the ASTM-E119 time-temperature curve, from below and the other double tee beams remain at room temperature, 20 °C.

The direction of the restraint moment is consistent with the restraint condition in all restraint cases. The flange restraint case experiences positive restraint moments throughout the fire duration and the web restraint case experiences negative restraint moments. The full restraint case, however, experiences negative restraint moment during the early stages of the fire and then the moment reverses in the 3 double tee beams system but doesn't reverse in the 5 double tee beams system. The reverse in moment direction in the 3 double tee beams system takes place at the 2.0 hr fire duration, but the reverse takes place at the 1.5 hr fire duration in the single span idealized boundary condition.

The magnitudes of the restraint forces in the 5 double tee beam system are less than the corresponding values of the restraint forces in the 3 double tee beam system. The restraint forces in both cases are less than the corresponding restraint forces in the idealized single span cases. This shows that the restraint forces in a structural member tend to decrease as the flexibility of the system they exist in increase. The lower flexibility in the 5 double tee beam system compared to the 3 double tee system is attributed to the larger lower axial stiffness in the former due to its larger length.

For both the 3 and 5 double team beam systems and at any given fire duration the strength of the double tee beam is slightly less when prescribed the full-restraint boundary conditions than the web-restraint boundary conditions. This is because the full-restraint case has its flange contributing to the restraint and thus diminishing the strength of the double tee. The strength is significantly less in the flange-only restraint case than both the full-restraint case the web-restraint case.

The strength of the double tee beam decreases as the number of spans increases in all restraint conditions. This effect, however, is lower in the flange-restraint case than in the other restraint cases.

Table 5.1: Restraint forces results for the 3 double tee beam system.

	0.5 hr	1.0 hr	1.5 hrs	2.0 hrs
Full-Restraint	3935 KN 326 KN.m	5966 KN 212 KN.m	7270 KN 67 KN.m	77 KN.m 7898 KN
Flange-Restraint	290 KN.m 2618 KN	493 KN.m 4130 KN	642 KN.m 5225 KN	721 KN.m 5876 KN
Web-Restraint	3582 KN 409 KN.m	5310 KN 356 KN.m	6390 KN 247 KN.m	6886 KN 121 KN.m

Table 5.2: Restraint forces results for the 5 double tee beam system.

	0.5 hr	1.0 hr	1.5 hrs	2.0 hrs
Full-Restraint	2556 KN 146 KN	4142 KN 274 KN.m	5404 KN 167 KN.m	6217 KN 36 KN.m
Flange-Restraint	196 KN.m 1770 KN	343 KN.m 2945 KN	479 KN.m 3939 KN	566 KN.m 4649 KN
Web-Restraint	2397 KN 380 KN.m	3826 KN 366 KN.m	4917 KN 292 KN.m	5587 KN 181 KN.m

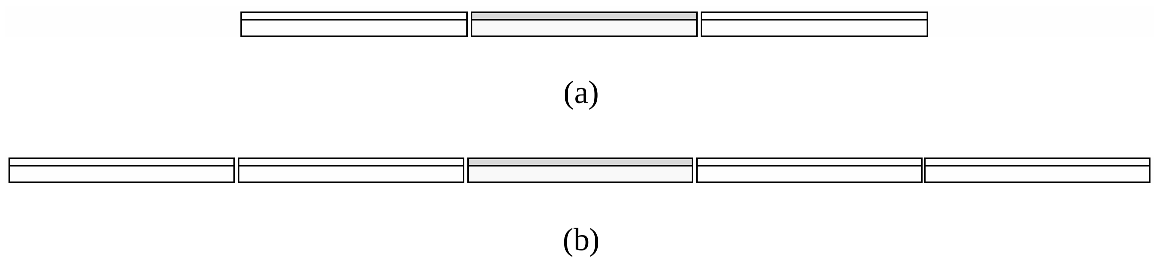

Figure 5.1: Double tee beam systems considered: (a) 3 double tee beam system; and (b) 5 double tee beam system.

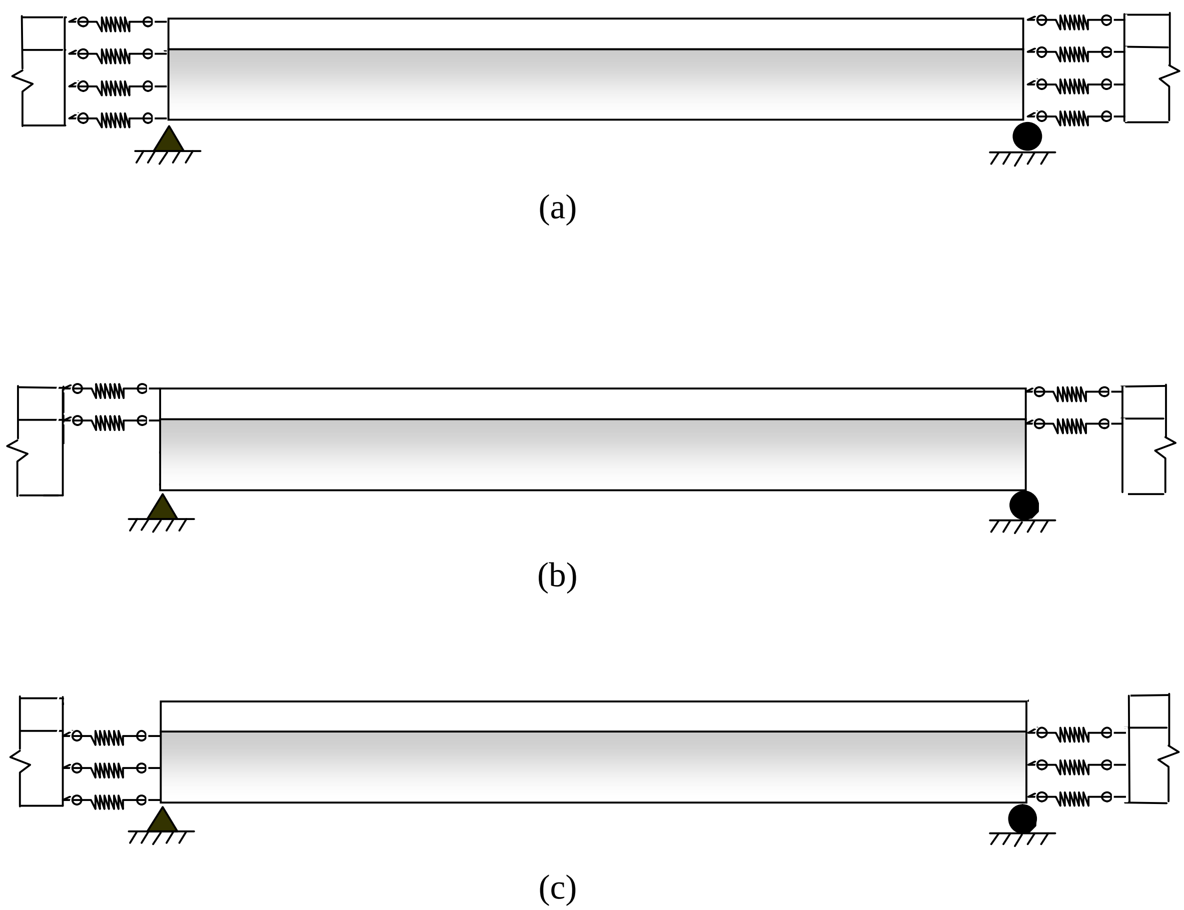

Figure 5.2: The different restraint cases considered between the double tee beams: (a) full-restraint; (b) flange-restraint; and (c) web-restraint.

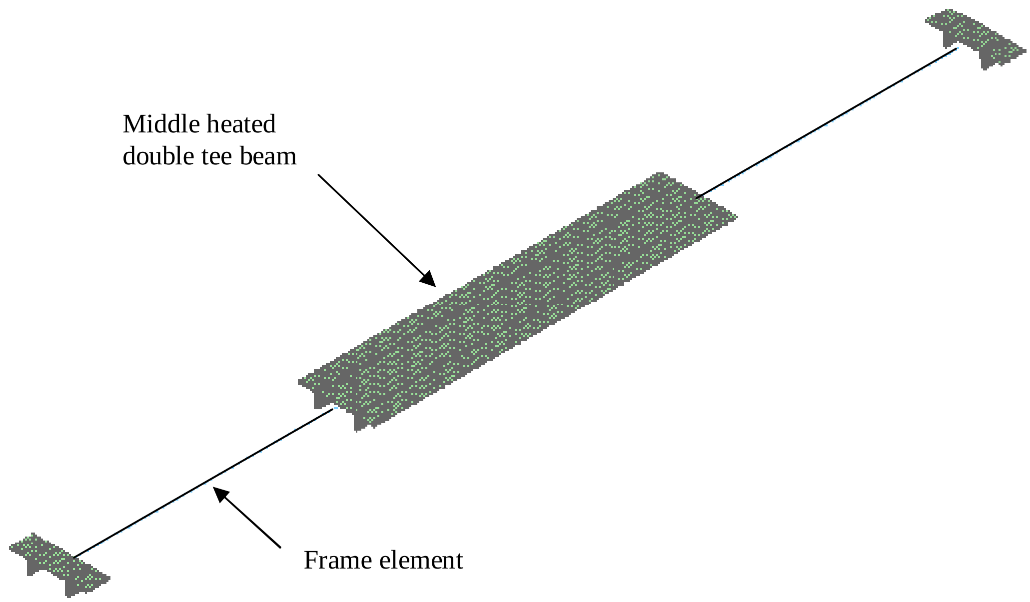

Figure 5.3: 3 double tee beam system.

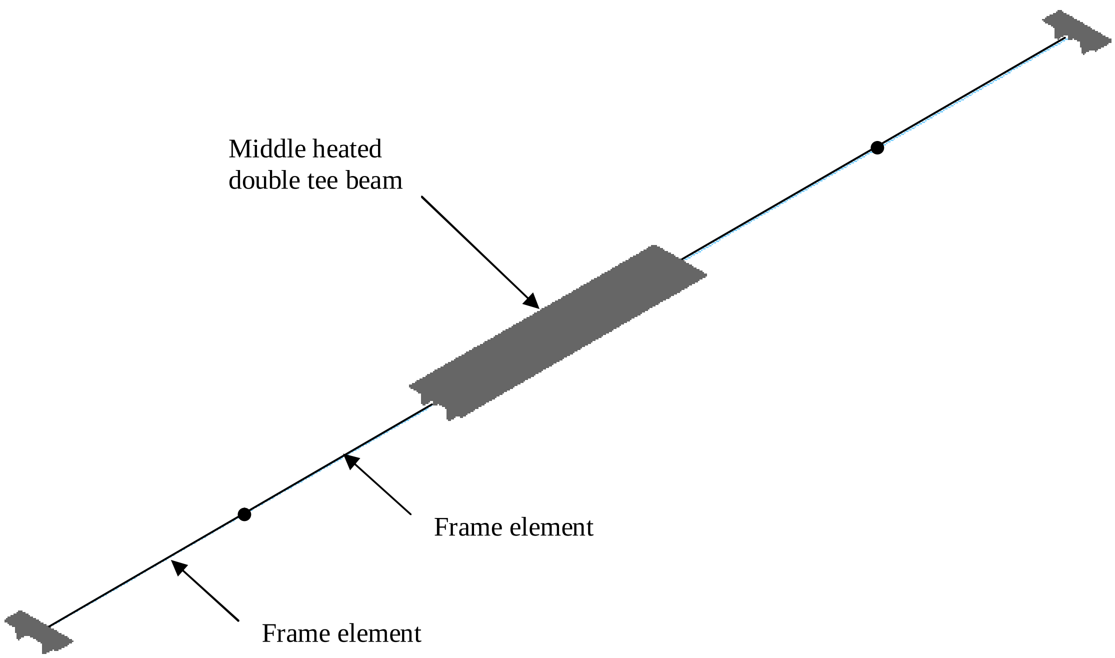

Figure 5.4: 5 double tee beam system.

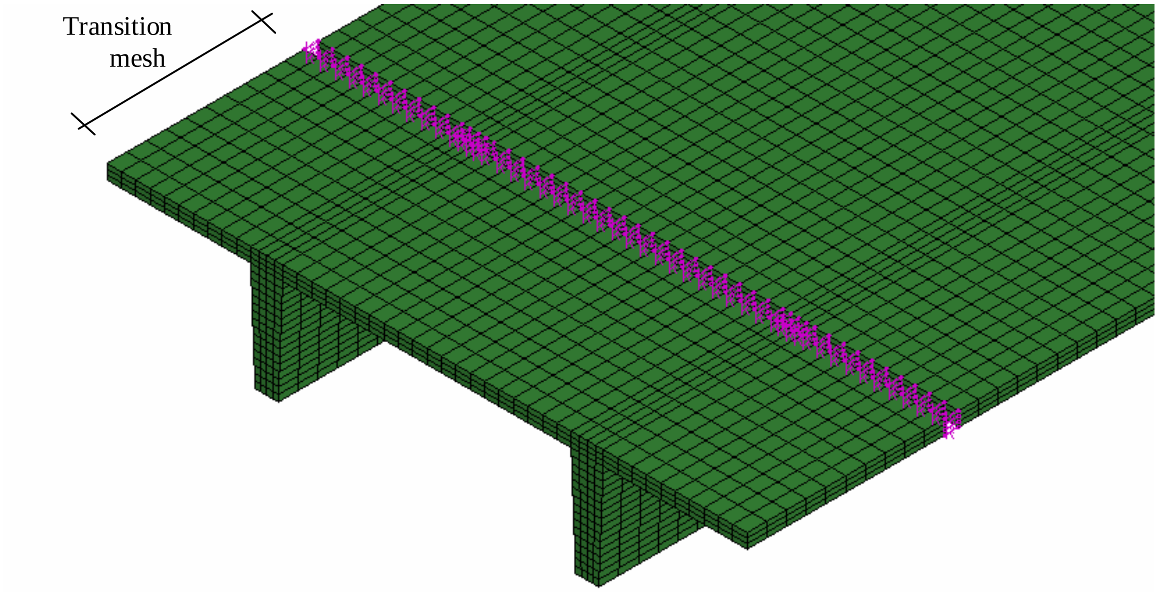

Figure 5.5: Connection between double tee beam and transition mesh.

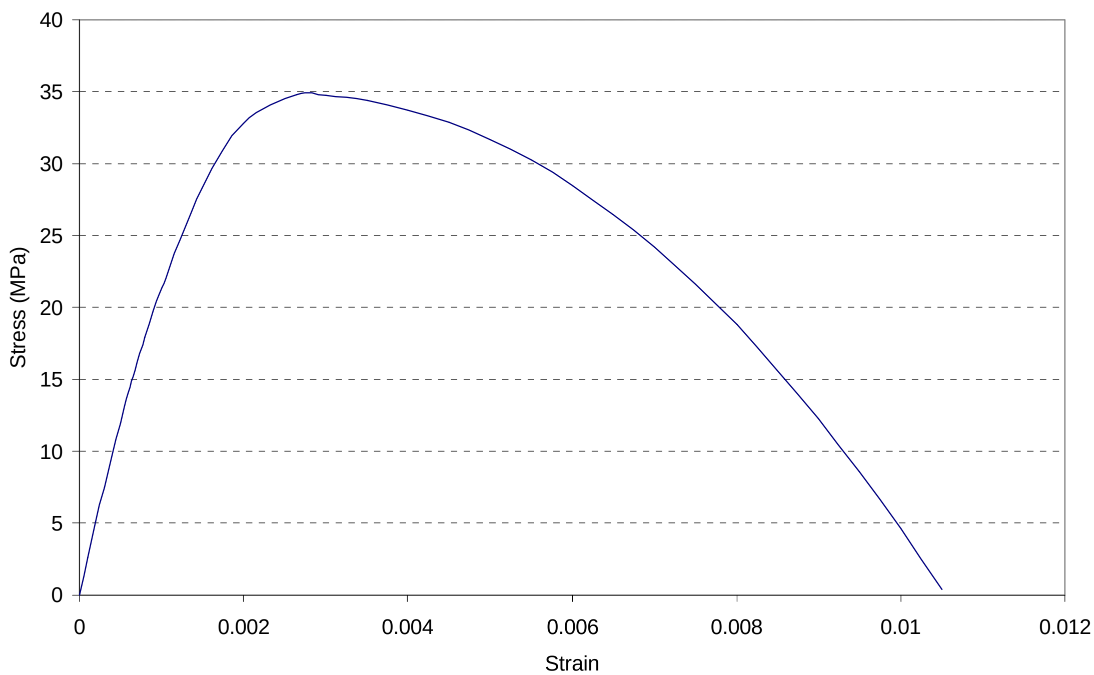

Figure 5.6: Concrete stress-strain curve (at room temperature) assigned to the transition meshes.

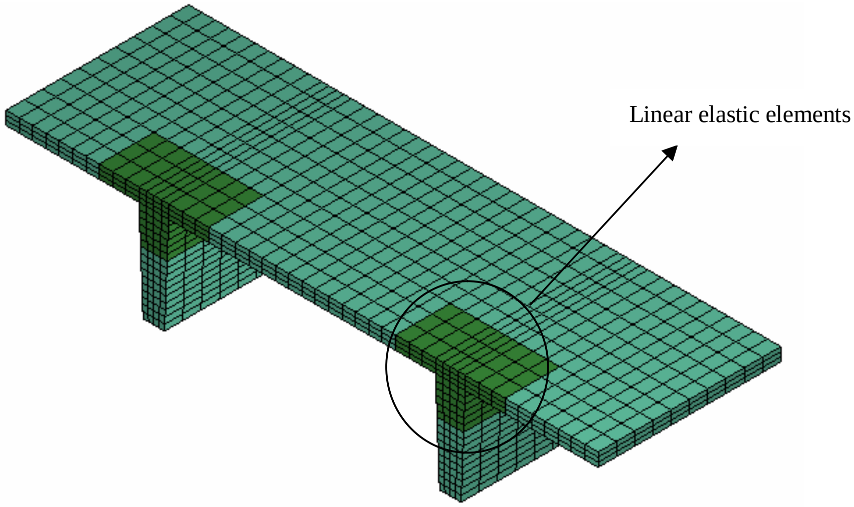

Figure 5.7: The elements assigned linear elastic room temperature properties in the transition mesh.

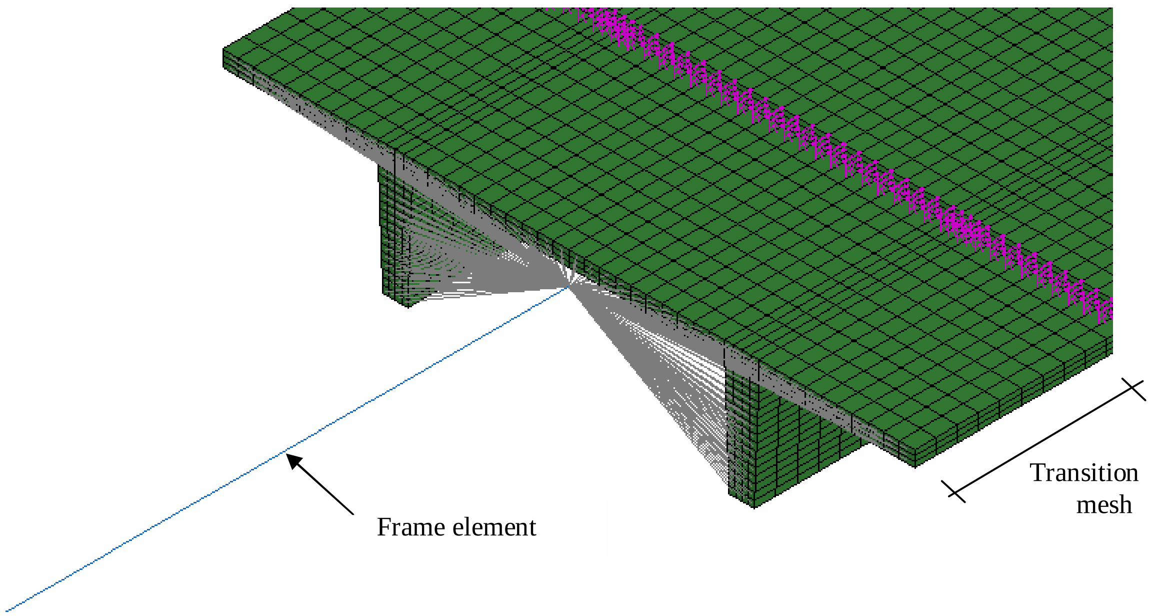

Figure 5.8: The kinematic coupling constraint between the frame element and the transition mesh.

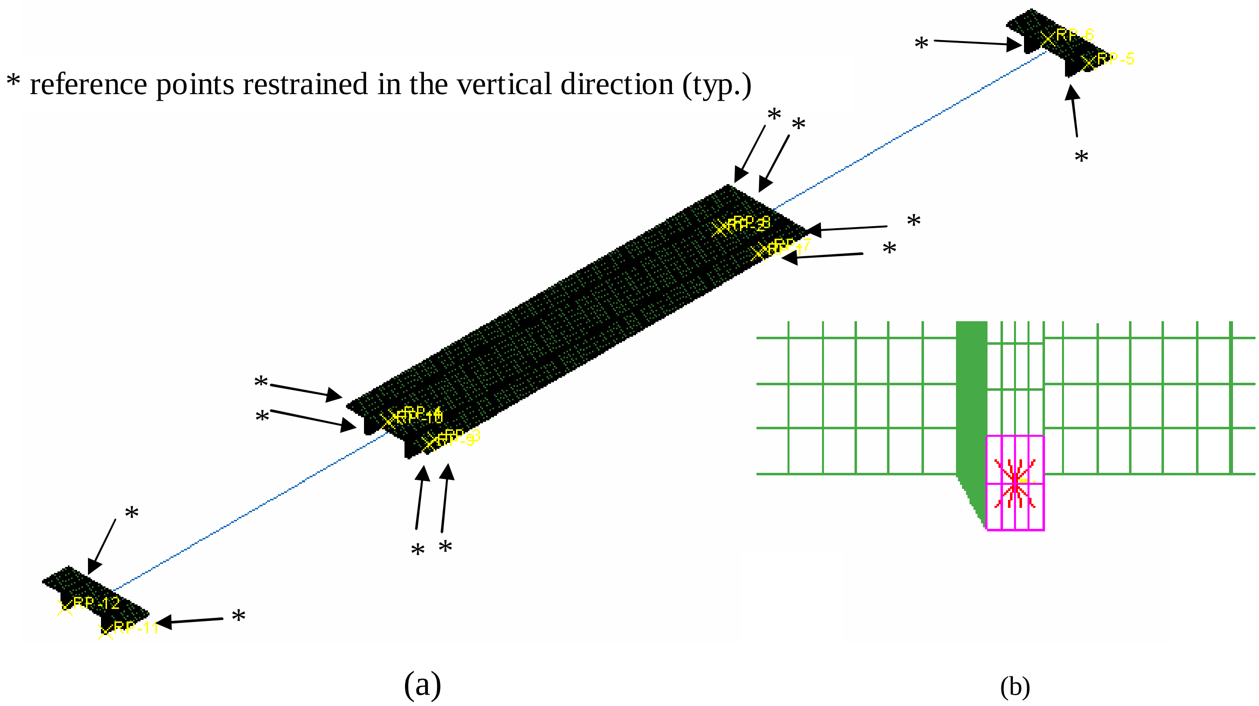

Figure 5.9: Vertical boundary conditions: (a) isometric view showing the locations of the reference points; and (b) bottom view of a web showing the kinematic coupling constraint area.

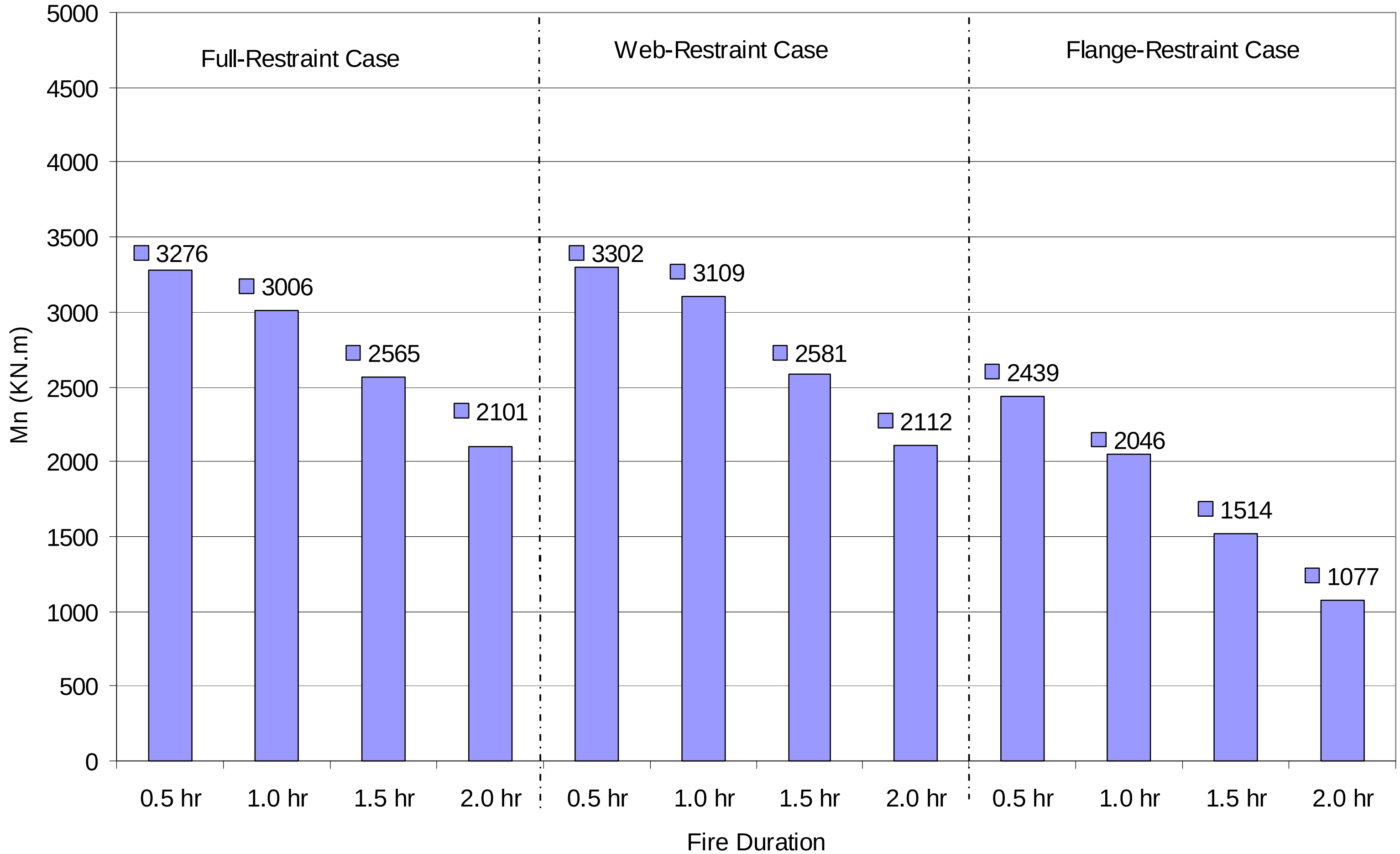

Figure 5.10 (a): Bar chart summary of the strength analyses for the 3 double tee beam system.

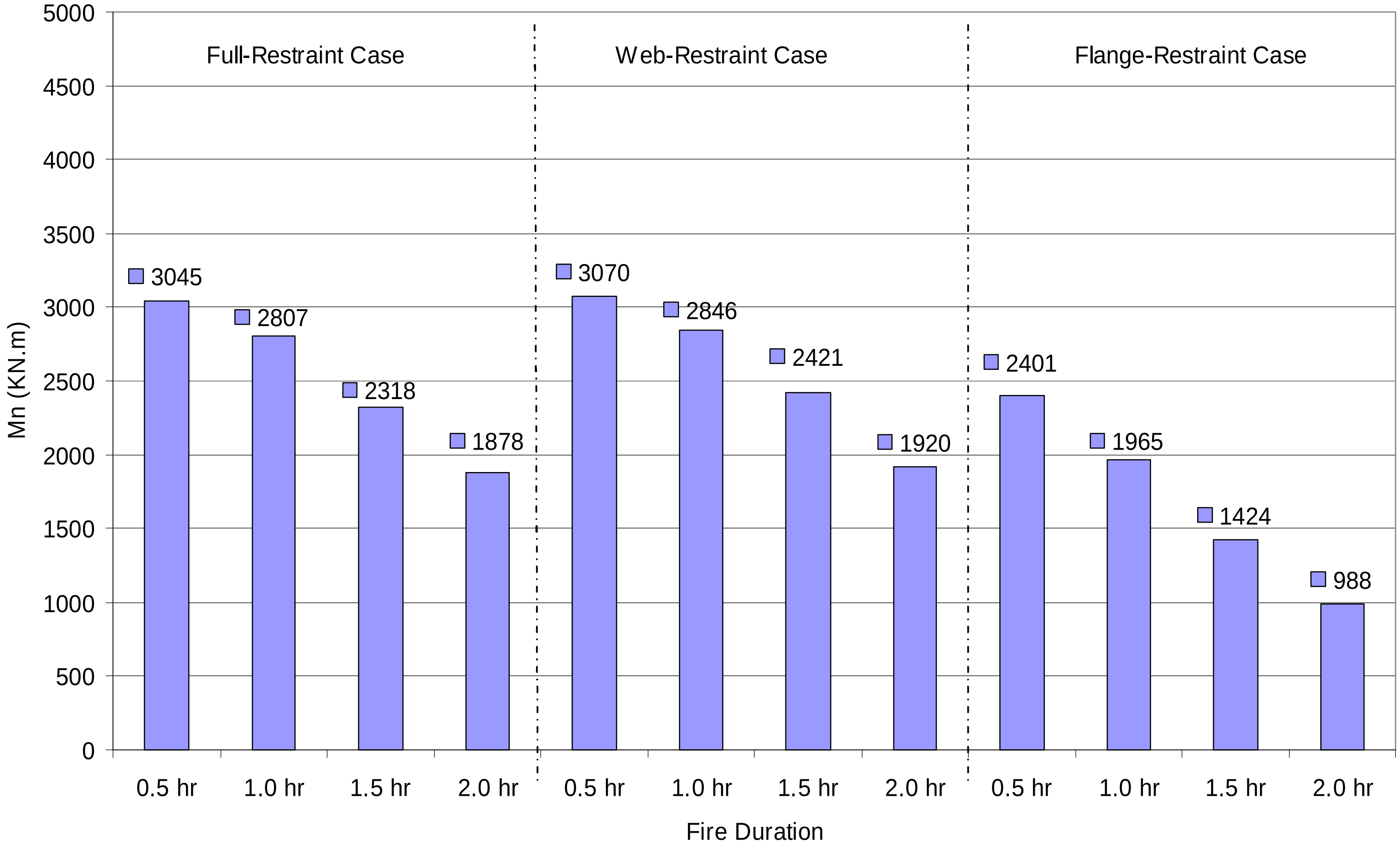

Figure 5.10 (b): Bar chart summary of the strength analyses for the 5 double tee beam system.

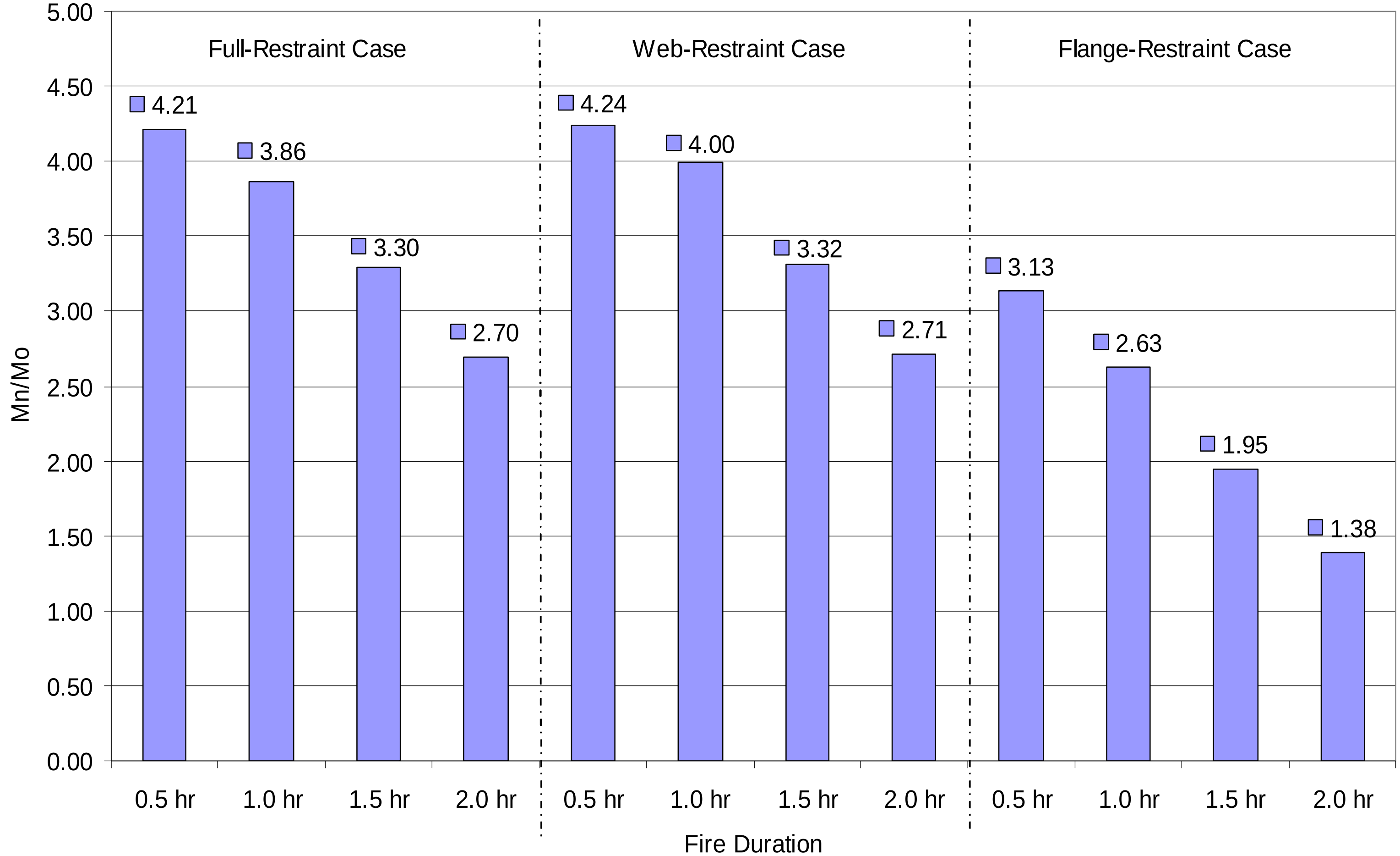

Figure 5.11 (a): Bar chart normalized summary of the strength analyses for the 3 double tee beam system.

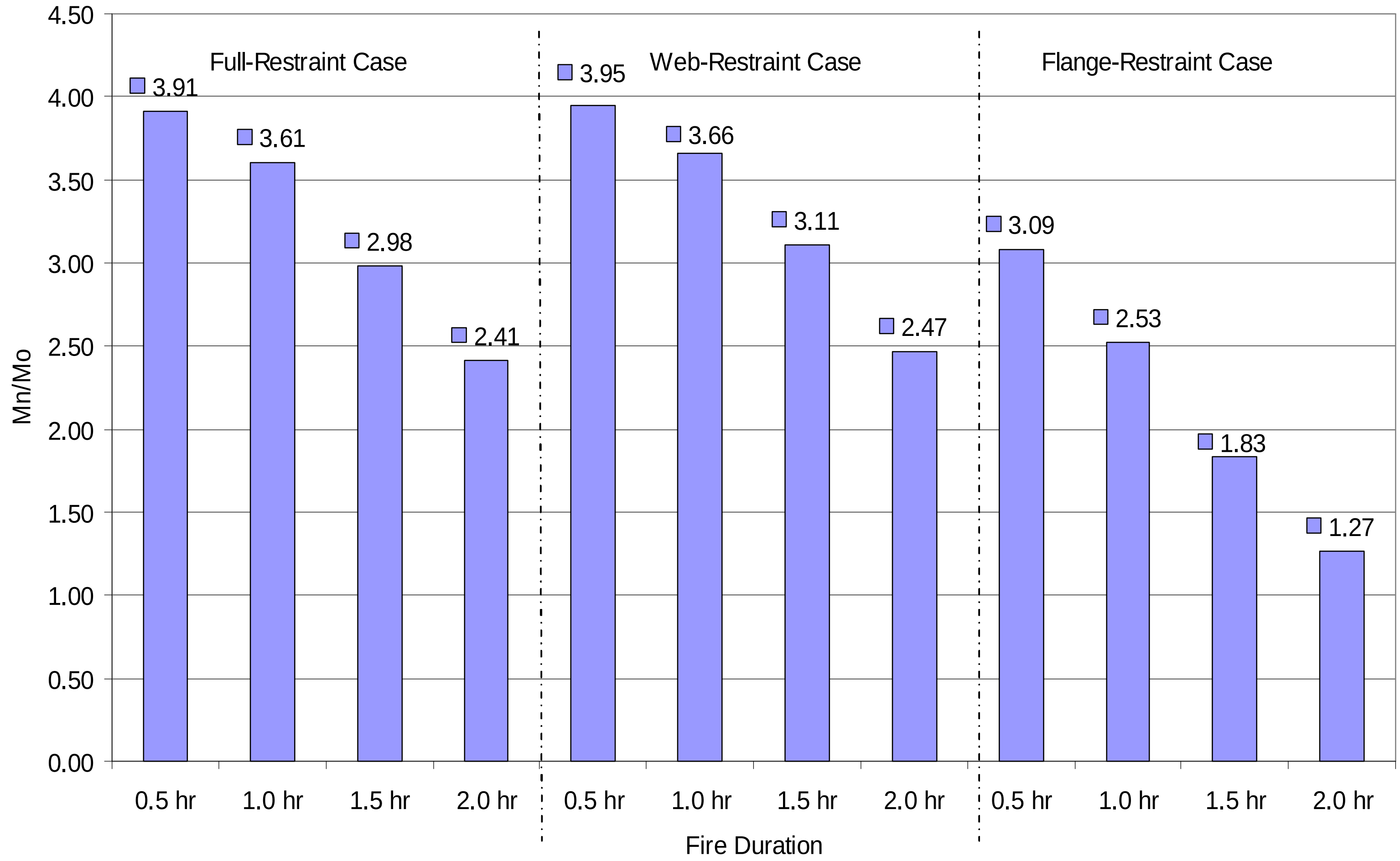

Figure 5.11 (b): Bar chart normalized summary of the strength analyses for the 5 double tee beam system.

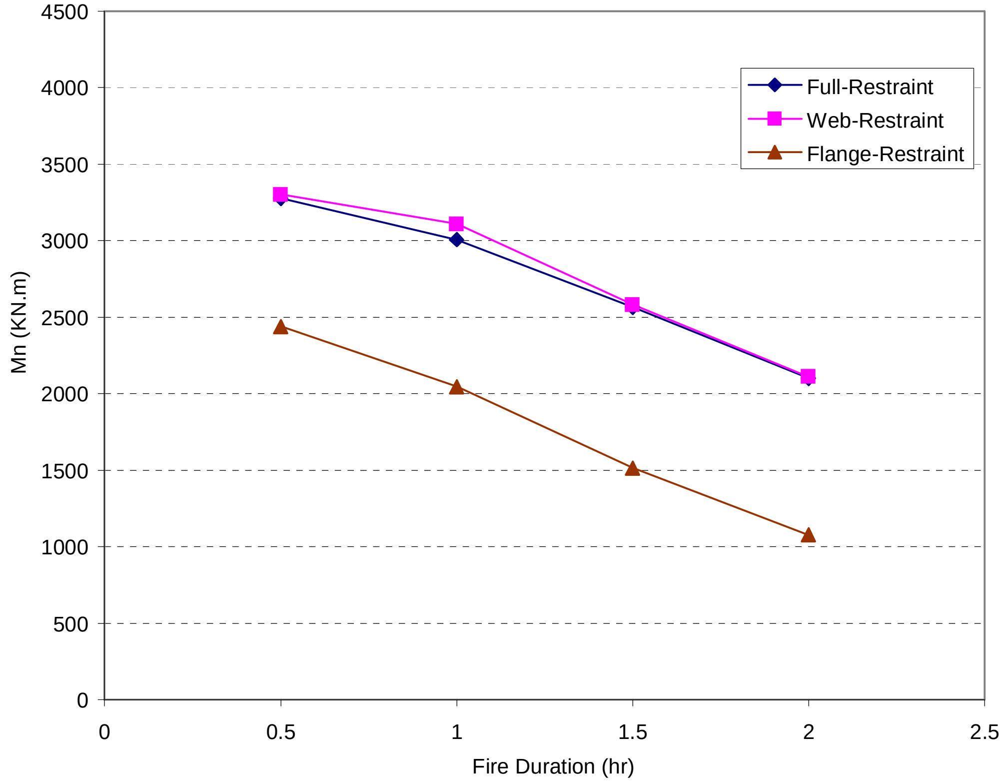

(a)

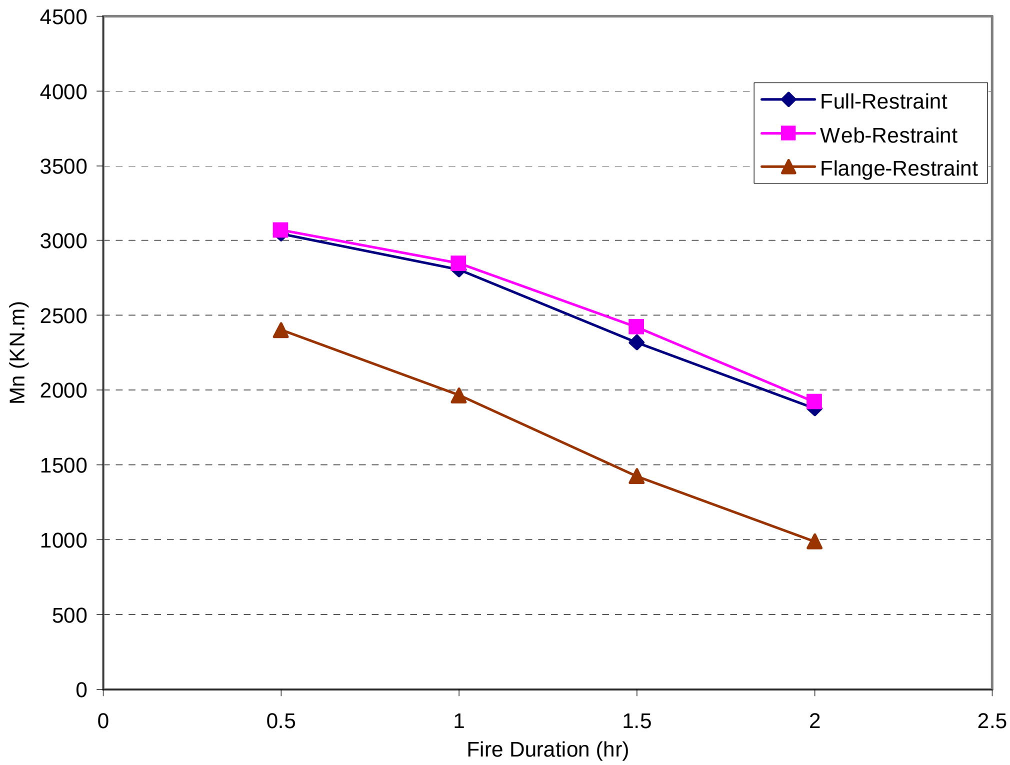

(b)

Figure 5.12: Summary of the strength analyses results for: (a) 3 double tee beam system; and (b) 5 double tee beam system.

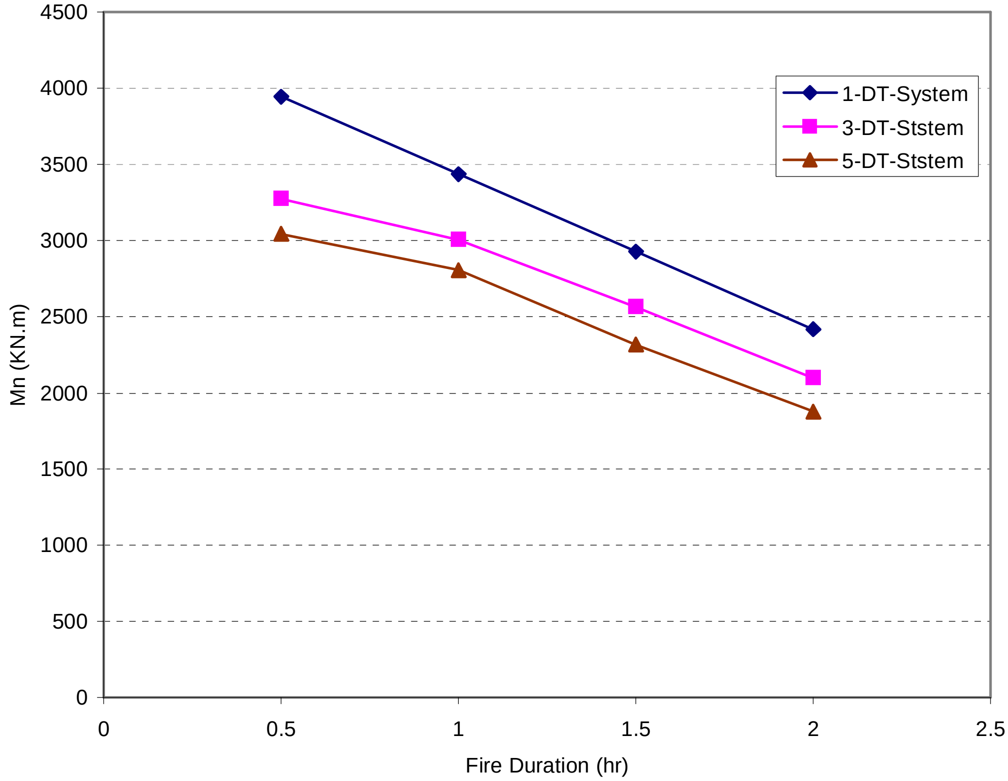

Figure 5.13 (a): Summary of the strength analyses results for the full-restraint case.

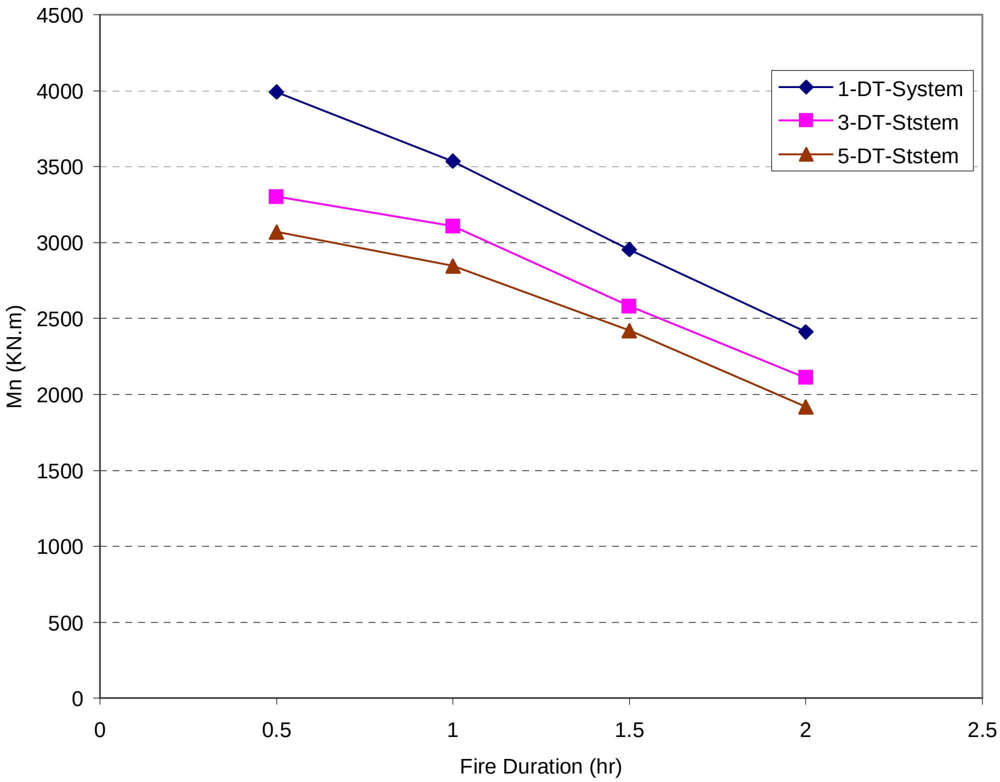

Figure 5.13 (b): Summary of the strength analyses results for the web-restraint case.

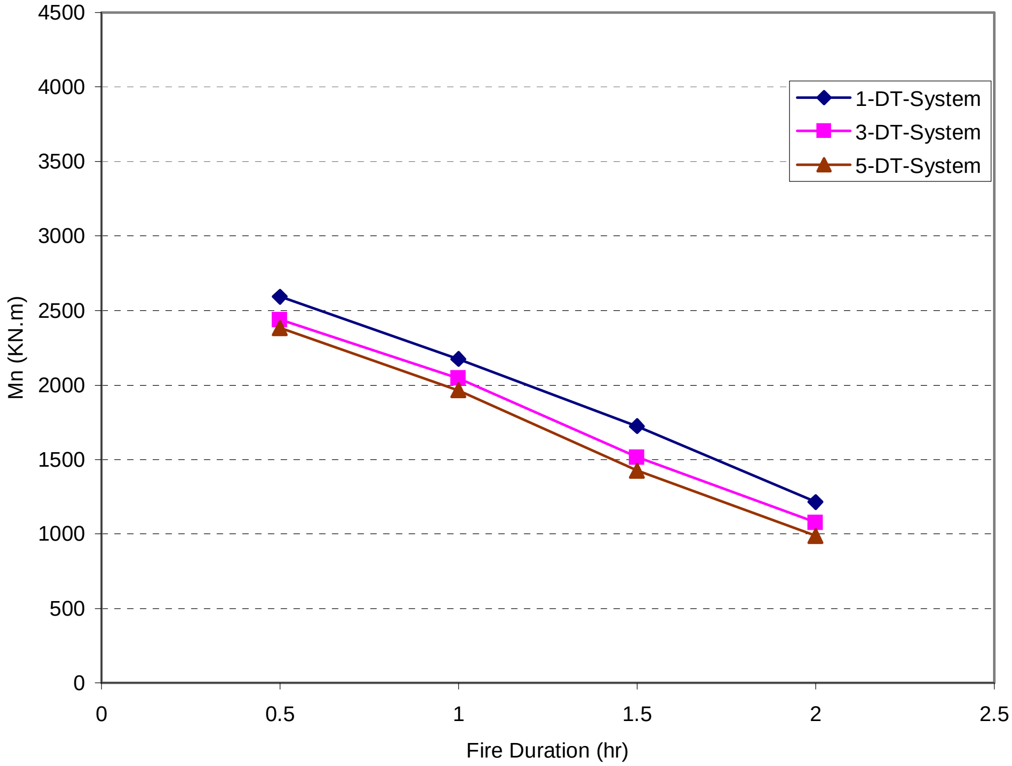

Figure 5.13 (c): Summary of the strength analyses results for the flange-restraint case.

CHAPTER 6

SPANDREL BEAMS AND INVERTED TEE GIRDERS RESTRAINT

6.1 INTODUCTION

This chapter presents results from the analyses of the precast prestressed double tee beam restrained longitudinally by flexible support elements at each end. As an example of flexible supports, a pocket spandrel beam and an inverted tee girder are analyzed in this chapter. These analyses present an insight to the restraint that the spandrel beam and the inverted tee girder provide to the double tee beam when subjected to a standard fire.

In precast structural systems, inverted tee girders collect the floor loads from the internal double tee beams, connected to it on both sides of the web, and transfer those loads to the columns. Spandrel beams are located on the perimeter of the floor system and they collect the loads from the external double tee beams from one side. The axial restraint to the double tee is provided in these cases by the weak-axis bending stiffness of the spandrel beam or inverted tee girder. Typically, three double tee beams are supported by one side of an inverted tee girder or spandrel beam. This chapter focuses on the behavior of a single double tee beam supported by a spandrel beam or inverted tee girder on their midspans. The impact of the restraint affected by the inverted tee and spandrel on the strength of the double tee beam to standard fire is explored.

Section 6.2 presents results from the structural analysis including the restraint forces developing in the double tee beam. The structural analyses models are described and the results are presented. Section 6.3 presents the strength analysis results in which the strength of the double tee beam is determined. Section 6.4 presents a summary of this chapter.

6.2 RESTRAINT FORCES ANALYSES

6.2.1 Description of the Models

Prototypes of a typical pocket spandrel beam and an inverted tee girder used in practice are used for the research presented in this report. Figure 6.1 shows the cross-section of the spandrel beam prototype and Figure 6.2 shows the cross-section of the inverted tee girder prototype. Figure 6.3 shows the model of the double tee beam – spandrel beam assembly. Figure 6.4 shows the model of the double tee beam – inverted tee girders assembly. The spandrel beam and the inverted tee girder have a span of 45 feet each.

Since only the middle double tee beam is the element that is subjected to fire, the same thermal histories generated in Chapter 4 can be used in theses analyses. Therefore, only the nonlinear finite element structural analyses are conducted using ABAQUS program and the thermal histories are used as a thermal load input. Theses analyses result in the restraint forces sought to be used in the fiber model analyses to compute the strength of the double tee beams for each case.

The double tee beam has the same geometry, mesh, element type, and material properties that are discussed and used in Chapter 4. In addition, only the double tee beam is exposed to the standard fire from below. The spandrel beam and inverted tee girder remain at room temperature and their properties remain at room temperature properties throughout the analyses. The compressive strength of the spandrel beam is 34.8 MPa (5 ksi) and the compressive strength of the inverted tee girder is 69.5 (10 ksi).

The spandrel beam and inverted tee girder are assigned linear elastic material properties. This is done to reduce the analyses run-time. The applicability of using linear elastic properties is checked by studying the stresses developing in the models. The stresses generated in the inverted tee girders and spandrels from the analyses added to the stresses from the self weight loads and the prestressing forces are found to be less than the linear elastic limits. However, these stresses were found to exceed the cracking stress of the concrete at several locations. Had the concreting cracking been taken into account in the model, the resulting restraint forces would have decreased. Since neglecting the cracking in concrete results in a conservative estimate of the restraint forces, and since the exaggeration in the values of the restraint forces are found to be moderate (as will be shown later in this section), assigning the linear elastic undamaged concrete properties is acceptable in these restraint force analyses.

The double tee beam is connected from its flange to the web of the spandrel beam and inverted tee girder through nonlinear compression only springs. These springs are connected between each node on the flange of the double tee beam at its end section and a corresponding node on the web of the spandrel beam or the inverted tee girder. The meshes, therefore, of the spandrel beam and the inverted tee girder are designed specifically for the purpose of providing the nodes required to connect with the corresponding nodes on the double tee beam by the nonlinear springs. Thus, the meshes of the spandrel beam and inverted tee girder are compatible with the mesh of the flange of the double tee beam in the region in contact with the double tee beam flange section. The mesh becomes coarser outside that region to reduce the analysis-run time. Figures 6.5 shows the mesh of the spandrel beam and Figure 6.6 shows the mesh of the inverted tee girder girder.

6.2.2 Boundary Conditions

The same boundary conditions prescribed to the double tee beam in the previous chapters are prescribed to the double tee beam in this chapter. The inverted tee girders and spandrel beams are prescribed boundary conditions so that they behave in a simply supported manner. The boundary conditions for the spandrel beam are described in Figure 6.7 and for the inverted tee girder in Figure 6.8. The farthest four corner nodes of each beam are restrained in direction 3. The two bottom nodes of theses nodes are restrained in direction 2. The two left side nodes of these nodes are restrained in direction 1. These boundary conditions are intended to represent the manner in which the spandrel or inverted tee are connected to the supporting column.

6.2.3 Restraint Forces

The models are run for each of the connection cases and for the prescribed fire durations. Since the systems are symmetric, the spring forces developing on each side of the double tee beam are the same. The forces in the springs between the flexible support elements and the double tee beam on one end are found using the technique discussed in Section 4.3. These forces are the restraint forces sought and they are shown in Table 6.1. The results in this table show that the restraint forces and moments are less in the spandrel beam case than the inverted tee girder case. This is attributed to the fact that the spandrel beam has larger bending stiffness than the inverted tee girder. The moments in the table are all positive in direction since the restraint is flange-restraint, which is consistent with the earlier observations.

6.3 STRENGTH ANALYSES

The resulting restraint forces from the previous step are used to analyze the moment capacity of the mid-span section of the double tee beam model, at the four different fire durations, by using nonlinear fiber analyses with the DRAIN-2DX program. The outcome of these analyses is the strength of the double tee beam subjected to different restraint conditions at different fire durations. This provides the insight needed to understand the effects of different restraint conditions on the precast concrete double tee beam subject to fire. The restraint cases considered here are the restraint provided by the spandrel beam and those provided by the inverted tee girder.

The same fiber models that have been explained and used in Chapter 4 are used here after replacing the previous restraint forces with the ones presented in Table 6.1. Figure 6.9 shows a bar chart displaying the summary of all the results achieved in the strength analyses of this chapter. This figure shows that the strength of the double tee beam has almost the same strength when either restrained by a spandrel beam or an inverted tee girder. Figure 6.10 provides normalized values of the analyses results in terms of the self-weight midspan moment of the simply supported double tee beam (i.e. M = 778 kN.m). Values in the chart higher than unity present the case where the double tee beam is expected to withstand its own self weight at the particular fire duration. It’s clear from this figure that the double tee beam will not be able of withstanding its own self weight at 2 hours of fire in both the spandrel beam restraint case and the inverted tee girder restraint case since they both have normalized value of strength less that 1.

Figure 6.11 presents curves for the summary of all the results achieved in the strength analyses in this chapter. This figure shows the similarity in the behavior of the double tee beam in both the spandrel beam restrain case and the inverted tee girder restraint case. Figure 6.12 compares between the results of this chapter and the results of Chapter 4 (idealized single span restraints). This figure shows that the behavior of the double tee beam in both the spandrel beam restraint case and the inverted tee girder restraint case is similar to the behavior of the simply supported case. In other words, the increase in strength due to the flexible support elements is negligible.

Figure 6.13 compares the results of this chapter and the results of flange-restraint cases of Chapter 5 (multiple span restraints). The flange-restraint case of Chapter 5 is chosen because the restraint between the double tee beam and the support element is through the flange as well. It is clear from this figure that the strength of the double tee beam in both the spandrel beam restraint case and the inverted tee girder restraint case is even lower than that of the multiple span cases and they both have negligible effects on the strength of the double tee beam during fire.

6.4 SUMMARY

This chapter presents results from the analyses of the precast prestressed double tee beam supported longitudinally by flexible support elements at each end. The support elements treated are a pocket spandrel beam and an inverted tee girder. These analyses provide insight to the restraint that the spandrel beam and the inverted tee girder provide to the double tee beam when subjected to a standard fire. This chapter focuses on the behavior of the double tee beam connected to the spandrel beam and inverted tee girder on their midspans. The impact of exposing this double tee beam to standard fire on its strength is explored.

The restraint forces and moments are found to be less in the spandrel beam case than the inverted tee girder case. This is attributed to the fact that the spandrel beam has larger bending stiffness than the inverted tee girder. The moments in both cases are all positive in direction since the restraint is flange-restraint, which is consistent with the earlier observations.

The strength of the double tee beam has almost the same strength when either restrained by a spandrel beam or an inverted tee girder. The double tee beam will not be able of withstanding its own self weight at 2 hours of fire in both the spandrel beam restraint case and the inverted tee girder restraint case.

The behavior of the double tee beam in both the spandrel beam restraint case and the inverted tee girder restraint case is similar to the behavior of the simply supported case. In other words, the increase in strength due to the flexible support elements is negligible. The strength of the double tee beam in both the spandrel beam restraint case and the inverted tee girder restraint case is even lower than that of the multiple span cases and they both have negligible effects on the strength of the double tee beam during fire.

Table 6.1: Restraint forces results for the flexible support elements cases.

	0.5 hr	1.0 hr	1.5 hrs	2.0 hrs
Spandrel	2 KN.m 15 KN	3 KN.m 28 KN	5 KN.m 42 KN	6 KN.m 57 KN
Inverted Tee	24 KN.m 192 KN	42 KN.m 340 KN	65 KN.m 497 KN	88 KN.m 660 KN

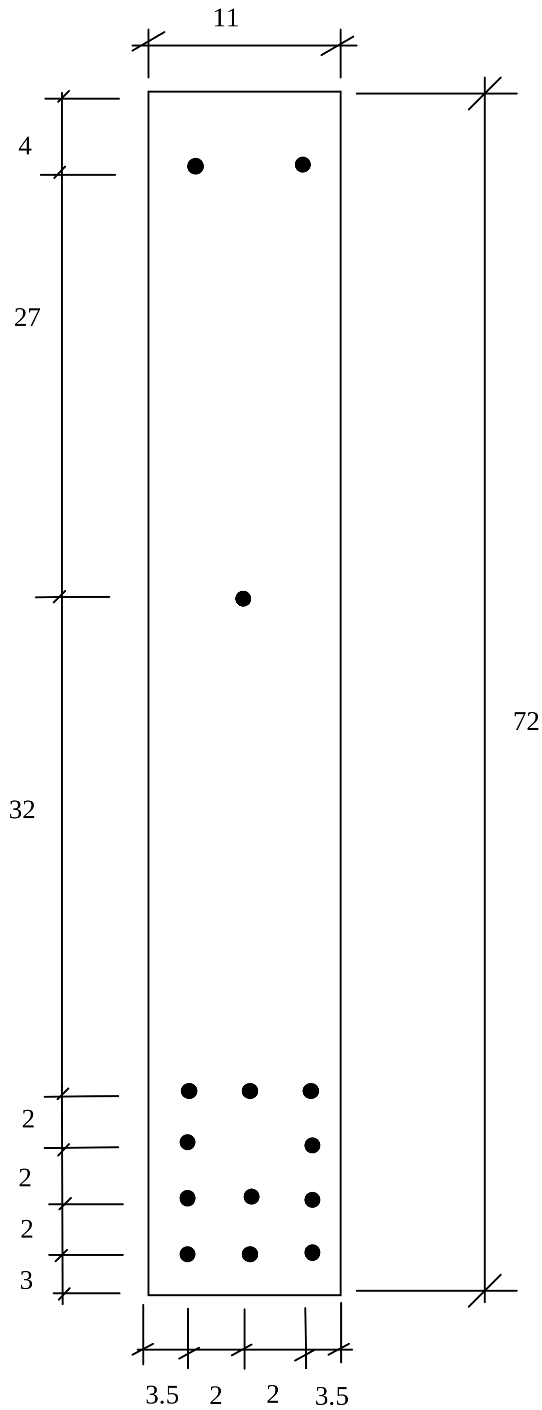

All dimensions
are in inches.

Figure 6.1: Cross-section of the prototype pocket spandrel beam (not to scale).

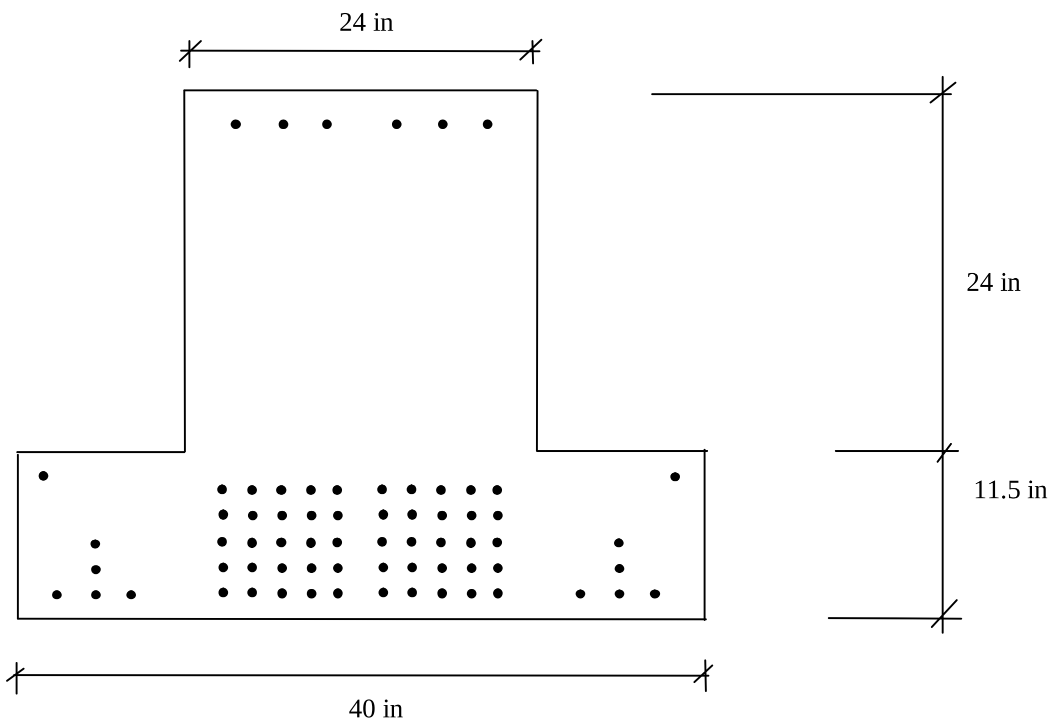

Figure 6.2: Cross-section of the prototype of the inverted tee girder (not to scale).

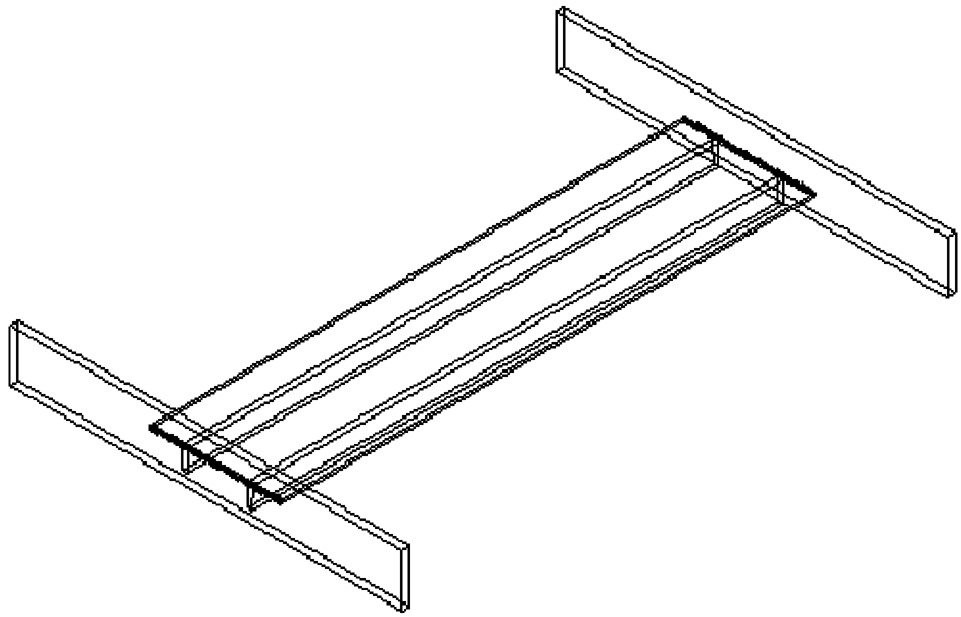

Figure 6.3: The double tee beam – spandrel beam assembly.

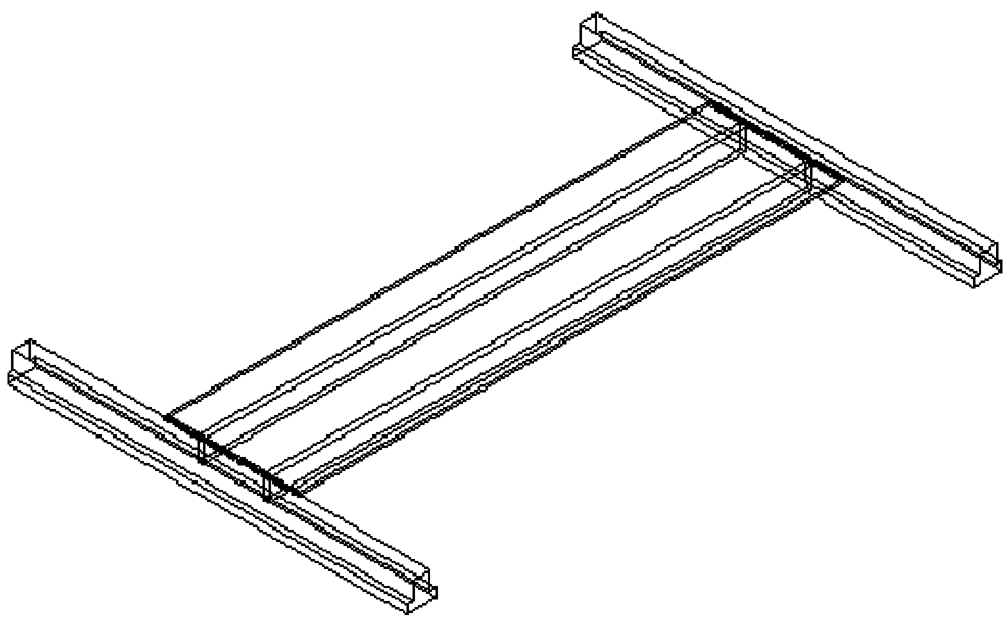

Figure 6.4: The double tee beam – inverted tee girder assembly.

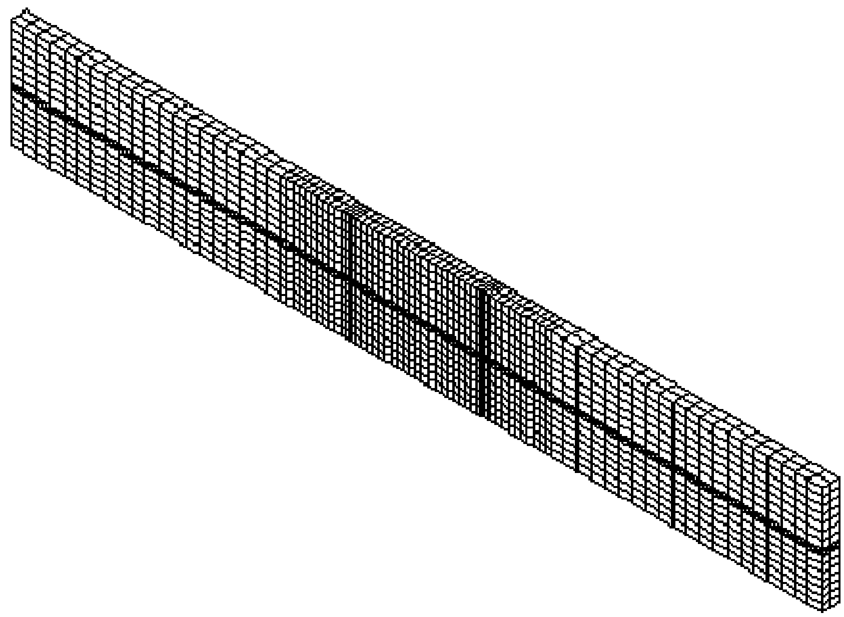

Figure 6.5: The spandrel beam mesh.

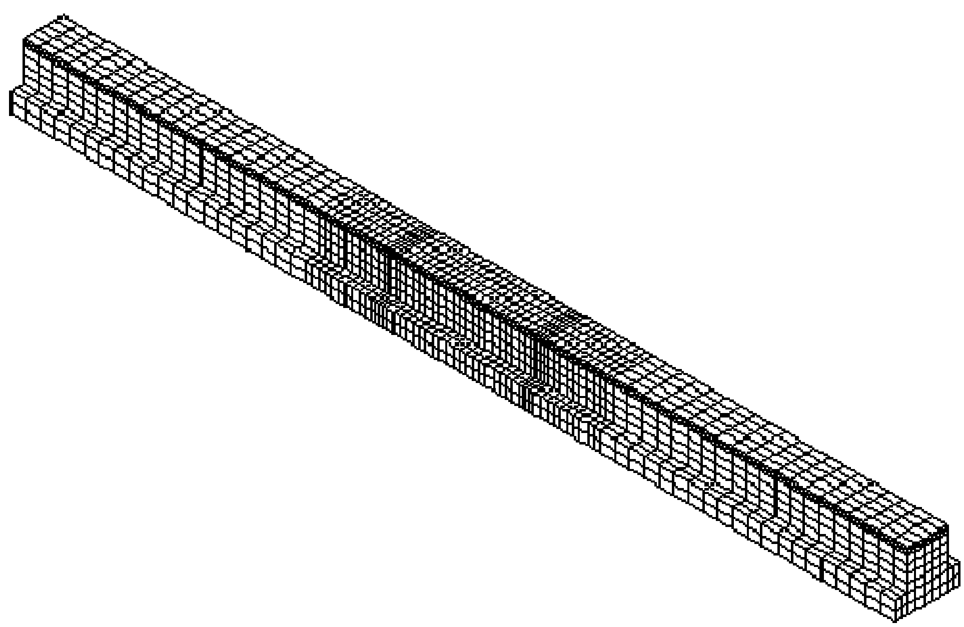

Figure 6.6: The inverted tee girder mesh.

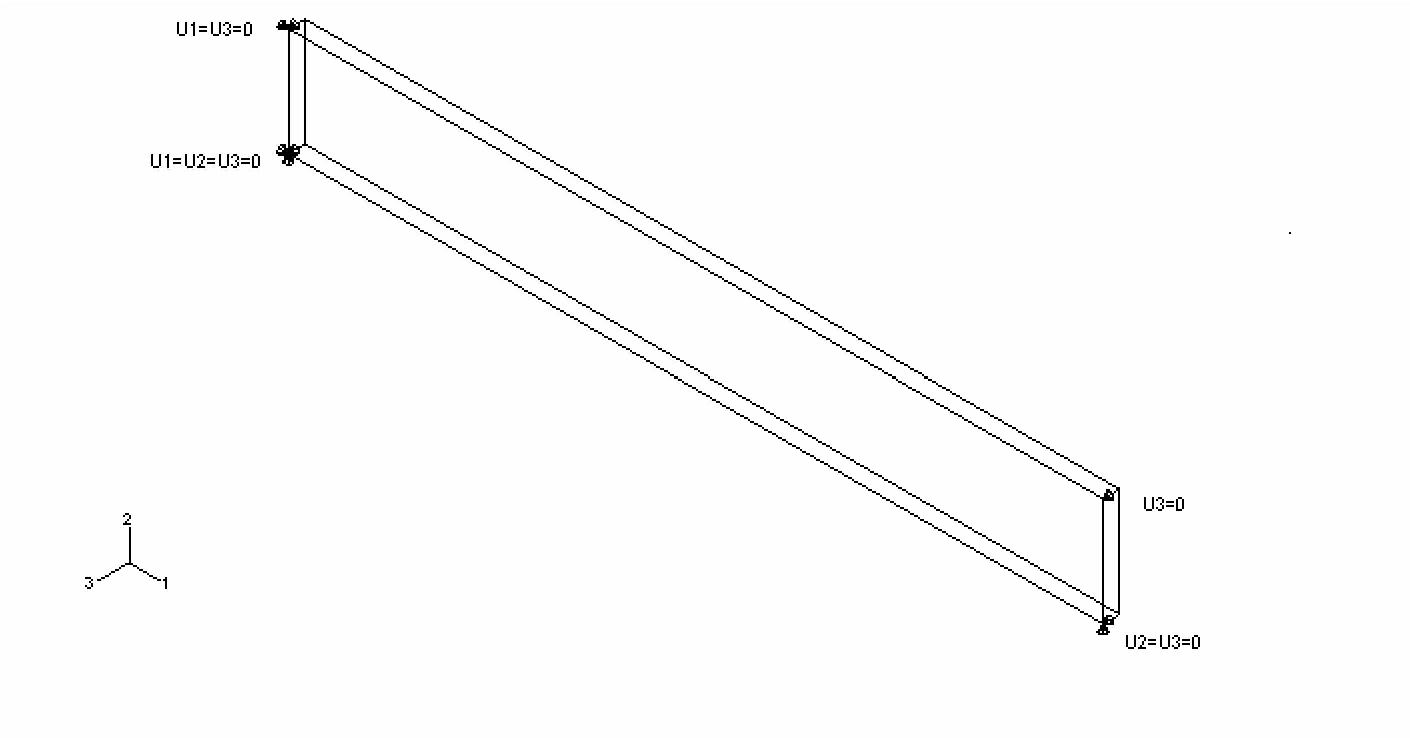

Figure 6.7: The spandrel beam boundary conditions.

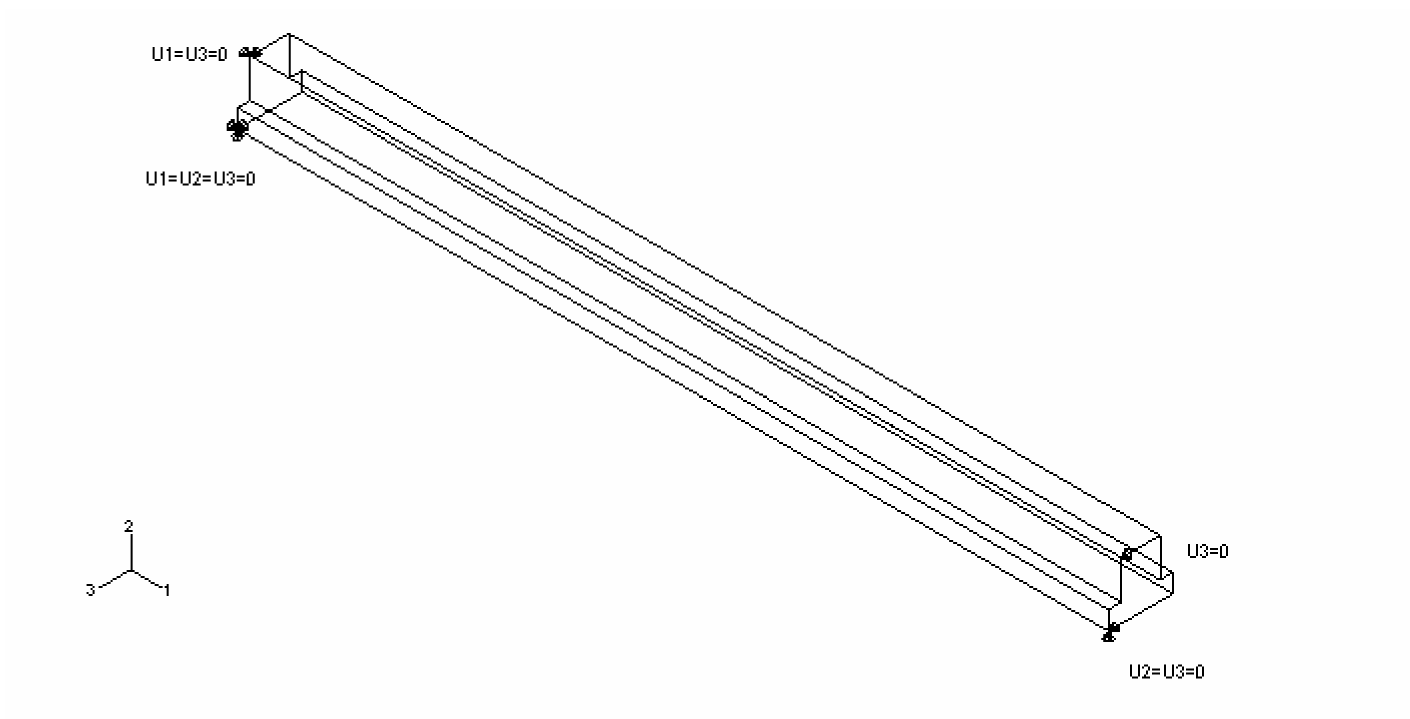

Figure 6.8: The inverted tee girder boundary conditions.

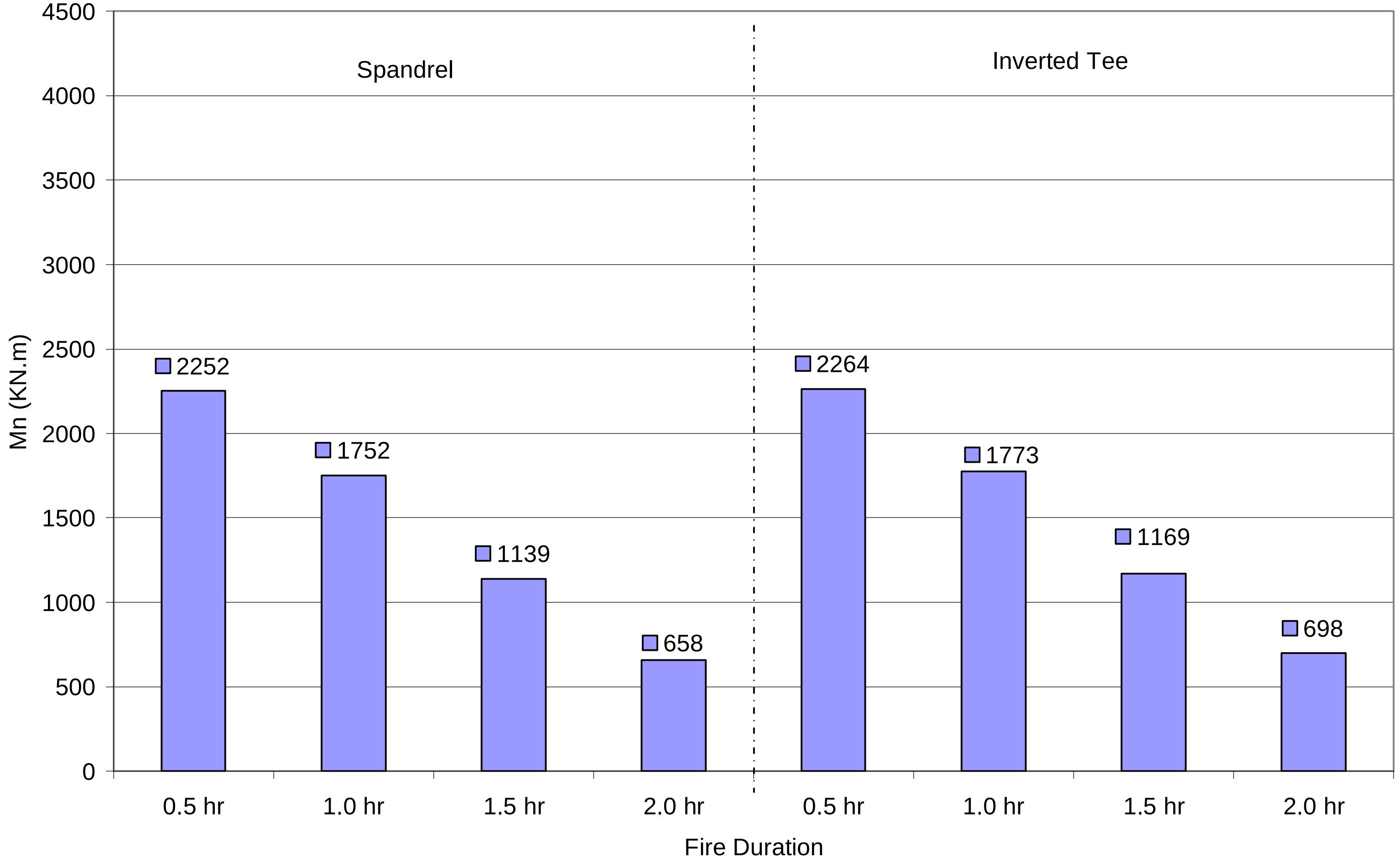

Figure 6.9: Bar chart strength analyses results for the flexible support elements cases.

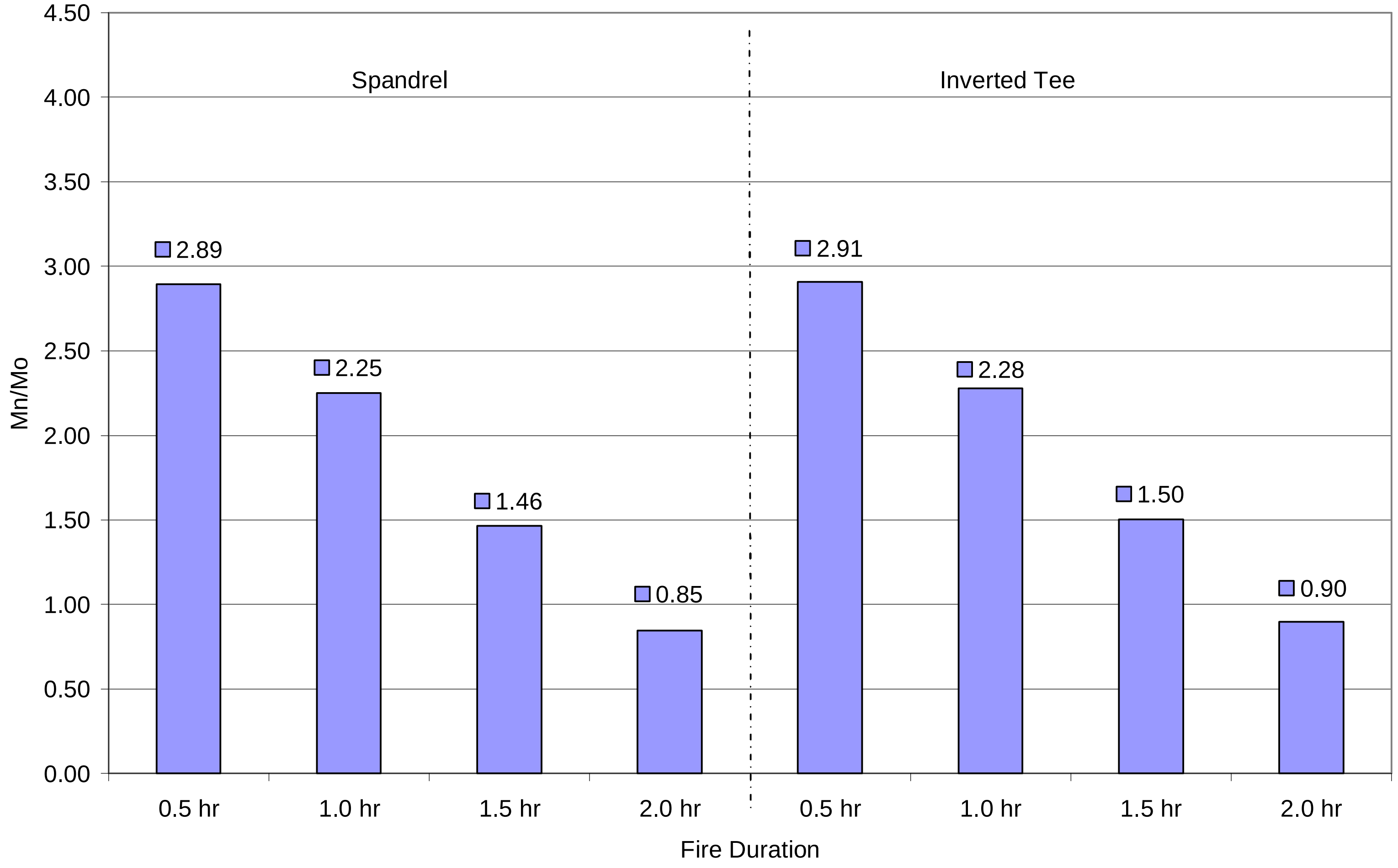

Figure 6.10: Bar chart normalized strength analyses results for the flexible support elements cases.

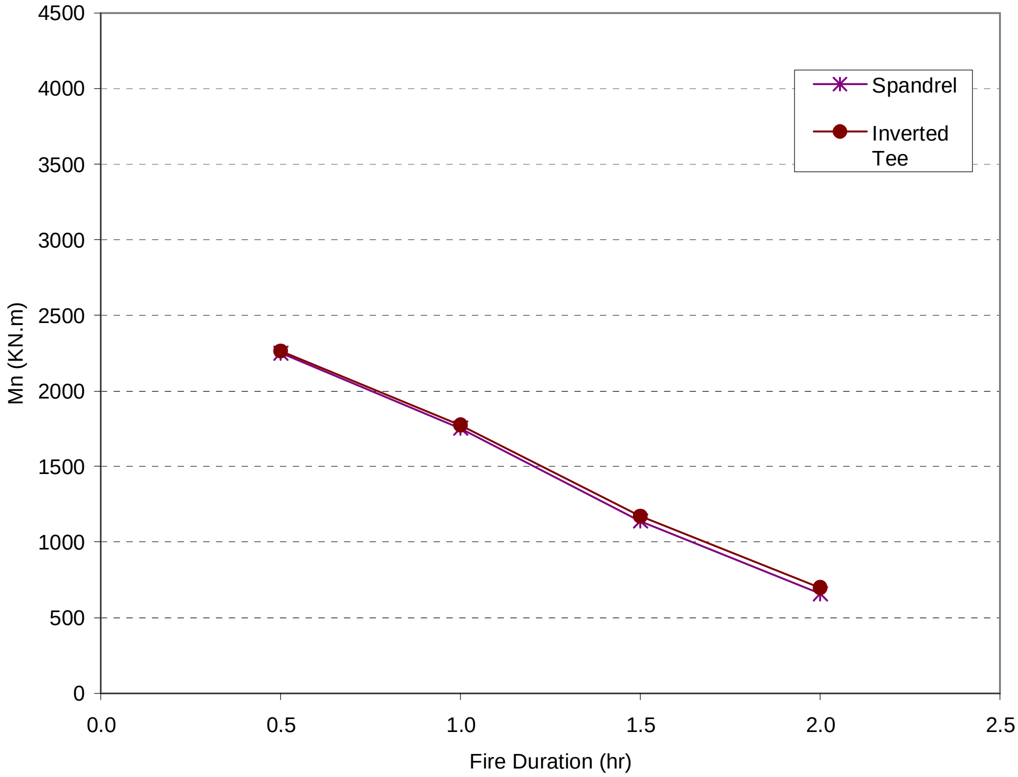

Figure 6.11: Strength analyses results for the flexible support elements cases.

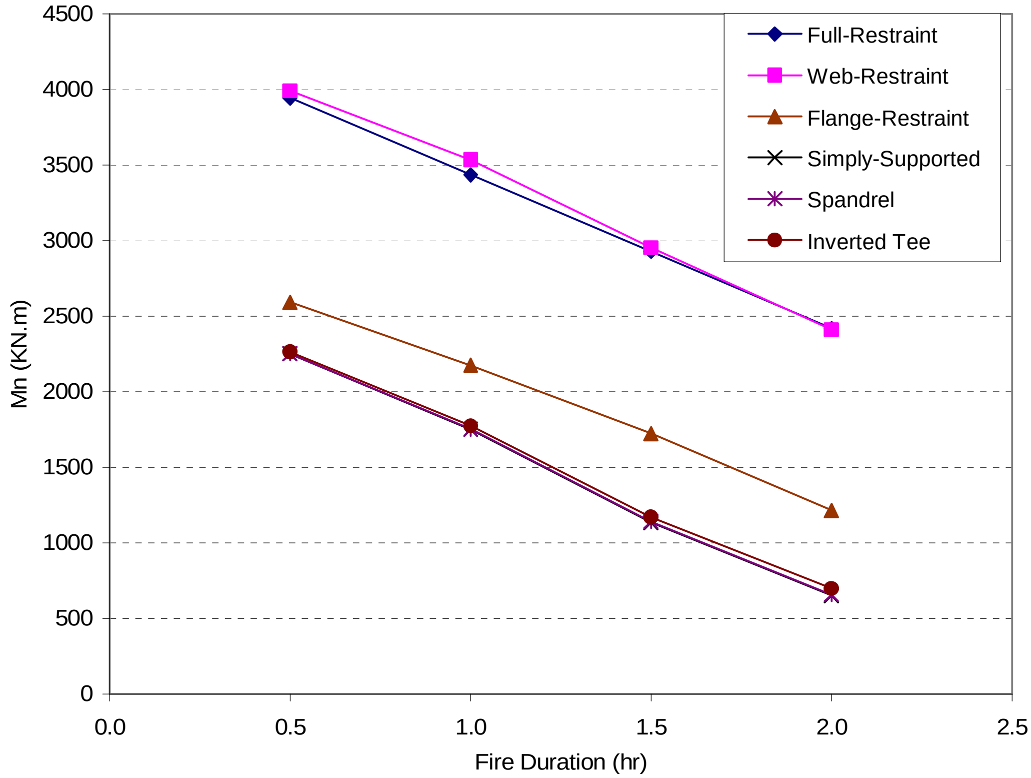

Figure 6.12: Strength analyses results for the flexible support elements cases compared with the idealized single span cases.

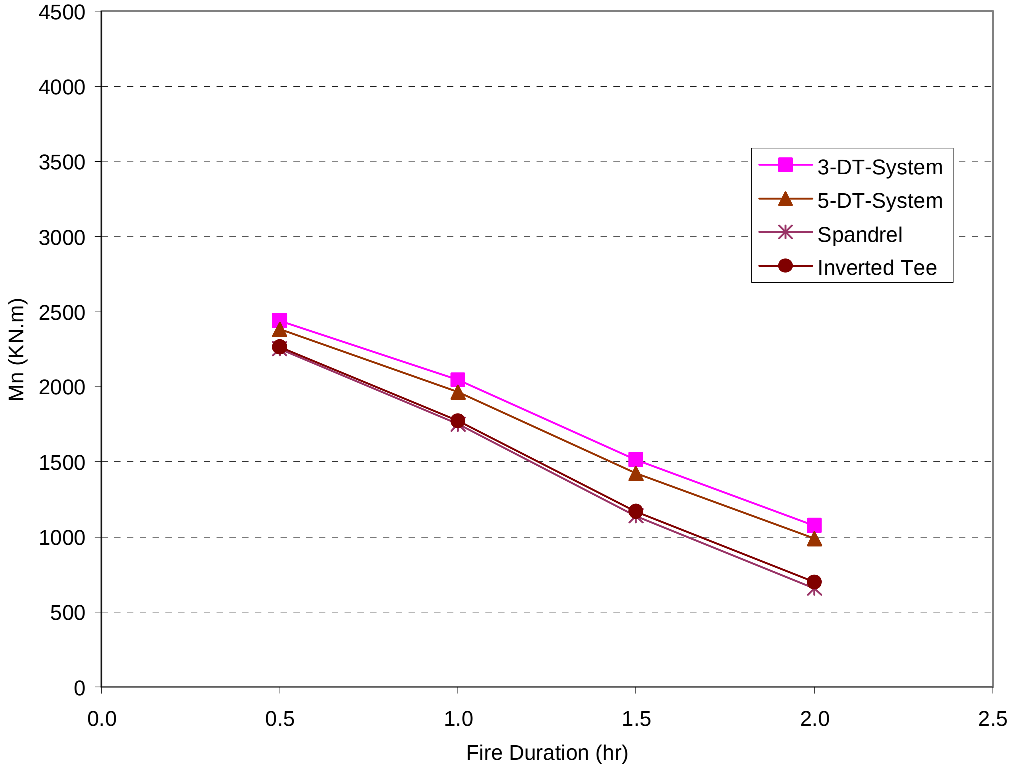

Figure 6.13: Strength analyses results for the flexible support elements cases compared with the multiple span flange restraint cases.

CHAPTER 7

FLANGE CONNECTORS RESTRAINT

7.1 INTODUCTION

It is common practice in many precast concrete building systems to use evenly spaced flange connectors to join adjacent double tee beams together. Flange connectors serve to compensate for varying camber, to align the flanges in the out of plane direction and to resist many types of diaphragm forces. Flange connectors also transfer shear between panels. This chapter presents results from the analyses of the precast prestressed double tee beam restrained along its span by flange connectors. The double tee beam is joined to an adjacent double tee beam on each side by flange connectors. The middle double tee beam is exposed to standard fire from below and the number of connectors is varied. Four different flange connectors cases are considered, where the number of flange connectors are varied along the span: (a) 3 flange connectors; (a) 5 flange connectors; (a) 9 flange connectors; and (a) 17 flange connectors. Figure 7.1 shows the top view of the 3 flange connectors case. The flange connectors in the other three cases are distributed evenly along the span between the flange connectors shown in Figure 7.1.

Section 7.2 presents results from the structural analyses including the restraint forces developing in the double tee beam. The structural analyses models are described and the results are presented. Section 7.3 presents the strength analyses results in which the strength of the double tee beam is determined. Section 7.4 presents a summary of this chapter.

7.2 RESTRAINT FORCES ANALYSES

This study explores the significance of using different numbers of flange connectors on the restraint forces and the strength of the double tee beam. The number of connectors used in practice varies depending on the diaphragm forces they are designed for. Typically, for double tee beams with the same span length of the double tee beam used in this report, 18.6 m (61 ft), the number of flange connectors used is between 8 and 10 flange connectors.

Each flange connector is modeled in the finite element analysis by three nonlinear springs. Each spring acts in a fixed direction parallel to one of the global Cartesian coordinate axes. The three directions simulate the behavior of the actual connectors in tension, horizontal shear and vertical shear.

7.2.1 Description of the Models

Many types of connectors are used by the precast concrete industry. While the purpose of these connectors is basically the same, their individual behaviors differ. Oliva et al. (1998) described the load deformation characteristics of flange connectors under horizontal shear, tension and combined loading. Based on their studies, the horizontal shear properties used in this report are shown in Figure 7.2 and the tension-compression properties are shown in Figure 7.3. The compression segment of Figure 7.3 is based on the assumption that the adjacent double tee beams are in contact. The vertical shear properties provided in Figure 7.4 are based on the JVI V-Connectors that were tested by Shaikh (2002).

The middle double tee beam has the same geometry, mesh, element type, and nonlinear material properties that were discussed and used in Chapter 4. In addition, only that double tee beam is exposed to the standard fire from below. The two adjacent double tee beams remain at room temperature and their properties remain at the room temperature properties. They, however, have the same geometry, mesh, element type as the middle double tee beam. They are also assigned nonlinear material properties, i.e. temperature dependent stress strain curves presented in Figure 3.3. Figure 7.5 shows the entire model of the 17 flange connectors case as an example of the other models considered.

Since only the middle double tee beam is the element that is subjected to fire, the same thermal histories generated in Chapter 4 can be used in theses analyses. Therefore, only the nonlinear finite element structural analyses are conducted using ABAQUS program and the thermal histories are used as a thermal load input. Theses analyses result in the restraint forces sought to be used to find the strength of the double tee beams for each case.

The flanges of the double tee beam contain three elements through the flange thickness. The flange connectors are connected to the bottom nodes of the first elements from the top of the flange. At each side of the spring, a kinematic coupling constraint is used between the double tee beam node connected to the spring, known as the reference point, and the faces of the four elements adjacent to that node. This is done to avoid the concentration of loads at one single node. Large point loads can cause numerical difficulties in finite element analysis. These nodes and constraint regions are shown in Figure 7.6.

7.2.2 Boundary Conditions

The same kinematic coupling constraints prescribed to the bottom of the webs of the double tee beam in the previous chapters are prescribed to the three double tee beams in this chapter. The boundary conditions prescribed to the models of this chapter are shown in Figure 7.7. These boundary conditions provide complete freedom of expansion to the three double tee beams. Therefore, minimum restraints are prescribed only to prevent rigid body motion and matrix singularities.

7.2.3 Restraint Forces

The models are analyzed for each of the connection cases and for the prescribed fire durations. Since the systems are symmetric, the spring forces developing on each side of the middle double tee beam are the same. The forces in the springs in the horizontal shear direction on one side of the middle double tee beam are found. The horizontal shear force in the middle span connector in all cases is found, as expected, to be zero. The restraint forces in each case are found as the sum of the spring horizontal shear forces in half the span on both sides of the middle double tee beam. These forces are shifted to the centroid of the uncracked gross non-heated section and shown in Table 7.1.

The restraint forces in Table 7.1 show that the flange connectors yield at an early stage of the fire. Thus, the restraint forces in most cases are constant in the four fire durations considered. The deformations in the springs are found to exceed the maximum deformations of the connectors provided by Oliva et al. (1998).

The restraint forces shown in Table 7.1 compared to the restraint forces in any of the previous chapters are very small. The impact of these forces on the strength is expected to be insignificant. By changing the connector properties with those of stronger connectors, the restraint forces are expected to increase accordingly. As an extreme case, the analyses are repeated using linear elastic properties in the three directions. In other words, the impact of using flange connectors with unlimited strength is used. The stiffnesses of the connectors prescribed in this case are the same as the initial stiffnesses used in the previous nonlinear connectors.

Table 7.2 presents the restraint forces resulting from the analyses using linear elastic flange connectors. As expected, the restraint forces in this case are significantly larger than the forces in the nonlinear case. In addition, in both linear and nonlinear flange connectors cases, the restraint forces developing in the double tee beam increase with the increase in the number of flange connectors. The largest restraint forces develop in the 17 linear flange connectors case. These restraint forces are less, however, than the restraint forces developed in the idealized flange-restraint case, which are the least among the other idealized cases.

7.3 STRENGTH ANALYSES

The resulting restraint forces from the previous step are used to analyze the mid-span section of the double tee beam model, at the four different fire durations, by using nonlinear fiber analysis with DRAIN-2DX program. The result of these analyses is the strength of the double tee beam subjected to different restraint conditions at different fire durations. This provides the insight needed to understand the effects of restraint on the strength of the precast concrete double tee beam subject to fire. The restraint cases considered here are the restraint provided by the different patterns of flange connectors.

The same fiber models were explained and used in Chapter 4 are used here after replacing the previous restraint forces with the forces presented in Tables 7.1 and 7.2. The strength analyses for both the linear and nonlinear connectors are conducted for only the cases of 3 and 17 flange connectors. This is because the restraint forces developing in the other two cases lie in between the 3 and 17 flange connectors restraint forces.

Figure 7.8 shows a bar chart displaying the summary of the results achieved in the strength analyses for the nonlinear flange connectors case. This figure shows that the strength of the double tee beam restrained by 3 flange connectors is similar to its strength when restrained by 17 flange connectors. Thus, varying the number of flange connectors along the span of the double tee beam has insignificant influence on the additional strength added to the double tee beam during fires. Figure 7.9 shows another bar chart displaying the summary of the strength analyses results for the linear flange connectors case. The values in Figure 7.9 are similar to the corresponding values in Figure 7.8. This implies that using flange connectors of any type leads to similar additional strengths provided to the double tee beam under fire loads.

Figure 7.10 provides normalized values of the results for the nonlinear flange connectors case in terms of the self-weight midspan moment of the simply supported double tee beam (i.e. M = 778 kN.m). Values in the chart higher than unity present the case where the double tee beam is expected to withstand its own self weight at the particular fire duration. Figure 7.11 provides normalized values for the linear flange connectors case. It’s clear form both figures that the double tee beam will not be able of withstanding its own self weight at 2 hours of fire in both the nonlinear flange connectors case and the linear flange connectors case with either 3 or 17 flange connectors used.

Figure 7.12 presents curves for the summary of all the results achieved in the strength analyses in this chapter. This figure confirms the findings of Figures 7.8 and 7.9. Figure 7.13 compares between the results of the nonlinear connectors case and the results of the idealized single span restraints. Figure 7.14 compares between the results of the linear connectors case and the idealized single span restraints. The results of both Figures 7.13 and 7.14 show that the strength of the double tee beam restrained by any type and any number of flange connectors is similar to the strength of the simply supported double tee beam. Therefore, flange connectors do not contribute to the restraint of double tee beams during fires.

7.4 SUMMARY

This chapter presents results from the analyses of the precast prestressed double tee beam restrained along its span by flange connectors. The double tee beam is joined to another double tee beam on each side by flange connectors. The middle double tee beam is exposed to standard fire from below and the number of connectors is varied. The impact of exposing this double tee beam to standard fire on its strength is explored. Four different flange connectors cases are considered, where the number of flange connectors are varied along the span: (a) 3 flange connectors; (a) 5 flange connectors; (a) 9 flange connectors; and (a) 17 flange connectors.

The restraint forces of the nonlinear flange connectors case compared to the restraint forces in any of the previous chapters are very small. The restraint forces resulting from the analyses using linear elastic flange connectors are significantly larger than the forces in the nonlinear case. In addition, in both linear and nonlinear flange connectors cases, the restraint forces developing in the double tee beam increase with the increase in the number of flange connectors. The largest restraint forces develop in the 17 linear flange connectors case. These restraint forces are less, however, than the restraint forces developed in the idealized flange-restraint case, which are the least among the other idealized cases.

Varying the number of flange connectors along the span of the double tee beam has insignificant influence on the additional strength added to the double tee beam during fires. Figure 7.9 shows another bar chart displaying the summary of the strength analyses results for the linear flange connectors case.

A double tee beam will not be able of withstanding its own self weight at 2 hours of fire in both the nonlinear flange connectors case and the linear flange connectors case with either 3 or 17 flange connectors used.

The strength of the double tee beam restrained by any type and any number of flange connectors is similar to the strength of the simply supported double tee beam. Therefore, flange connectors do not contribute to the restraint of double tee beams during fires.

Table 7.1: Restraint forces results for the nonlinear connectors case.

# of Connectors	0.5 hr	1.0 hr	1.5 hrs	2.0 hrs
3	25 KN.m 142 KN	25 KN.m 142 KN	25 KN.m 142 KN	25 KN.m 142 KN
5	51 KN.m 285 KN	51 KN.m 285 KN	51 KN.m 285 KN	51 KN.m 285 KN
9	98 KN.m 550 KN	102 KN.m 569 KN	102 KN.m 569 KN	102 KN.m 569 KN
17	178 KN.m 996 KN	198 KN.m 1112 KN	203 KN.m 1139 KN	203 KN.m 1139 KN

Table 7.2: Restraint forces results for the linear connectors case.

# of Connectors	0.5 hr	1.0 hr	1.5 hrs	2.0 hrs
3	89 KN.m 469 KN	164 KN.m 921 KN	231 KN.m 1239 KN	282 KN.m 1577 KN
5	123 KN.m 690 KN	234 KN.m 1312 KN	339 KN.m 1899 KN	426 KN.m 2390 KN
9	178 KN.m 996 KN	334 KN.m 1871 KN	478 KN.m 2671 KN	594 KN.m 3330 KN
17	257 KN.m 1439 KN	469 KN.m 2626 KN	655 KN.m 3670 KN	799 KN.m 4475 KN

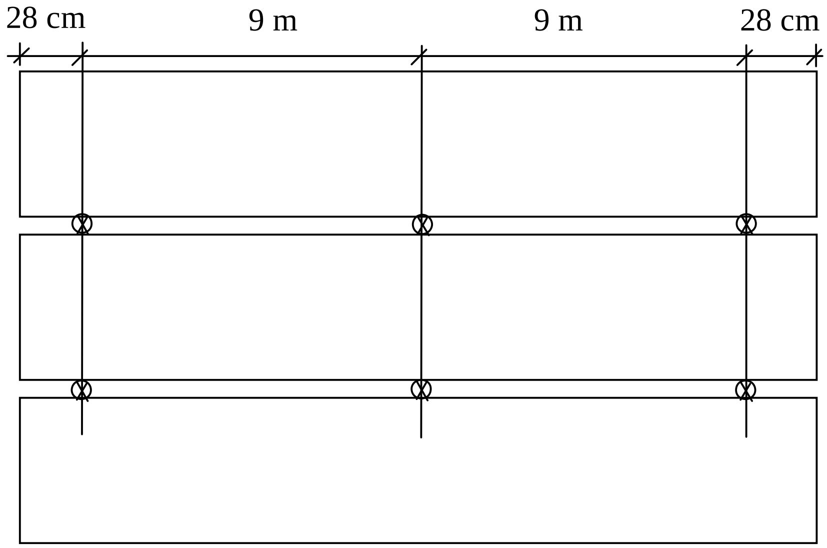

Figure 7.1: Top view of the 3 flange connectors case.

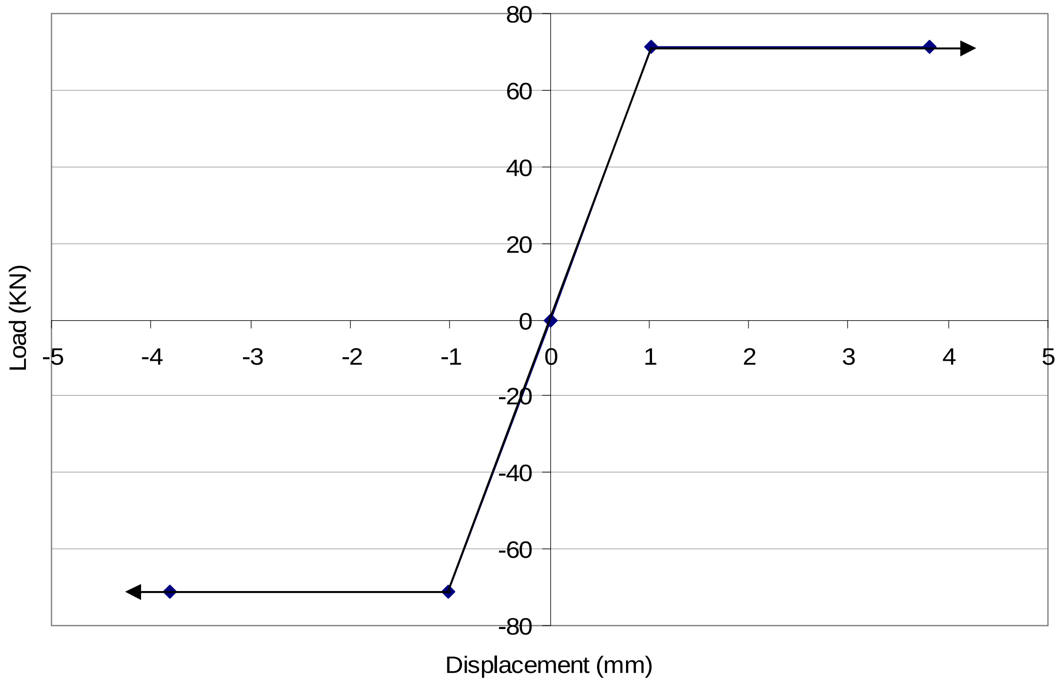

Figure 7.2: Flange connector load deformation properties in horizontal shear for ABAQUS.

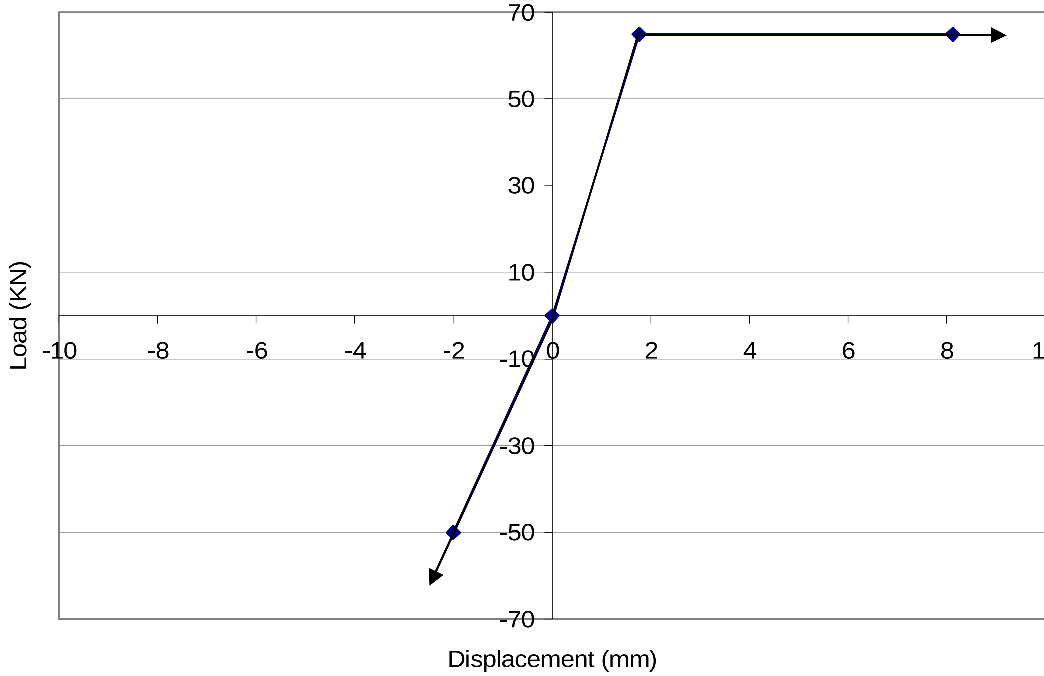

Figure 7.3: Flange connector load deformation properties in tension-compression for ABAQUS.

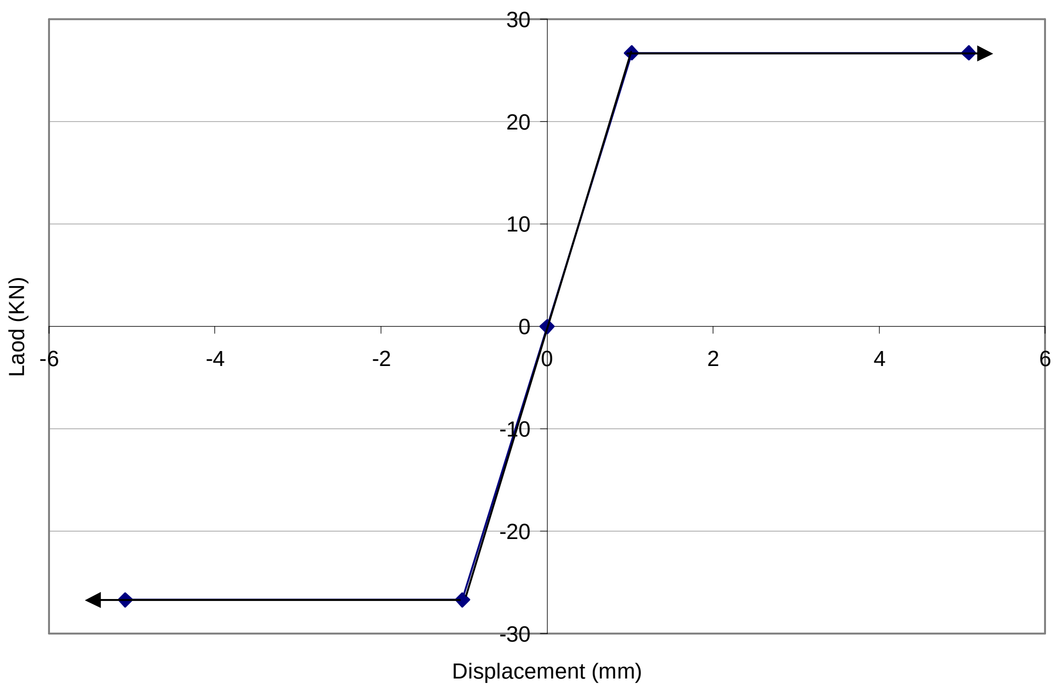

Figure 7.4: Flange connector load deformation properties in vertical shear for ABAQUS.

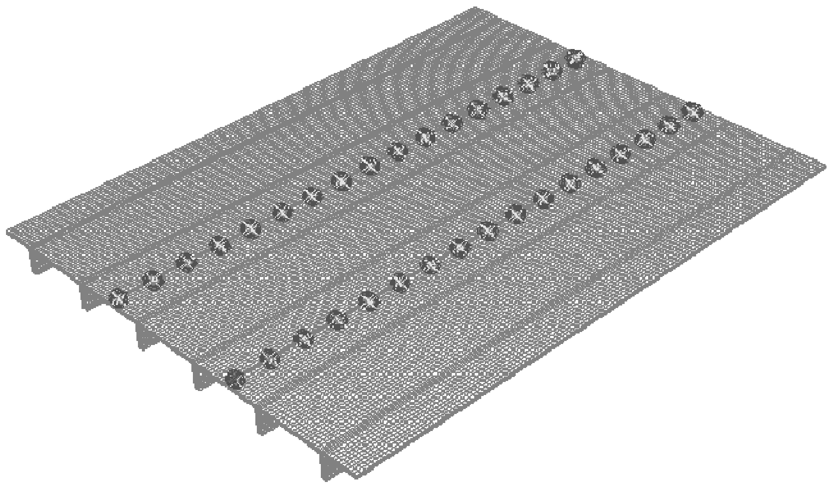

Figure 7.5: ABAQUS model for the 17 flange connectors case.

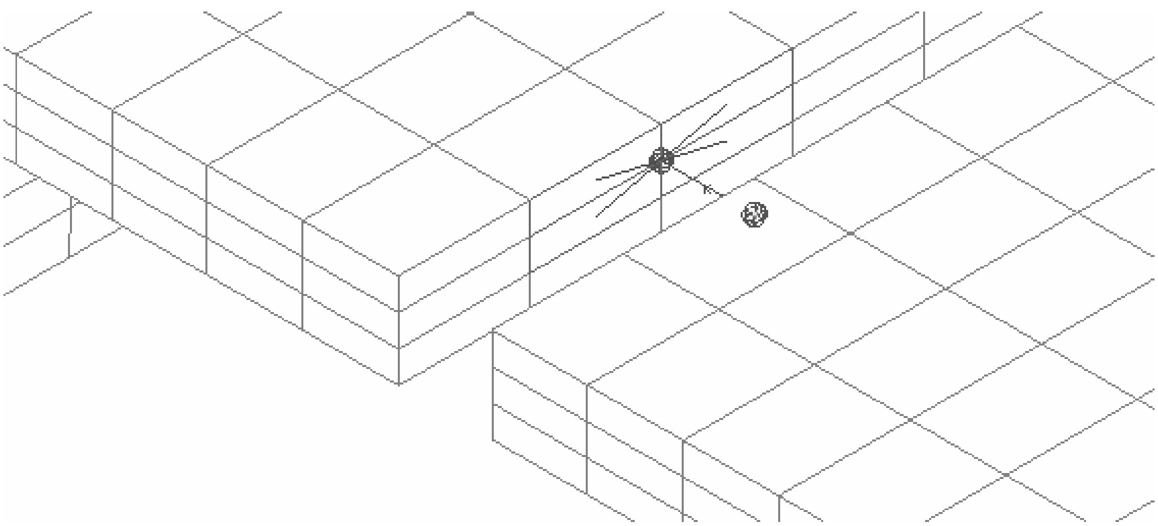

Figure 7.6: The double tee beam constraint regions and connection with the spring.

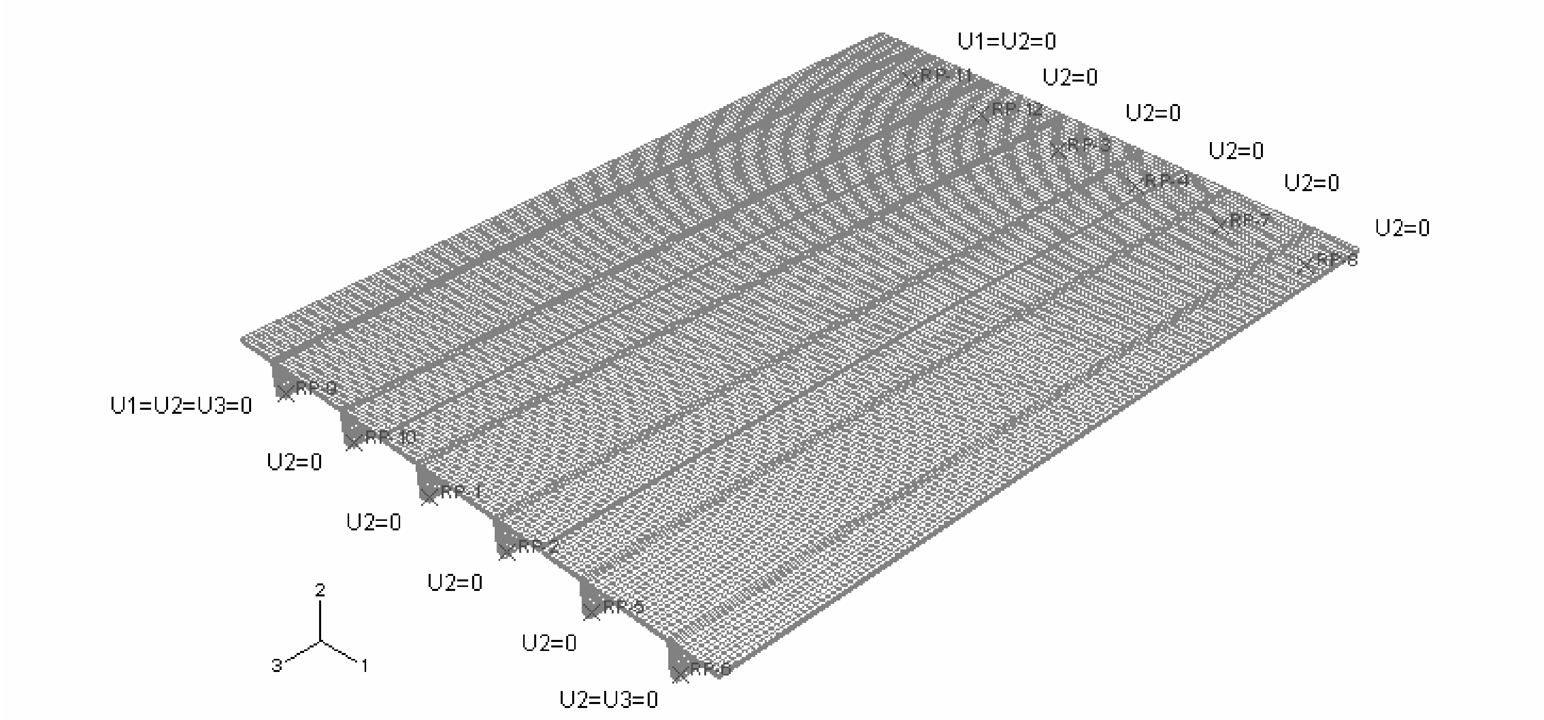

Figure 7.7: Boundary conditions prescribed to the ABAQUS models for the flange connectors analyses.

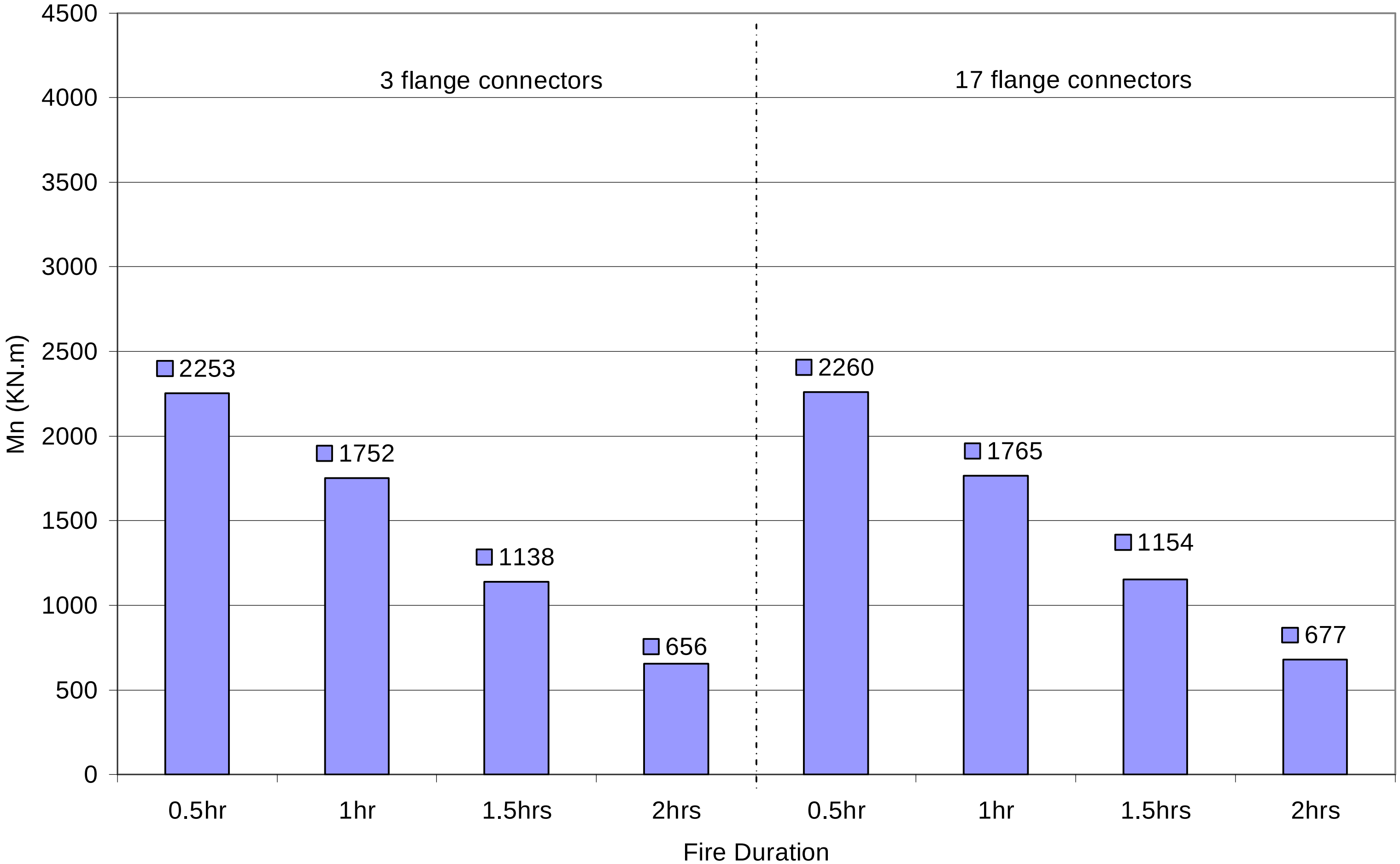

Figure 7.8: Strength analyses results for the nonlinear flange connectors restraints.

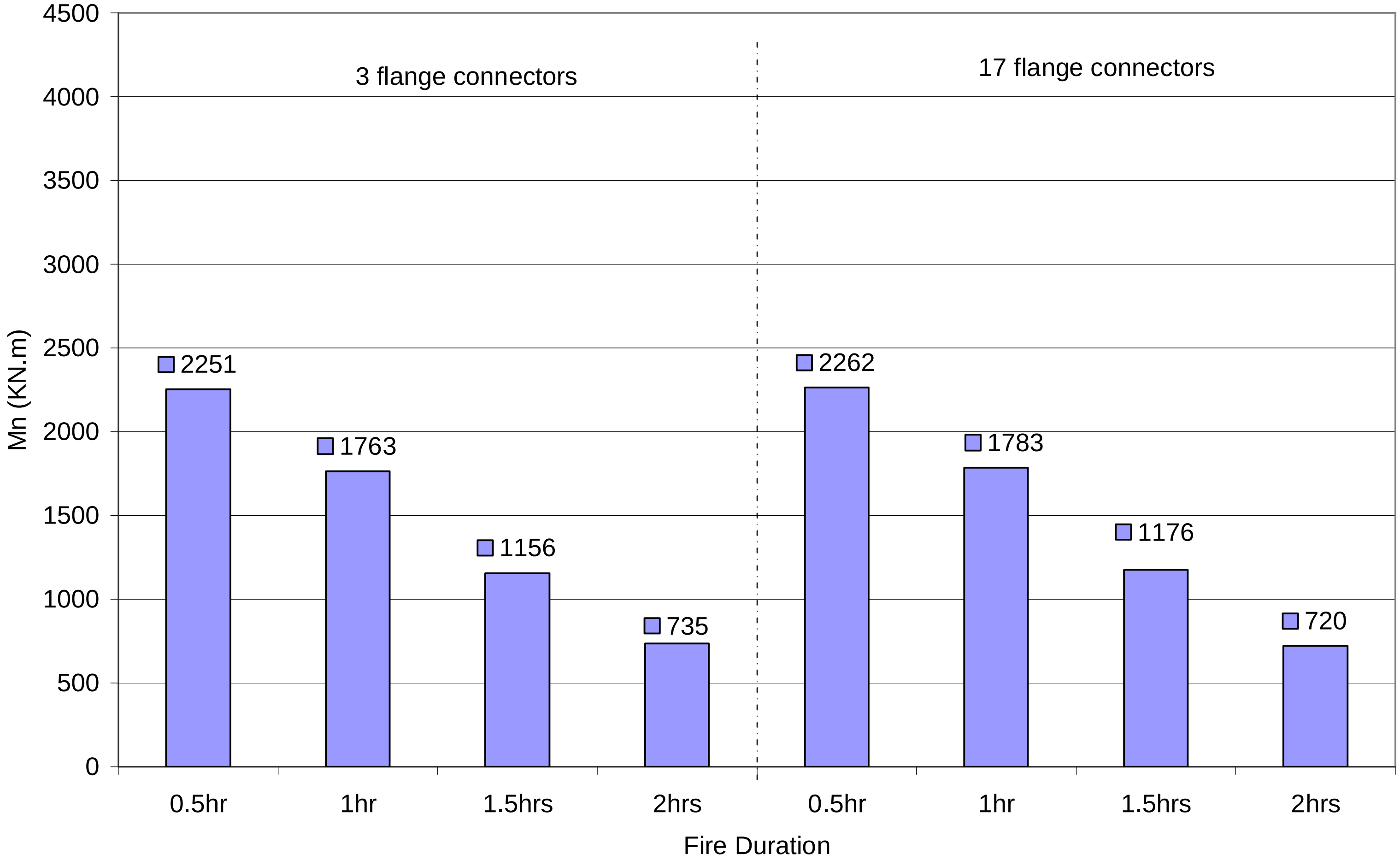

Figure 7.9: Strength analyses results for the linear flange connectors restraints.

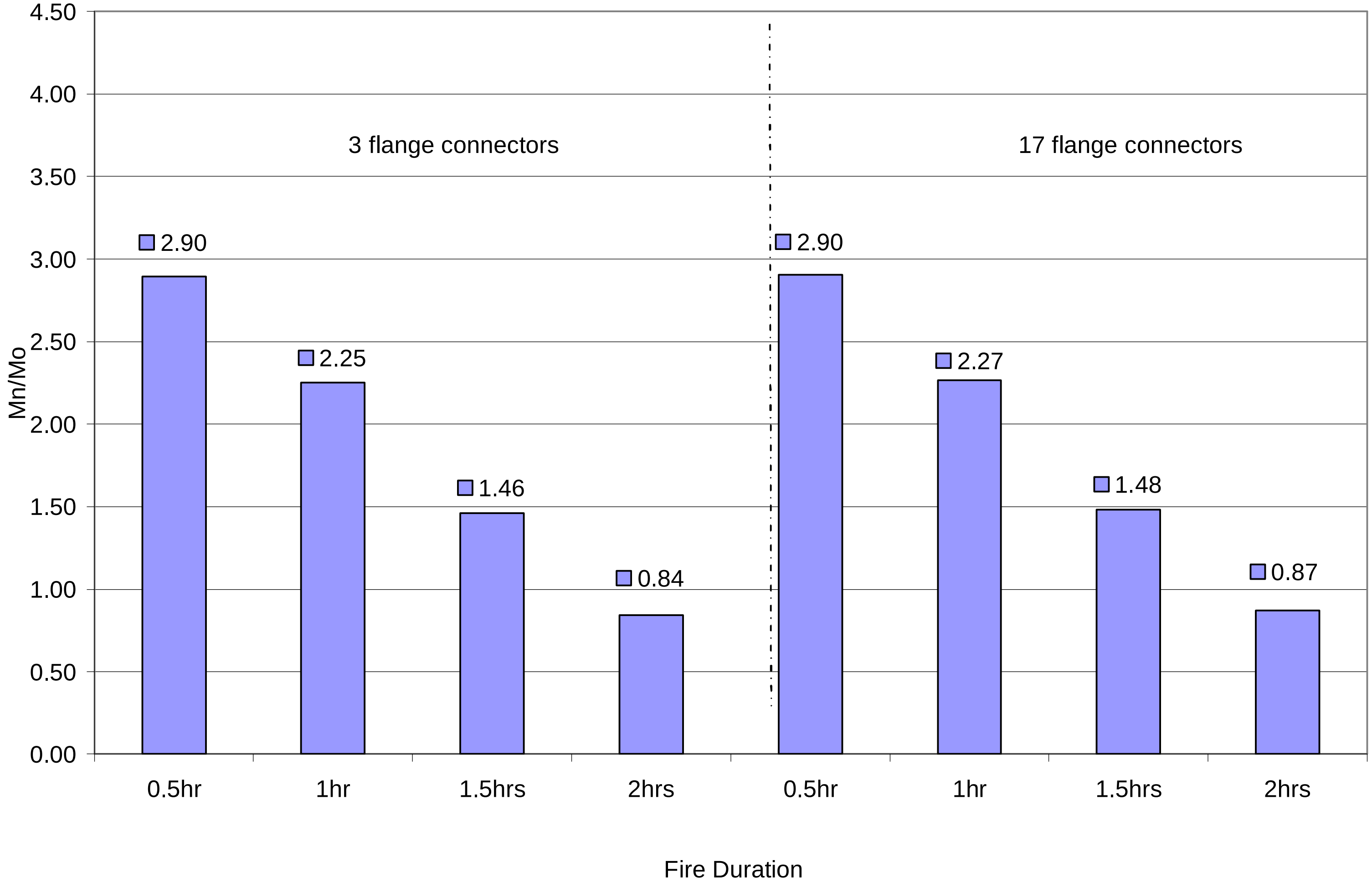

Figure 7.10: Normalized strength analyses results for the nonlinear flange connectors restraints.

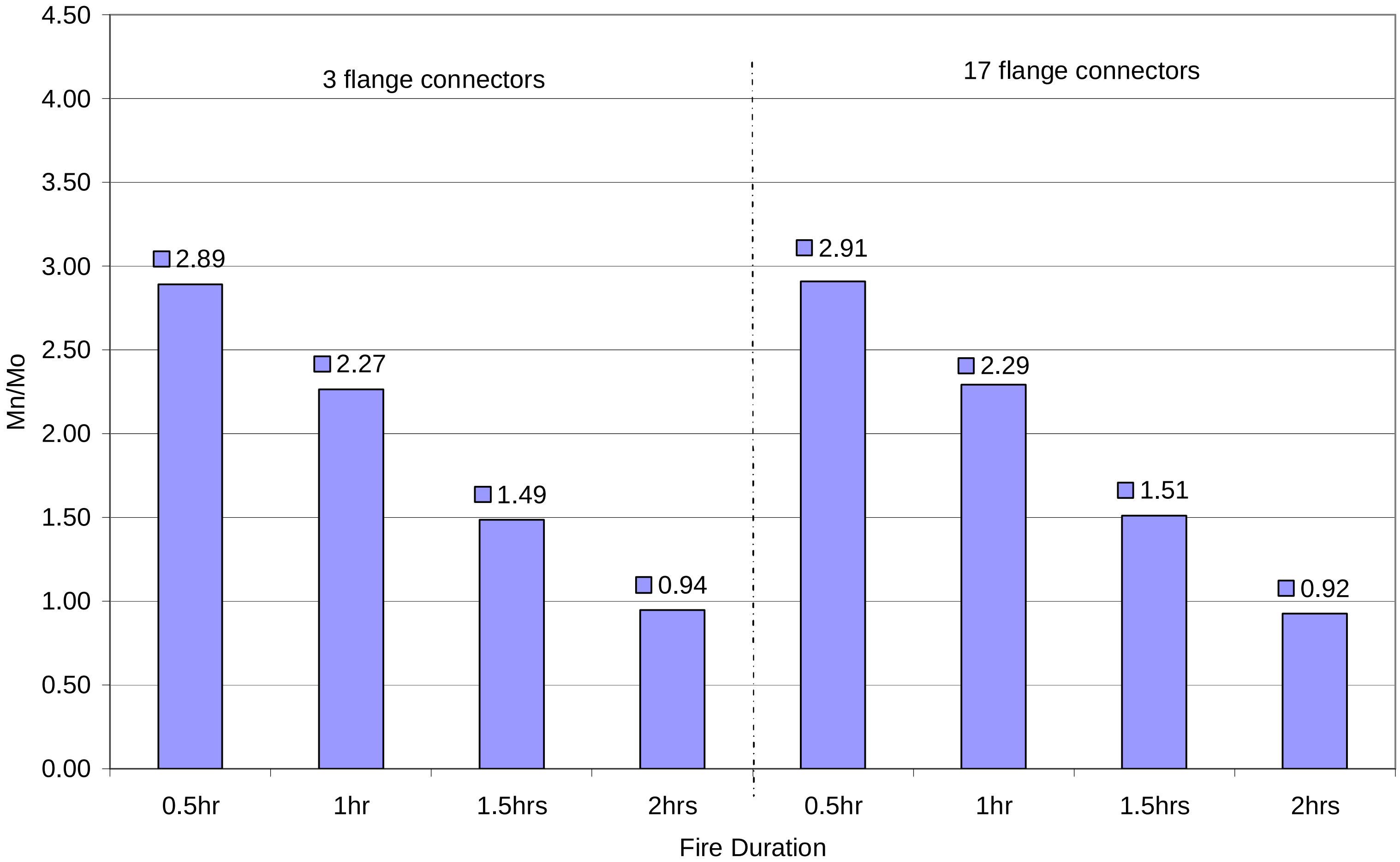

Figure 7.11: Normalized strength analyses results for the linear flange connectors restraints.

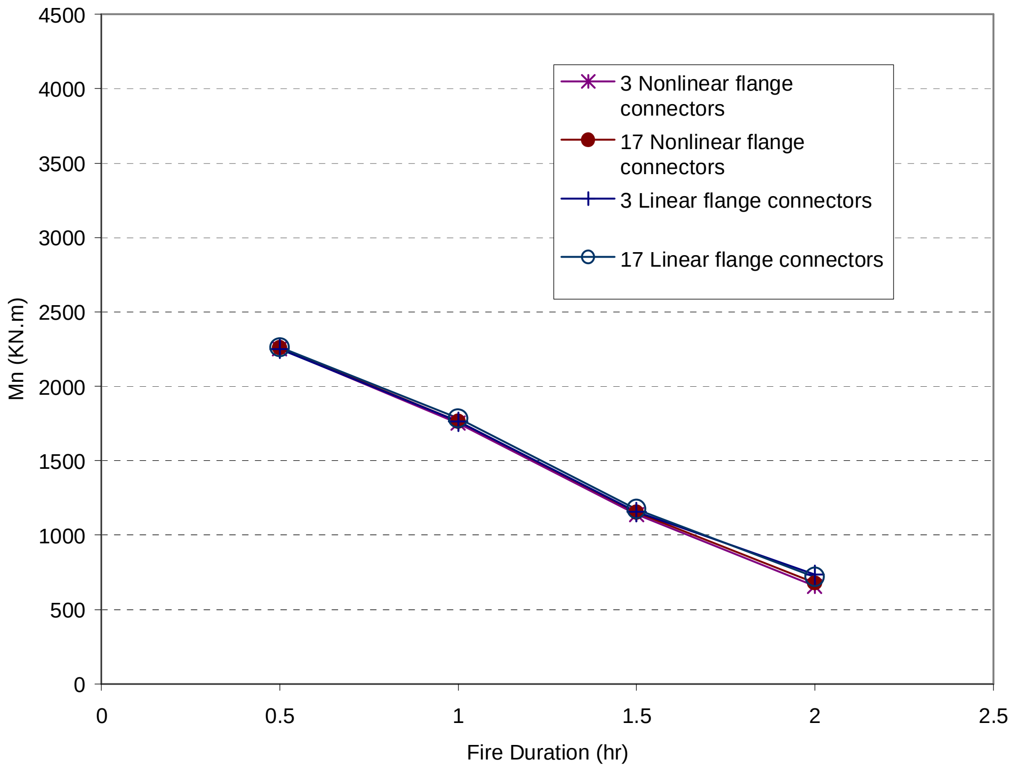

Figure 7.12: Strength analyses results for the nonlinear flange connectors and the linear flange connectors restraints.

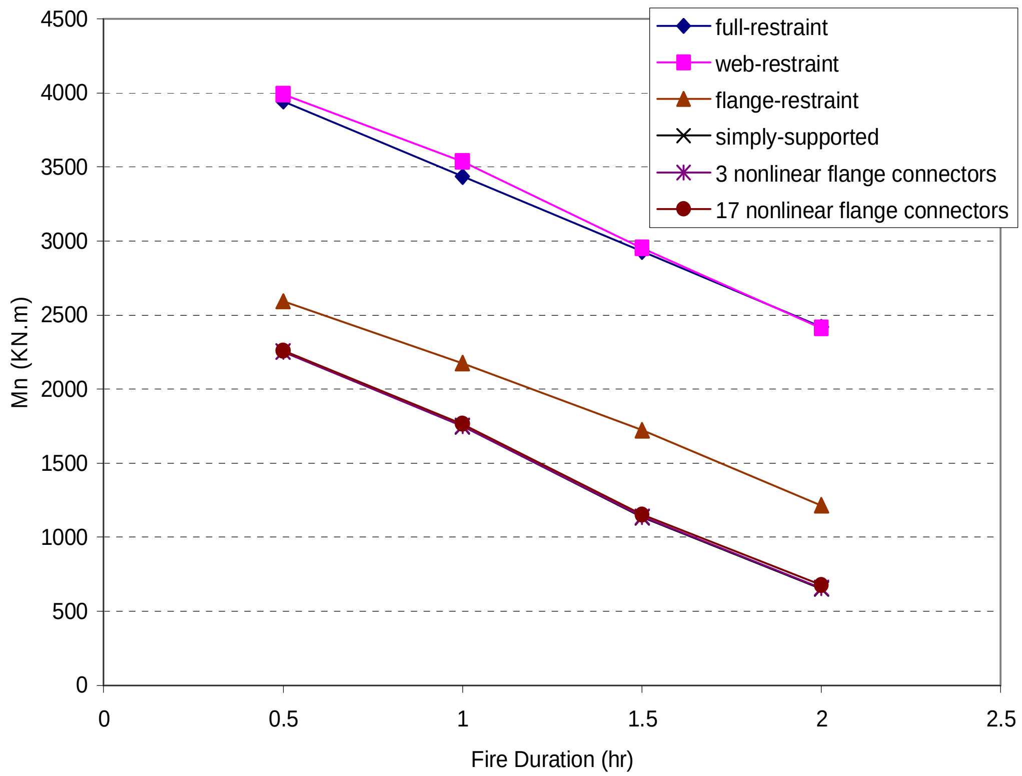

Figure 7.13: Strength analyses results for the nonlinear flange connectors cases compared with the idealized single span cases.

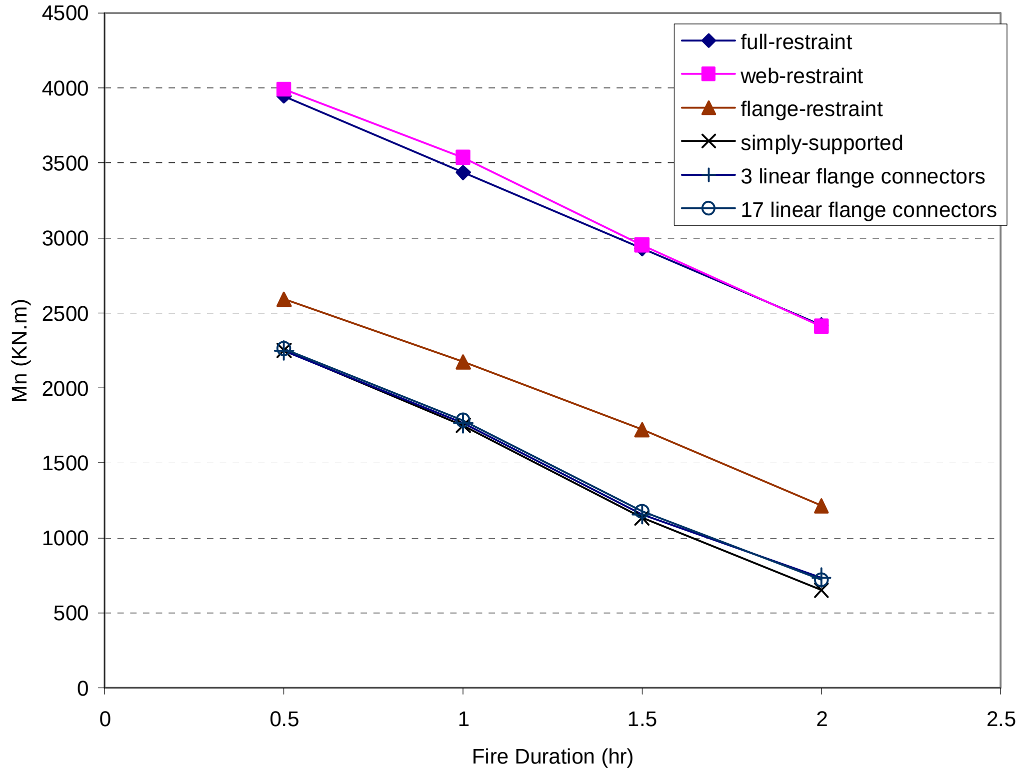

Figure 7.14: Strength analyses results for the linear flange connectors cases compared with the idealized single span cases.

CHAPTER 8

SUMMARY, CONCLUSIONS, AND FUTURE RESEARCH

8.1 SUMMARY

The objective of the research presented in this report is to analytically investigate the development of restraint mechanisms in precast prestressed concrete floor systems subjected to fire loading. A prototype precast prestressed double tee beam typically used in practice for precast parking structures is considered in this research. The restraint mechanisms are investigated through their influence on the strength of the double tee beam section. The analytical approach consisted of three sequential analysis steps: (1) nonlinear heat transfer analysis; (2) nonlinear structural analysis; and (3) nonlinear strength analysis. Each step used the results from the previous analysis step.

Four different restraint cases, where restraint forces develop in the prototype double tee beam from different sources, are explored: (1) idealized single span restraints; (2) multiple span restraints; (3) flexible support elements restraints; and (4) flange connectors restraints.

8.2 CONCLUSIONS

The following conclusions are drawn from the results of the research work presented in this report:

1. From the idealized single span restraints analyses, the strength of the double tee beam was found to vary significantly with the type of boundary conditions prescribed and when subjected to different durations of standard fire. The strength is significantly less in the flange-restraint case, and even less in the simply supported case as compared to the web-restraint case and the full-restraint case. The strength of the double tee beam in the web-restraint case is slightly higher than in the full-restraint case. This is attributed to the fact that the flange contributes to the restraint in the full-restraint case, which tends to decrease the strength, and doesn’t in the web-restraint case.

2. From the multiple span restraints analyses, in both the 3 and 5 double tee beam systems, the strength of the beam in the web-restrained case is slightly higher than that of the full-restraint case, and it’s considerably higher in both cases than in the flange-restraint case. This is consistent with the findings of the idealized single span restraint analyses. In addition, the strength of the double tee beam decreases as the number of spans increases in all restraint conditions. This effect, however, is lower in the flange-restraint case than in the other restraint cases.

3. From the flexible supports elements (spandrel beams and inverted tee girders) restraints analyses, the strength of the double tee beam restrained by the flexible

support elements is only slightly higher than the strength of the simply supported double tee beam.

4. From the flange connectors restraints analyses, varying the number of flange connectors along the span of the double tee beam has insignificant influence on the restraint mechanisms and the additional strength added to the double tee beam during fires. Using flange connectors of any type leads to the same additional strengths provided to the double tee beam subjected to fire. The strength of the double tee beam restrained by any type and any number of flange connectors is only slightly higher than the strength of the simply supported double tee beam.

8.3 FUTURE RESEARCH

Further research is suggested in the following areas:

1. Conducting further research work additional restraint mechanisms such as support walls and topping slabs.

2. Conducting further research work to create models of the entire floor system or the entire building, in which the different restraint cases are simultaneously considered, to further understand the development of restraint mechanisms.

3. Repeating the analyses in the report for time-temperature curves that represent real fires.

REFERENCES

ABAQUS (2005), ABAQUS/Standard Version 6.5 User's Manuals, Hibbit, Karlsson, and Sorenson, Inc., Pawtucket, Rhode Island.

ACI Committee 216 (1989), "Guide for Determining the Fire Endurance of Concrete Elements (ACI 216R-89)," American Concrete Institute, Farmington Hills, MI, 48 pp.

ACI Committee 318 (2005), "Building Code Requirements for Structural Concrete (ACI 318-05)," American Concrete Institute, Farmington Hills, MI, 430 pp.

ASTM (1999), "Standard Test Methods for Fire Tests of Building Construction and Materials," E119, American Society for Testing and Materials, W. Conshohocken, PA, 21 pp.

Eurocode 2 ENV 1992-1-2 (1996), "Design of Concrete Structures," Part 1.2, General Rules-Structural Fire Design, European committee for standardization, Brussels, 63 pp.

Gustaferro, A.H., Martin, L.D., (1989), "Design for Fire Resistance of Precast Prestressed Concrete," Second Edition, Precast/Prestressed Concrete institute, (MNL-124-89), 85 pp.

Lie, T.T., (1992), "Structural Fire Protection," American Society of Civil Engineers, ASCE Manuals and Reports on Engineering Practice No. 78. ASCE, 1992, 241 pp.

Mills, A.F., "Heat Transfer," (1998), Prentice Hall, 2nd Edition, 954 pp.

Oliva, M.G., Pincheira, J.A. and Kusumo-Richard, F.I. (1998), "Test on Double tee beam Flange Connectors Subjected to Monotonic and Cyclic Loading," PCI JOURNAL, V. 43, No. 3, May-June 1998, pp. 82-96.

PCI (2004), PCI Design Handbook, Precast and Prestressed Concrete, Sixth Edition, Precast/Prestressed Concrete Institute, Chicago, IL, 736 pp.

Prakash, V., Powell G.H., Campbell, S., (1993), "DRAIN-2DX Base Program Description and User Guide," Version 1.10, November 1993, 90pp.

Shaikh, A.F. and Feile, E.P., (2002), "Testing of JVI Vector Connector," Structural Engineering Testing Report, University of Wisconsin-Milwaukee, WI, September 2002, 50 pp.

Thompson, J.M., (2004), "Behavior and Design of Precast Prestressed Concrete Inverted Tee Girders With Multiple Web Openings for Service Systems," Ph.D. Dissertation, Lehigh University, 511 pp.

Varma, A.H., Srisa-Ard, J., and Hong, S. (2004), "Behavior of CFT Columns Under Fire Loading," Proceedings of the ASCE Structures Congress – 2004, Nashville, Tennessee, pp. 557-580.

Wang, Y.C., Steel and Composite Structures, (2002), "Behavior and Design for Fire Safety," Spon Press, New York, 2002, 332 pp.